RECOVERY OF RARE EARTH ELEMENTS FROM ALASKAN COAL AND COAL COMBUSTION PRODUCTS

By

Tushar Gupta

A Thesis Submitted in Partial Fulfillment of the Requirements

for the Degree of

Master of Science

in

Mining Engineering

University of Alaska Fairbanks

December 2016

APPROVED:

Tathagata Ghosh, Committee Chair
Guven Akdogan, Committee Co-Chair
Sukumar Bandopadhyay, Committee Member
Debasmita Misra, Committee Member
Margaret Darrow, Chair
Department of Mining and Geological Engineering
Douglas Goering, Dean
College of Engineering and Mines
Michael Castellini,
Dean of the Graduate School

Abstract

Owing to the monopolistic supply and rapid demand growth of Rare Earth Elements (REEs), cost effective and eco-friendly technologies for extraction of REEs from coal and coal byproducts are being widely explored. Physical separation tests, like magnetic separation, float-sink and froth flotation, were conducted at a laboratory scale, for identification and characterization of REEs in two Alaskan coal samples. The studies revealed that the samples are enriched in critical REEs, and have elevated REE concentrations as compared to average world coal estimates. The selected coal samples from Healy and Wishbone Hill regions were found to possess an overall concentration of 524 ppm and 286 ppm, respectively, of REEs in coal on ash basis and some density fractions have total REE concentrations as high as 857 ppm.

Based on the characterization studies, detailed investigations were conducted to enrich the REEs and produce a concentrate for downstream extraction. A three-factor three-level Box-Behnken design for modeling and optimization of froth flotation revealed that the optimum flotation conditions for maximum REE Enrichment in the froth fraction was independent of collector dosage for both coal samples. The response variable was maximized at 4.2% solids and 32.7 ppm of frother dosage for Healy Coal sample and 10% solids and 37.9 ppm of frother dosage for Wishbone Hill Coal sample.

A processing flowsheet for REE enrichment in clean coal is proposed, which aims at concentrating REEs in lower density fractions by a combination of dense medium separation and froth flotation processes. The overall REE recovery of the process is

calculated to be 76% for Healy and 60% for Wishbone Hill with clean coal fractions enriched in REE concentrations above the cut-off value required for the commercial exploitation. The coals are found to possess the potential to be used as a REE resource under favorable socio-economic and geo-political scenarios.

Dedicated to

Amma Ji and Naani for their unconditional love and inspiration.

Table of Contents **Page**

Title Page i

Abstract iii

Dedication v

Table of Contents vii

List of Figures xi

List of Tables xv

List of Appendices xix

Acknowledgements xxi

CHAPTER 1 INTRODUCTION 1

1.1 Introduction 1

1.2 Objective of the Work 4

1.3 Thesis Outline 5

CHAPTER 2 BACKGROUND 7

2.1 What are REEs 7

2.2 Classification of REEs 8

2.3 Properties 10

2.3.1 Reactivity 10

2.3.2 Boiling and Melting Points 10

2.3.3 Ionization Potential 11

2.3.4 Magnetic Properties 11

2.3.5 Lanthanide Contraction 12

2.4 Applications of Rare Earth Elements 14

2.5 Global Demand/Supply 21

2.6 Abundance 27

2.7 Resources 30

2.8 Prices 32

2.9 REE Resources in Alaska 35

2.10 REE in Coal 38

2.10.1 Abundance 38

2.10.2 Mineralization and Size 40

2.10.3 Separation 42

2.10.3.1 Physical Beneficiation of REEs 43

2.10.3.2 Chemical Beneficiation of REEs 50

CHAPTER 3 METHODS AND MATERIALS 53

3.1 Characterizing REEs in Alaskan Coal 53

3.1.1 Samples and Their Origin 53

3.1.1.1 Coal Samples 53

3.1.1.2 Ash samples from UAF Power Plant 55

3.1.2 Size Analysis 56

3.1.3 Float and Sink Tests 58

3.1.4 Magnetic Separation 59

3.1.4.1 Dry High Intensity Magnetic Separation (Carpco) 59

3.1.4.2 Wet High Intensity Magnetic Separation (Carpco) 60

3.1.5 Scanning Microscope Analysis 61

3.1.6 Preliminary Froth Flotation Studies 62

3.2 Statistically Designed Experimental Program for Froth Flotation 64

3.2.1 Sample Preparation and Grinding Tests 64

3.2.2 Box-Behnken Design 66

3.3 Leaching and Extraction 68

CHAPTER 4 RESULTS AND DISCUSSION 73

4.1 Characterizing REEs in Alaskan Coal 73

4.1.1 Size Analysis 73

4.1.2 Float and Sink Tests 78

4.1.3 Magnetic Separation 82

4.1.4 Scanning Electron Microscope Analysis 83

4.1.5 Preliminary Froth Flotation Studies 89

4.1.6 REE Content in Ash Samples from UAF Power Plant 91

4.2 Statistically Designed Experimental Program for Froth Flotation 92

4.2.1 Sample Preparation and Grinding Tests 92

4.2.2 Box-Behnken Design 93

CHAPTER 5 FLOWHEET AND ECONOMIC ANALYSIS 107

5.1 Flowsheet 107

5.2 Economic Analysis 111

CHAPTER 6 CONCLUSIONS AND RECOMMENDATIONS 117

6.1 Conclusions 117

6.2 Recommendations 121

REFERENCES 123

APPENDICES 133

List of Figures **Page**

Figure 1. Energy-Critical Minerals in the Medium Term (2015-2025) (Department of Energy, 2011). 3

Figure 2. Lanthanide Contraction (Krishnamurthy & Gupta, 2004). 13

Figure 3. Rare earth application by demand in the US and world in 2015 (Humphries, 2012). 15

Figure 4. Worldwide production of rare-earth oxides from 1987 to 2010 (U.S. Geological Survey, 2012). 23

Figure 5. Abundance (atom fraction) of the chemical elements in earth's upper continental crust as a function of atomic number (Haxel et al., 2002) 28

Figure 6. Location map of Alaska rare-earth-element occurrences and anomalies (Modified from Szumigala & Werdon, 2011). 35

Figure 7. Physical beneficiation of monazite in beach sand minerals (Krishnamurthy & Gupta, 2004) 45

Figure 8. Simplified flowsheet for the recovery of bastnasite at the Mountain Pass Molycorp plant (Aplan, 1989). 47

Figure 9. Schemes for the physical beneficiation of Bayan Obo ore (Andresen, 1986; Houot et al., 1991) 49

Figure 10. Locations of the handpicked sample from Wishbone Hill and the procured sample from Usibelli Coal Mine, Healy (Modified from Google Earth) 54

Figure 11. Single Toggle Jaw Crusher..... 57

Figure 12. Single Smooth Roll Crusher. 58

Figure 13. A washability float and sink test for coal. 59

Figure 14. Carpco wet magnetic separator..... 60

Figure 15. Sample mount on the Quanta 200 ESEM..... 62

Figure 16. Flotation cell setup at MIRL, UAF. 63

Figure 17. Sample drying oven. 64

Figure 18. Tumbling ball mill with timer..... 65

Figure 19. Flowsheet for extraction of REEs from coal ash (Joshi et al., 2015). 70

Figure 20. REE extraction using microbial biosorption and desorption as a function of pH (Bonificio & Clarke, 2016). 71

Figure 21. Percentage distribution of individual REEs in the coal samples.. 75

Figure 22. Distribution of HREE and LREE in Healy and Wishbone Hill coal samples 76

Figure 23. REE distribution on the basis of size for Healy..... 77

Figure 24. REE distribution on the basis of size for Wishbone Hill..... 77

Figure 25 REE distribution on the basis of specific gravity for Healy..... 79

Figure 26. REE distribution on the basis of specific gravity for Wishbone Hill.. 79

Figure 27. Washability Curves for composite Healy coal sample..... 80

Figure 28. Washability Curves for composite Wishbone Hill coal sample. 81

Figure 29. Distribution of magnetic and non-magnetic material in the coal samples of Healy and Wishbone Hill..... 82

Figure 30. Distribution of LREE and HREE in magnetics and non-magnetics of Wishbone Hill Coal. 83

Figure 31. SEM images of Cinders with Quanta 200 ESEM with (a) lower and (b) higher magnification..... 85

Figure 32. SEM images of Fly Ash with Quanta 200 ESEM with (a) lower and (b) higher magnification..... 86

Figure 33. SEM images of Bottom Ash with Quanta 200 ESEM with (a) lower and (b) higher magnification..... 87

Figure 34. SEM images of (a) Healy and (b) Wishbone Hill Coal samples with Quanta 200 ESEM. 88

Figure 35. Total HREE and LREE distribution in the flotation products of Healy. 90

Figure 36. Total HREE and LREE distribution in the flotation products of Wishbone Hill..... 90

Figure 37. Distribution of individual REEs in coal combustion products..... 91

Figure 38. REE distributions of UAF power plant products. 92

Figure 39. Optimum grinding time for the coal and ash samples..... 93

Figure 40. Response surface for maximizing REE enrichment for Healy as a function of pulp density (% Solids) and frother dosage (ppm). 99

Figure 41. Response surface for REE recovery for Healy as a function of pulp density (% Solids) and frother dosage (ppm). 99

Figure 42. Response surface for REE concentration for Healy as a function of pulp density (% Solids) and frother dosage (ppm). 100

Figure 43. Response surface for Maximizing REE enrichment for Wishbone Hill as a function of pulp density (% Solids) and frother dosage (ppm). 102

Figure 44. Response surface for REE recovery for Wishbone Hill as a function of pulp density (% Solids) and frother dosage (ppm). 103

Figure 45. Response surface for REE concentration for Wishbone Hill as a function of pulp density (% Solids) and frother dosage (ppm). 103

Figure 46. Schematic Flowsheet for commercial extraction of REEs from Alaskan coals. 108

Figure 47. Comparison of REE concentrations in Alaskan coals to world coals..... 119

List of Tables **Page**

Table 1. Rare earth elements, their chemical symbols, atomic numbers, electronic ground state configurations, and common oxidation states. (* indicates radioactive) 12

Table 2. Application of Rare Earth Elements (Department of Energy, 2011; Krishnamurthy & Gupta, 2004; Swift et al., 2014). 17

Table 3. Distribution of rare earth elements in major applications (Bleiwas & Gambogi, 2013). 19

Table 4. World mine production and reserves (REE Oxides) (Ober, 2016). (NA-Not Available, *-Included with other countries) 25

Table 5. Rare earth element's abundance (mg/kg) in the earth's crust (Krishnamurthy & Gupta, 2004). 29

Table 6. Minerals that contain REEs and occur in economic or potentially economic deposits (Castor & Hedrick, 2006). (Ln=Lanthanide Element). 31

Table 7. Rare earth metal and oxide prices (USD kg-1) from December 2013 to July 2016 (HEFA, 2014; MineralPrices, 2016). 33

Table 8. Comparison of REE concentrations of coals across the globe (Modified from W. Zhang et al., 2015). 40

Table 9. Physical properties of common REE bearing minerals (W. Zhang et al., 2015). 44

Table 10. Types of collectors used in Floatation of REEs. 46

Table 11. Levels of Independent variables and their levels for Box-Behnken design. 67

Table 12. Size-by-size proximate analysis of the Healy coal sample..... 73

Table 13. Size-by-size proximate analysis of the Wishbone Hill coal sample. 74

Table 14. Mineralogical composition analysis of the samples. 84

Table 15. Parameter values and the results for Healy coal flotation achieved from an experimental program conducted using three-level Box-Behnken design where three factors are: A – % solids, B – frother dosage in ppm, C – collector dosage in lbs/ton. 95

Table 16. Parameter values and the results for Wishbone Hill Coal flotation achieved from an experimental program conducted using three-level Box-Behnken design where three factors are: A – % solids, B – frother dosage in ppm, C – collector dosage in lbs/ton..... 96

Table 17. ANOVA table for REE Enrichment model for Healy..... 97

Table 18. ANOVA table for REE Enrichment model for Wishbone Hill. 101

Table 19. Set of optimum parameters from the Box-Behnken Design to maximize REE enrichment and the value of other output variables on the optimum conditions... 105

Table 20. Overall REE Recovery from the processing plant..... 110

Table 21. Economic potential of the REEs in Alaskan coal samples based on REE metal prices from July 2016. 112

Table 22. Installation and hourly operation cost of the equipment used. 113

Table 23. Supplementary costs. 114

Table 24. Technical, financial, and operational project parameters. 115

List of Appendices **Page**

Appendix A. Float-Sink data of the Healy coal sample. 135

Appendix B. Float-Sink data of the Wishbone Hill coal sample. 136

Appendix C. REE analysis of the Healy coal sample with size and density fractions (data reported on "Whole Coal" basis). 137

Appendix D. REE analysis of the Wishbone Hill coal sample with size and density fractions (data reported on "Whole Coal" basis). 138

Appendix E. REE analysis of the Healy and the Wishbone Hill composite coal samples with size and density fractions (data reported on "Whole Coal" basis). 139

Appendix F. Wet High Intensity Magnetic Separation (WHIMS) of the Healy and the Wishbone Hill coal samples (<100 Mesh fractions). 140

Appendix G. REE distributions after Wet High Intensity Magnetic Separation (WHIMS) of the Healy and the Wishbone Hill samples (<100 Mesh fractions) on whole coal basis. 140

Appendix H. Flotation of Healy and the Wishbone Hill Samples (<100 Mesh fractions) on whole coal basis. 140

Appendix I. REE Distribution after flotation of Healy and the Wishbone Hill Samples (<100 Mesh fractions) on whole coal basis. 141

Appendix J. Proximate and sulfur analysis of UAF power plant products. 141

Appendix K. REE distribution of UAF power plat products on ash basis. 141

Appendix L. Proximate Analysis of the 17 Box-Behnken Flotation products for Wishbone Hill. 142

Appendix M. Proximate Analysis 17 Box-Behnken Flotation products for Healy. 143

Appendix N. REE distribution in 17 Box-Behnken Flotation products for Wishbone Hill. 144

Appendix O. REE distribution in 17 Box-Behnken Flotation products for Healy. 145

Appendix P. Cost analysis of the project over a period of 7 years. 146

Acknowledgements

I want to express my gratitude to my advisors Dr. Tathagata Ghosh and Dr. Guven Akdogan for their valuable support, guidance, and motivation over the span of my studies. Their attitude towards research and life has inspired me and contributed to the success of this investigation. I also wish to thank my committee members Dr. Sukumar Bandopadhyay and Dr. Debasmita Misra for their valuable time and vital assistance in completing the thesis work. The doors to their homes and offices were always open whenever I ran into a troubled spot in my life or in my research.

The financial support provided by the University of Alaska Fairbanks: Department of Mining and Geological Engineering and from U.S. Department of Energy/National Energy Technology Laboratory is gratefully acknowledged. I likewise want to recognize J. Ekmann from LTI and Howard Shafer from ALS, as their guidance and expertise played a crucial role in this project.

I remain grateful to my parents, Mr. Vipin Gupta and Mrs. Seema Gupta and my siblings Shristy, Purva, and Prakhar for their endless love and encouragement throughout my study at the University of Alaska Fairbanks. I would definitely like to thank Abhinav Gupta, who has always been supportive and caring like an older brother through thick and thin. Shanu Gupta, Vaibhav Raj, Bindu Gadamsetty and Vaibhav Srivastava also deserve my appreciation for being very supportive and helpful during the critical times. Special thanks are given to Priyamvada Sharma, Saurav Bhowmick, Taraprasad Bhowmick and Aaron Kruse for their support and

friendship. I would finally like to thank all my fellow graduate students and faculty at University of Alaska Fairbanks who made my stay in Fairbanks one of the most memorable and enjoyable experiences in my lifetime.

CHAPTER 1 INTRODUCTION

1.1 Introduction

In the 18th Century, the Industrial Revolution was facilitated by the invention of the steam engine and the substantial use of iron and steel in the manufacturing industry. Analogously, the Information Revolution that followed the Industrial Revolution was a result of pioneering innovations in science and technology, which are all invariably dependent on Rare Earth Elements (REEs) (Haxel, Hedrick, Orris, Stauffer, & Hendley II, 2002). REEs are a class of 17 naturally occurring elements, including scandium (Sc) and yttrium (Y) along with 15 of the lanthanide elements namely: lanthanum (La), cerium (Ce), praseodymium (Pr), neodymium (Nd), promethium (Pm), samarium (Sm), europium (Eu), gadolinium (Gd), terbium (Tb), dysprosium (Dy), holmium (Ho), erbium (Er), thulium (Tm), ytterbium (Yb), lutetium (Lu). REEs are vital in countless hi-tech modern day technologies owing to a diverse set of electrical, chemical, nuclear, optical, metallurgical and catalytic properties (Krishnamurthy & Gupta, 2004). Thus, they are critical in the fabrication of a wide variety of sophisticated technological products that constitute a significant part of the industrial and manufacturing economy of the major developed nations across the globe (Haxel et al., 2002). The United States was once self-sustainable in the production of REEs; however, it in 2015 was dependent on imports from China (71%), Estonia (7%), France (6%), Japan (6%) and others (10%) for all of its domestic consumption (Ober, 2016). Over the last 25 years, China mined, processed, and refined these elements at prices that nations across the globe were happy to pay and

thus has emerged as a monopolistic giant in the market. In 2010, China disrupted the world's REE supply by cutting down the export quotas, thus raising concerns for countries, like the United States, of losing their leadership in manufacturing high-value products. The Chinese export-to-production ratio of REEs steadily decreased from 64% in 2000 to 19% in 2010, thus creating an unstable supply-demand scenario (W. Zhang et al., 2015).

With China having 42% of the world's known REE reserves and producing 85% of all REEs of the world, the realization of quotas and export restrictions on these critical elements presented a huge risk of supply in the international market (Kingsnorth, 2011; Ober, 2016; Polinares, 2012). In 2010, the European Commission in 2010 included REEs as critical raw materials on the list of the 14 most critical materials for the European Union owing to dependence on imports and unavailability of suitable substitutes. The United States Department of Energy in the 2011 Critical Materials Strategy Report identified 16 elements that are essential for the development of clean energy technologies, of which eight are REEs. The report delineated five REEs that are of most critical importance in the next decade in terms of growing global demand and shortage of supply, namely dysprosium (Dy), terbium (Tb), europium (Eu), neodymium (Nd) and yttrium (Y) (Figure 1) (Department of Energy, 2011).

The analysts have placed the lower and upper bounds of annual growth for total REE demand, considering the continued dependence of technology on REEs, at 5% and 9%, respectively, over the next 25 years (Alonso et al., 2012). The REE demand is expected

to grow up to 250,000-300,000 tons of Rare Earth Oxides (REO) by the year 2020, with China producing 150,000 tons of these crucial elements (Kingsnorth, 2011; Ober, 2016).

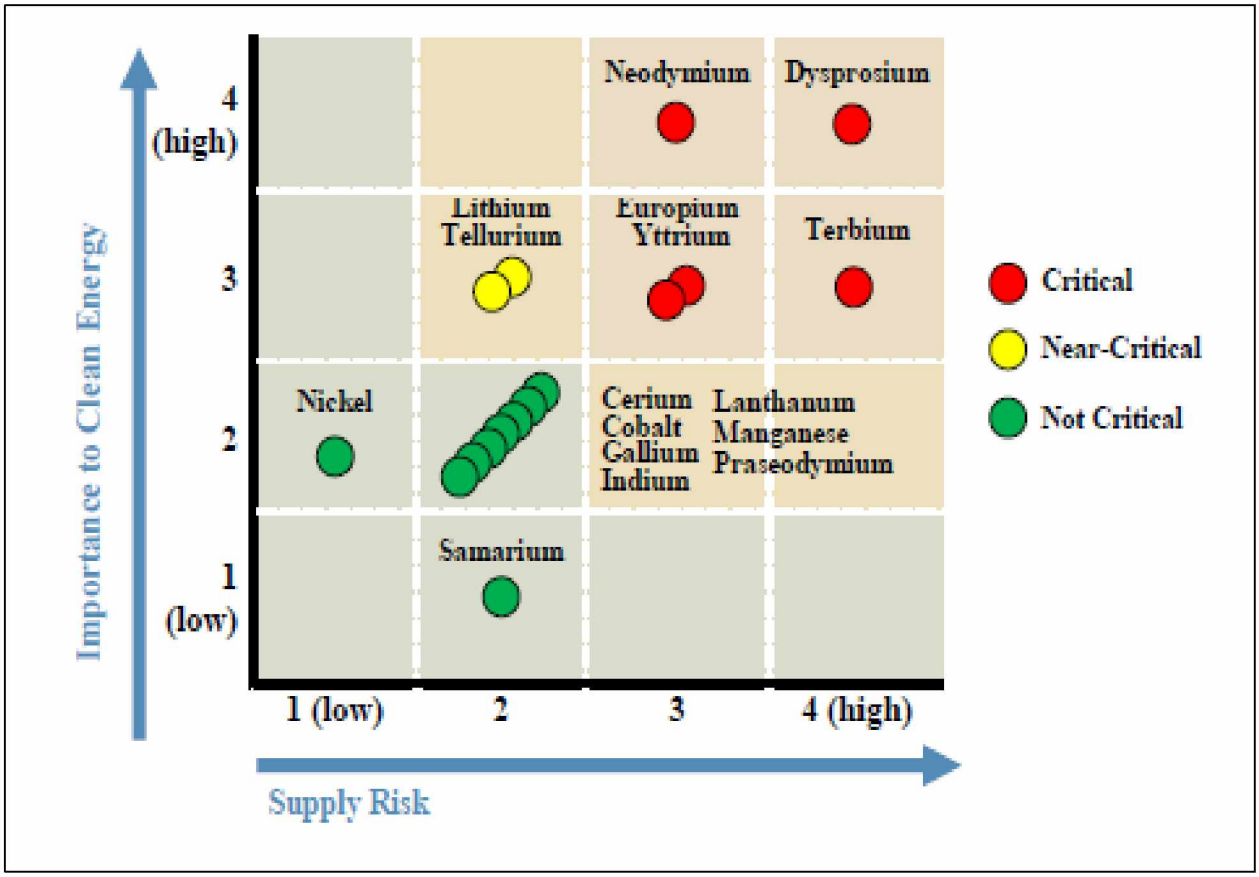

Figure 1. Energy-Critical Minerals in the Medium Term (2015-2025) (Department of Energy, 2011).

The ever increasing demand of REEs for next generation applications and monopolistic supply has raised global concerns surrounding stable access to REE mineral supplies. The manifold rise of the prices of these elements over the last few years has forced many countries to re-evaluate the possibility of production from indigenous REE resources and has attracted considerable attention for REE recovery from waste materials, particularly for the critical elements. Opportunities are being

extensively explored for extraction of REEs from various non-conventional mineral sources to meet the domestic requirement in a cost-effective and eco-friendly manner. There is also a desire to increase production from previously productive sites to stabilize the supply chain and to expand the production from new alternate sources including coal and coal byproducts (Bleiwas & Gambogi, 2013).

1.2 Objective of the Work

Coals from certain parts of the world (Russia, China, U.S., etc.) can be rich in REEs and can approach a total concentration of 1000 ppm (Seredin & Dai, 2012). The U.S. Department of Energy (DOE) wanted to investigate and quantify the presence of REEs in Alaskan coals. The DOE was also interested in investigations into combustion products (fly ash, bottom ash, and cinders) from Alaskan power plants to assess the enrichment of REE into the coal combustion products, and perhaps, preferential REE groupings in these streams. Systematic investigations of REE in Alaskan coal and coal ash have not been performed to date. Therefore, this investigation aimed to address these questions.

The main objectives of the research included:

(A) Collection of two Alaskan coal samples: one from Healy coal mine, Seam No. 4 and another from an oblique-slip fault outcrop at Wishbone Hill; and the collection of fly ash, bottom ash and cinder samples from the University of Alaska Fairbanks power plant, depending on the availability of quality samples and access.

(B) Conducting laboratory classification, float-sink, magnetic and flotation tests to ascertain the distributions of REE in terms of size and specific gravity.

(C) Analyses of the composite samples and products of classification, float-sink, magnetic and flotation tests for proximate, sulfur, and REE+Y+Sc content with ICP-MS (Inductively Coupled Plasma-Mass Spectrometry)/ICP-OES (Inductively Coupled Plasma-Optical Emission Spectrometry).

(D) Develop a commercially viable flowsheet for REE enrichment.

1.3 Thesis Outline

This first chapter provides the backdrop needed to appreciate the research performed for the thesis. It introduces the economic importance of REEs and the downside effects of supply and demand deficit on the major world economies. Chapter 2 provides the background necessary to understand these vital elements, explaining their physical and chemical properties, classification, resources and applications along with a brief discussion on prevalent REE processing techniques and the previous research done on the extraction of REEs from coal. A detailed description of sample origin and collection, laboratory experiments, and experiment procedures is presented in Chapter 3. Chapter 4 systematically outlines the results of the study and discusses them in a fundamental context. Chapter 5 proposes a viable flowsheet to extract REEs from coal along with a detailed economic evaluation of the extraction processes. A summary of the research and the conclusions are highlighted in Chapter 6 along with the recommendations for future work.

CHAPTER 2 BACKGROUND

2.1 What are REEs

REEs are the largest chemically coherent group of elements in the periodic table, which consists of the 15 lanthanide elements, lanthanum (La) to lutetium (Lu). Yttrium (Y) is grouped with the REEs because of its chemically equivalent characteristics to the lanthanide elements and its general availability in rare earth bearing minerals. Scandium (Sc) is also associated with most REE deposits in minor amounts and is also classified as a REE. These metals have similar properties, which results in them being clustered together in mineral deposits. The REEs possess metallic properties and so are also called "rare earth metals" (Binnemans et al., 2013; Haxel et al., 2002; Peramaki, 2014; Ren, Song, Lopez & Lu, 2000; Szumigala & Werdon, 2011).

These valuable elements are commonly referred to as 'rare' because they are highly dispersed in the earth's crust, and difficult to find in concentrations viable for commercial extraction. Bastnasite, monazite, xenotime, and ion-adsorption clays are the primary ores of REEs. Bastnasite deposits in China and the United States compose the largest percentage of the world's rare earth economic resources, followed by the mineral monazite. Xenotime and ion-adsorption clays are important sources of yttrium and other heavy group rare earths but account for a much smaller part of the total production (U.S. Geological Survey, 2010; Ober, 2016; Gambogi, 2013; U.S. Geological Survey, 2015; Virta, 2011).

2.2 Classification of REEs

The most common classification of REEs is based on the atomic number of the element. The REEs are subdivided into "light rare earth elements" (LREEs) and "heavy rare earth elements" (HREEs). Lanthanum, cerium, praseodymium, neodymium, promethium, samarium, europium and gadolinium, with atomic numbers 57 through 64, are generally referred to as the LREEs or the cerium subgroup. Yttrium however, with an atomic number of 39, is lighter than the LREEs; it is included in the heavy group because of its chemical and physical associations with heavy rare earths in natural deposits. Therefore, yttrium, terbium, dysprosium, holmium, erbium, thulium, ytterbium, and lutetium, with atomic numbers 39 and 65 through 71, are generally considered the HREEs or the yttrium subgroup (Dai et al., 2008; Jackson & Christiansen, 1993; Moldoveanu & Papangelakis, 2013). Scandium is also included in the LREEs or the cerium group owing to its small size and low atomic number (Castor & Hedrick, 2006; Gschneidner Jr, 1964).

In a different classification, researchers attribute the first six rare earths lanthanum to samarium as LREEs and the remaining ten rare earths from europium to lutetium, together with yttrium to the HREEs (McGill, 2012; Szumigala & Werdon, 2011). Another classification assigns the rare earths into three subgroups: lanthanum to neodymium are called "light rare earths"; samarium to dysprosium are known as "medium rare earths"; holmium to lutetium, including yttrium, are called "heavy rare earths" (Bunzli, 2000). The densities of the pure LREEs range from 2.9 g/cm^3 (scandium) to 7.9 g/cm^3 (gadolinium) and those of the HREEs are from 8.2 g/cm^3 to

9.8 g/cm^3, with the exception of yttrium (4.47 g/cm^3) and ytterbium (6.9-7 g/cm^3). The distinction between the light and heavy groups is based more on atomic volume and geological behavior than on the densities of the individual elements.

Kremers (1961) in his classification of REEs, named the light rare earths, from lanthanum to samarium, as the "cerium group"; the middle rare earths, europium to dysprosium, as the "terbium group"; and the heavies, holmium to lutetium and yttrium, as the "yttrium group".

Yet another classification of REEs is based on the supply and demand relationship of individual element and divides REEs into critical (Nd, Eu, Tb, Dy, Y, and Er), noncritical (La, Pr, Sm, and Gd), and excessive (Ce, Ho, Tm, Yb, and Lu) categories (Seredin & Dai, 2012).

The multitude of classification of REEs can lead to serious confusion, so for this thesis, light rare earth elements (LREEs), or the cerium group, are elements from lanthanum to gadolinium, and scandium and heavy rare earth elements (HREEs), or the yttrium group, are the elements from terbium to lutetium, and yttrium.

2.3 Properties

2.3.1 Reactivity

Except for europium, which readily oxidizes under all conditions, other rare earth metals react relatively slowly at room temperature with oxygen or dry air and rapidly in moist air. At higher temperatures, all rare earth metals ignite in air and react with the majority of nonmetallic elements (McGill, 2012).

Generally, light rare earth metals react slowly with water at room temperature and vigorously at a higher temperature; however, the heavy rare earths react very slowly. Europium, the most reactive rare earth, forms hydroxides even with cold water (Krishnamurthy & Gupta, 2004).

REEs are reactive with acids. All rare earth metals readily dissolve in dilute mineral acids with the formation of RE^{3+} ions and hydrogen (Gschneidner & Daane, 1988; McGill, 2012). Rare earth metals react at slower rates with common organic acids than mineral acids of the same concentration. Rare earth metals react, but slowly, with strong bases, like sodium hydroxide, and no reaction is observed with a weak base, like ammonium hydroxide (Gschneidner & Daane, 1988; Krishnamurthy & Gupta, 2004; McGill, 2012).

2.3.2 Boiling and Melting Points

Melting points for the REEs range from 798°C for cerium(Ce) to 1,663°C for lutetium (Lu) and the boiling points range from 1194°C (Yb) to 3512°C (Pr) (Cordier & Hedrick,

2011; McGill, 2012). REEs have an iron gray to a silvery luster and are typically soft, malleable, and ductile (Krishnamurthy & Gupta, 2004).

2.3.3 Ionization Potential

REEs have low ionization potentials and are therefore highly electropositive and occur primarily as ionic compounds. This is the consequence of their valence shells consisting of deeply buried 4f orbitals, where the 4f electrons are not available for covalent bonding (Krishnamurthy & Gupta, 2004).

2.3.4 Magnetic Properties

The magnetic behavior of the REEs is determined by the number of unpaired electrons in the outermost shell (4f orbital). The magnetic effects of electrons cancel each other out in the completed 4f subshell, which does not happen for the incomplete 4f subshell. All REEs, except scandium, yttrium, lanthanum, ytterbium, and lutetium, are strongly paramagnetic. On cooling many REEs become antiferromagnetic, and on cooling further, a number of these elements develop ferromagnetic properties. Upon application of a magnetic field of sufficient strength, all paramagnetic rare earths become ferromagnetic at low temperatures. The rare earth metals are strongly anisotropic and their magnetic behavior are determined by the crystal axis (Krishnamurthy & Gupta, 2004).

2.3.5 Lanthanide Contraction

The root cause for the similarity of chemical properties between REEs and their compounds is lanthanide contraction, which is based on the atomic configuration (Table 1). Lanthanide contraction is the significant and steady decrease in the size of atoms and ions with the increase in atomic number from lanthanum to lutetium. Thus, as shown in Figure 2, lanthanum has the greatest radius and lutetium has the smallest. The general consensus for the cause of this contraction is stated to be the imperfect shielding of one electron by another in the same subshell.

Table 1. Rare earth elements, their chemical symbols, atomic numbers, electronic ground state configurations, and common oxidation states. (* indicates radioactive)

Element	Symbol	Atomic number	Configuration	Oxidation states
Scandium	Sc	21	[Ar]4s23d1	3
Yttrium	Y	39	[Kr]5s24d1	3
Lanthanum	La	57	[Xe]6s25d1	3
Cerium	Ce	58	[Xe]4f16s25d1	3, 4
Praseodymium	Pr	59	[Xe]4f36s2	3, 4
Neodymium	Nd	60	[Xe]4f46s2	3
Promethium*	Pm	61	[Xe]4f56s2	3
Samarium	Sm	62	[Xe]4f66s2	3, 2
Europium	Eu	63	[Xe]4f76s2	3, 2
Gadolinium	Gd	64	[Xe]4f76s25d1	3
Terbium	Tb	65	[Xe]4f96s2	3, 4
Dysprosium	Dy	66	[Xe]4f106s2	3
Holmium	Ho	67	[Xe]4f116s2	3
Erbium	Er	68	[Xe]4f126s2	3
Thulium	Tm	69	[Xe]4f136s2	3, 2
Ytterbium	Yb	70	[Xe]4f146s2	3, 2
Lutetium	Lu	71	[Xe]4f146s25d1	3

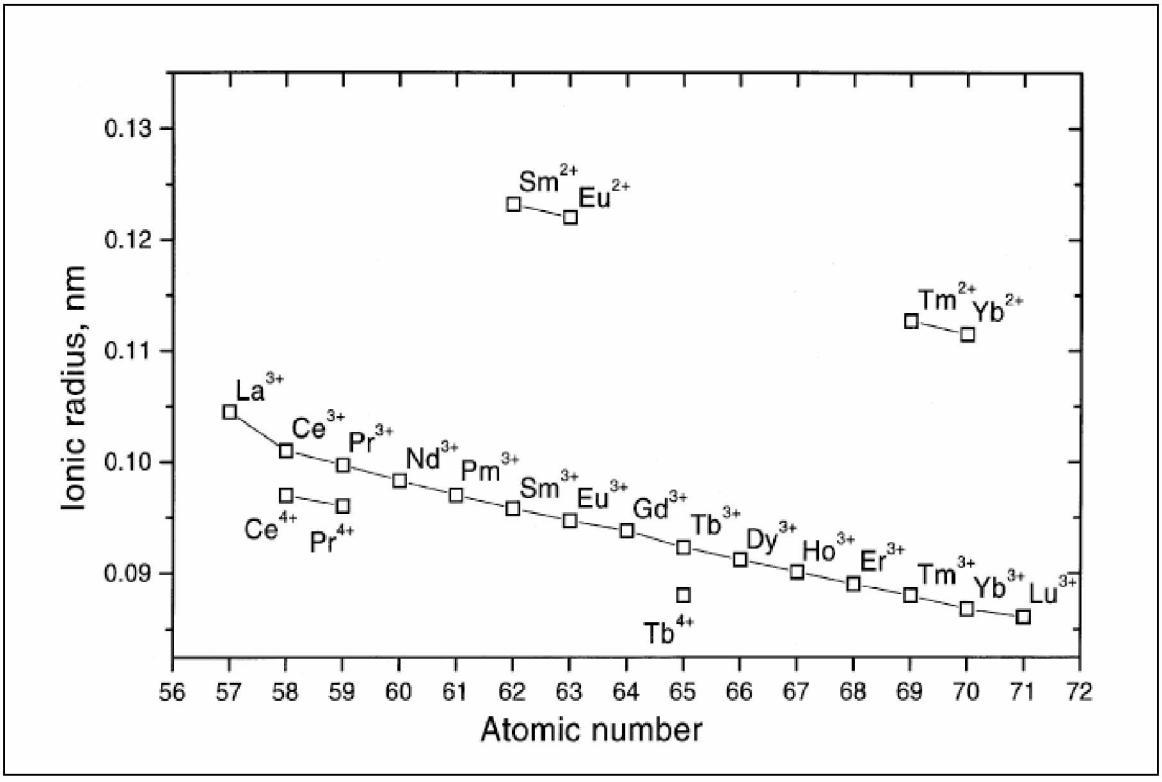

Figure 2. Lanthanide Contraction (Krishnamurthy & Gupta, 2004).

As one moves from lanthanum to lutetium, both the nuclear charge and the number of 4f electrons increase by one for each element. As a result of the shape of the orbitals, the mutual shielding of 4f-electrons is very imperfect, and with the increase of the atomic number the effective nuclear charge experienced by the 4f electron increases. The magnitude of such contractions add up and results in the steady decrease in size across the lanthanoid series. The association of yttrium with the heavier lanthanides is explained by the similarity in the outer electronic configuration and the similarity in ionic size. Yttrium compounds have atomic and ionic radii in the holmium to erbium range, and thus associate with those of the heavier lanthanide elements and exhibit similar solubility, crystal structure, and overall chemical properties. The atomic and trivalent ionic radii of scandium, however, is far too small and lanthanide

contraction is insufficient for decreasing the atomic and ionic size of the REEs to that of scandium. Thus, its chemistry is significantly different from that of the other REEs (Krishnamurthy & Gupta, 2004; McGill, 2012).

2.4 Applications of Rare Earth Elements

Modern society has immense reliance on common consumer products like hybrid vehicles, rechargeable batteries, wind turbines, renewable energy, mobile phones, flat screen televisions, compact fluorescent light bulbs, laptop computers, disk storage and catalytic converters; however, it is not widely noted that these products, amongst many others, are dependent on the distinctive properties of REEs. Although more expensive, REEs possess fewer environmental problems upon disposal or recycling as compared to their heavy metal counterparts (Haxel et al., 2002).

The distribution of REE end use in the United States in 2015 had catalysts (43%) as the most common area of application. They also have an important application in industrial utilization as in metallurgy and for alloys, which accounts for 8% of the total end-use. REEs are also used in permanent magnets (13%) and glass polishing (21%) and various other areas of industry. Catalysts have gained more end use in the U.S. in recent years; in 2015, it should be noted that the data for end use was rather different for rest of the world (Figure 3).

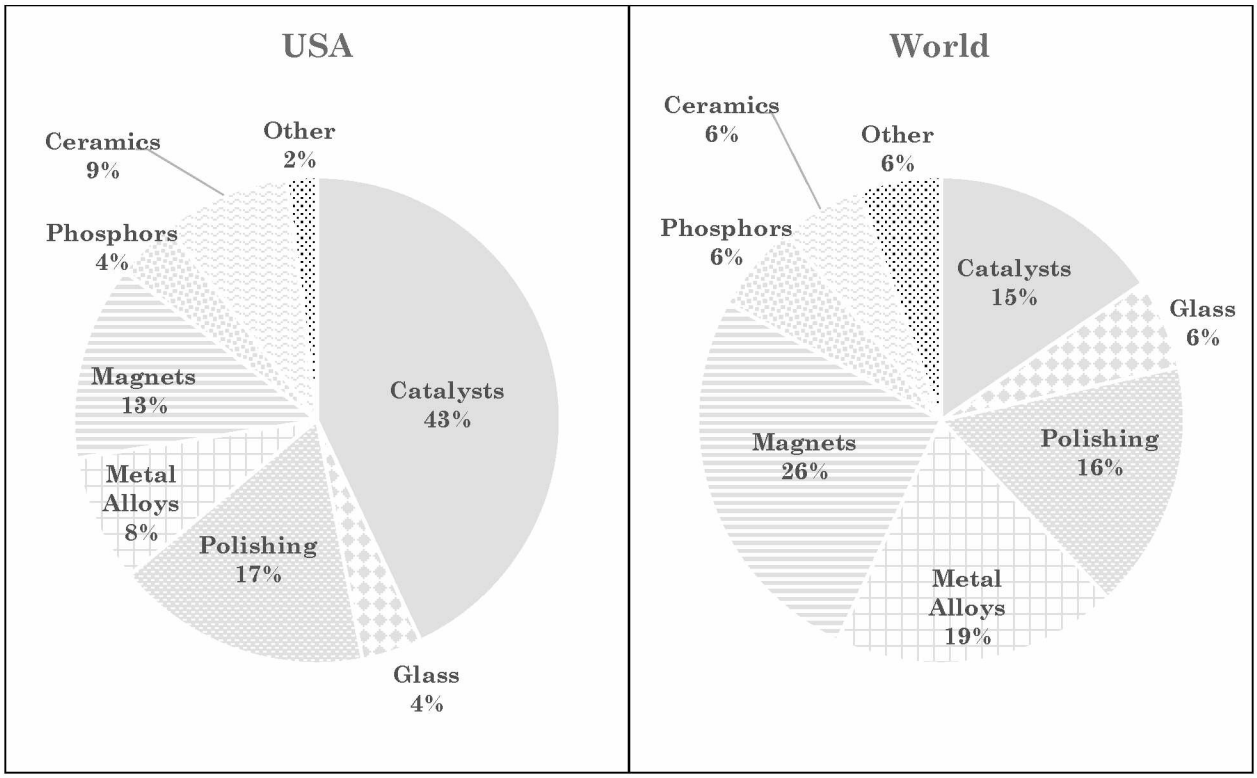

Figure 3. Rare earth application by demand in the US and world in 2015 (Humphries, 2012).

The REE's have special electronic, catalytic, magnetic and optical properties, which gives them a vast and expanding market and technology value. Rare earth elements and alloys are used in a multitude of applications ranging from mundane consumer goods (such as lighter flints, glass polishing, fluorescent lighting) to high-tech products (like computer storage, phosphors, lasers, magnets, magnetic refrigeration, rechargeable batteries, cell phones, vehicle catalytic converters, magnets) to futuristic technologies (namely high temperature superconductivity, safe storage, green energy and transport of hydrogen for a post-hydrocarbon economy) (U.S. Geological Survey, 2002; Haxel et al., 2002; Szumigala & Werdon, 2011). For example, the potential of cerium-doped glass to block ultraviolet light is exploited in

the manufacturing of medical glassware and aero-space windows. Praseodymium, because of its optimum reflectance of 560 nm, is used in amplification of telecommunication systems, including as a doping agent in fluoride fibers. The absorption band of Neodymium is very close to the human vision sensitivity, thus making it useful in welding goggles. Samarium is employed in laser applications and is valued for its ability to operate at high temperatures. Gadolinium, when mixed with EDTA (Ethylenediaminetetraacetic acid) dopants, is used as an injectable contrast agent for magnetic resonance imaging (MRI). Yttrium is used in many applications because it has the highest thermodynamic affinity for oxygen than any element. Yttria-stabilized zirconium oxide is used in thermal plasma sprays to protect aerospace component surfaces at high temperatures. Terbium has high efficiency for response to x-ray excitation and is, therefore, deployed in x-ray phosphors. Dysprosium, owing to its high magnetic moment, is an essential additive in Neodymium magnet production. Holmium has the highest magnetic moment (10.6μB) amongst all naturally occurring elements and is used to create the highest known magnetic fields. The electrical resistance of Ytterbium increases under very high stresses. This property is used in manufacturing strain gauges for monitoring ground deformations from earthquakes and nuclear explosions. Unlike most rare earths, lutetium lacks a magnetic moment and has the smallest metallic radius of any other REE. It is an ideal host for x-ray phosphors because it produces the densest known stable white material, lutetium tantalate (density of 9.81 g/cm^3) (Krishnamurthy & Gupta, 2004). The major applications of REEs are summarized in

Table 2. Dysprosium, europium, neodymium, terbium, and yttrium are among the most important HREEs used in advanced technologies (Krishnamurthy & Gupta, 2004). The classification of selected REEs in common applications is presented in Table 3.

Table 2. Application of Rare Earth Elements (Department of Energy, 2011; Krishnamurthy & Gupta, 2004; Swift et al., 2014).

Rare Earth	Supply/ Demand	Applications
Scandium	-	Ceramics, lasers, and phosphors and in certain high-performance alloys.
Lanthanum	Critical	Components in FCC catalysts for petroleum refining, hydrogen storage batteries, telescope lenses, hybrid engines, and in night vision goggles.
Cerium	Near Critical	Glass and glass polishing, phosphors, ceramics, catalysts, metallurgy, in reducing automotive emissions and polishing computer chips.
Praseodymium	Not-Critical	Magnets for wind turbines, optical fibers and strengthening agent for other alloys.
Neodymium	Critical	Lasers, glass tinting, dielectrics and permanent magnets. These permanent magnets have wide application in starter motors, brake systems, seat adjusters and car stereo speakers, voice coil motors, computer disk drives, hand tools, and headphones.
Promethium	-	Pacemakers, watches, and compact fluorescent bulbs.
Samarium	Not-Critical	Nuclear reactors, lasers, electronic watches, aerospace equipment, microwave technology and in radiation treatments in cancer.
Europium	Critical	Energy efficient fluorescent lighting, commercial red phosphors for color television, computer screens, and fluorescent lamps. Its luminescence is also valuable in medical, surgical and biochemical applications.

Table 2 continued.

Gadolinium	-	Gadolinium is especially useful in healthcare, as it can target tumors, enrich MRIs and even aid in diagnosing cancer. It also acts as a host for x-ray cassettes and in scintillated materials for computer tomography.
Yttrium	Critical	Cancer treatment drugs, surgical arthritis medication, superconductors, light bulbs, camera lenses, ceramics, fluorescent lighting phosphors, computer displays, metallic alloys and automotive fuel consumption sensors.
Terbium	Critical	X-ray screens, color televisions and fluorescent lighting, and in defense technologies.
Dysprosium	Critical	Nuclear reactors, energy-efficient vehicles, and hard computer disks.
Holmium	-	Adds color to glass, and it is used in microwave equipment as well as nuclear control rods.
Erbium	-	Glass coloring, fiber optics, lasers for medical and dental use, eyewear and decorative glassware. Erbium amplifies wavelengths, making it an important for amplifiers of fiber optic communications systems.
Thulium	-	Crystals and in X-rays and lasers in medical and dental applications.
Ytterbium	-	Fiber amplifier and fiber optic technologies and in various lasing applications. It is also used in cancer treatments, strengthening stainless steel and monitoring earthquakes
Lutetium	-	Dopant in matching lattice parameters of certain substrate garnet crystals, due to its lack of a magnetic moment. It is important in petroleum refining and can be used to identify the age of items such as meteorites.

Table 3. Distribution of rare earth elements in major applications (Bleiwas & Gambogi, 2013).

Application	Sc	La	Ce	Pr	Nd	Pm	Sm	Eu	Gd	Y	Tb	Dy	Ho	Er	Tm	Yb	Lu
Alloys & metallurgical uses	■	■	■	■	■		■	■	■	■	■	■	■	■	■	■	■
Batteries		■	■	■	■	■					■						
Catalysts		■	■	■	■		■		■	■							■
Ceramics	■	■	■	■	■		■	■	■	■		■	■	■	■		■
Electronics		■	■	■	■					■	■	■		■			
Fertilizers		■	■		■												
Glass	■																■
Lamps	■	■	■	■	■		■	■		■	■	■	■	■	■		
Lasers	■	■	■	■	■	■	■	■	■	■	■	■	■	■	■	■	■
Magnets			■	■	■		■	■	■		■	■	■				
Medical & pharmaceutical uses		■	■		■		■	■	■				■	■			■
Neutron absorption			■				■	■	■	■		■	■	■			
Phosphors	■	■	■			■	■	■	■	■	■	■	■	■	■	■	■

The largest application of REEs is in the manufacture of rare earth containing zeolite cracking catalysts, which are required for petroleum refining and automotive pollution-control catalytic converters (Wallace, 1981). In petroleum refining, catalysts are used to break down heavier oil fractions into simpler, small chain hydrocarbons and increase the yield of gasoline by cracking. Zeolite cracking catalysts provide considerable enhancement to the process performance and have largely replaced the amorphous silica–alumina catalysts used previously for cracking. REEs are also used as catalysts in a number of other reactions. REEs' high affinity to oxygen and sulfur are utilized in metallurgy, where mischmetal (a mixture of

mainly Ce, La, and Nd) is employed to trap O and S to improve the properties of steel or cast iron (Krishnamurthy & Gupta, 2004).

It is evident that the REEs are remarkably useful materials in an extensive range of cutting edge technological fields. They are simply un-substitutable in applications such as air pollution control, illuminated screens on electronic devices, and optical-quality glass. Thus, the demand for all of these products is expected to rise (U.S. Geological Survey, 2010; Cordier & Hedrick, 2011; Martin, 2010; Szumigala & Werdon, 2011). The superior properties of rare earth magnets not only permitted extensive miniaturization in a wide variety of consumer and industrial products but also resulted in performance characteristics formerly unattainable (Haxel et al., 2002; Kilbourn, 1993; Krishnamurthy & Gupta, 2004). REEs are extremely useful materials and are relatively abundant in the earth's crust, but discovered minable concentrations are less common than for most other ores. The logical effort is to produce sufficient quantities of required quality in a cost effective manner by development of better extraction techniques.

2.5 Global Demand/Supply

Although the REEs are abundant in nature, conventional REE extraction requires grinding large volumes of rock and removing REEs by acid digestion, which generates huge amounts of toxic waste. The process is harmful to the environment and is not lucrative. This has resulted in a shift of the current rare earth users to rely on imports for the vast majority of REEs and has initiated a search for a cheaper alternative. The substitution of REEs can occur in two ways. One is through the development of new technologies that consume lesser amounts of REEs and the other is through the use of other substances (Falconnet, 1988; Greinacher, 1980). REEs are substitutable for applications that depend on their metallurgical and magnetic properties, but substitution appears less likely in applications that rely on the optical, chemical and special magnetic properties of REEs. The substitutes are usually far less effective and may have a higher cost, thus ensuring that the demand for REEs will be long lasting in glass polishing, catalysts, phosphors, magnets, optical components, tinting of glass, pigments, and x-ray intensifiers.

All technologies need to be sustainable in the near future by being energy independent and reducing impact on climate. This will boost the demand and sales of electric vehicles and renewable energy systems like wind turbines and solar power panels, in turn dramatically increasing the demand for batteries made with REE compounds. The future demand of rare earths, in applications such as automotive pollution catalysts, fiber optics, permanent magnets and rechargeable NiMH batteries will continue to increase with a growing demand for electronic equipment,

automobiles, computers and dental and surgical equipment. Future growth is also expected for REEs in MRI contrast agents, positron emission tomography (PET), medical isotopes, lasers, and magnetic refrigeration alloys (Hedrick, 1999).

The largest percentage of the world's REE economic resource is found in the bastnasite deposits in China and the United States, followed by monazite deposits that constitute the second largest segment (Ober, 2016). The U.S. mine production of bastnasite and finished REE product increased to meet growing demand during the 1970's and 1980's. With the expansion of electronics and high-value applications, the demand shifted away from mischmetal and mixed compounds in the 1980's. The demand and production were hit during 1985 because of the decreased demand for REE containing petroleum cracking catalysts. The rare earths industry rebounded during the next 5 years as a result of stable demand in conventional markets and strong demand in new applications. In 1990, REEs were produced by at least 14 countries across the globe, primarily in the United States, China, Australia, India, and Malaysia. Due to a favorable exchange rate, cheap labor, and lax environmental standards, however, China in the last decade of the 20th century flooded the market with cheap REE's, driving out the competition and eventually capturing the global market. In 1999-2000, the majority of countries became net importers of finished REE goods. The indigenous producers including the Mountain Pass Mine in California, which was once the world's leading producer, could not compete with the cheap prices and thus more than 90% of REE required by the U.S. industry started coming from deposits in China (Figure 4) (Haxel et al., 2002).

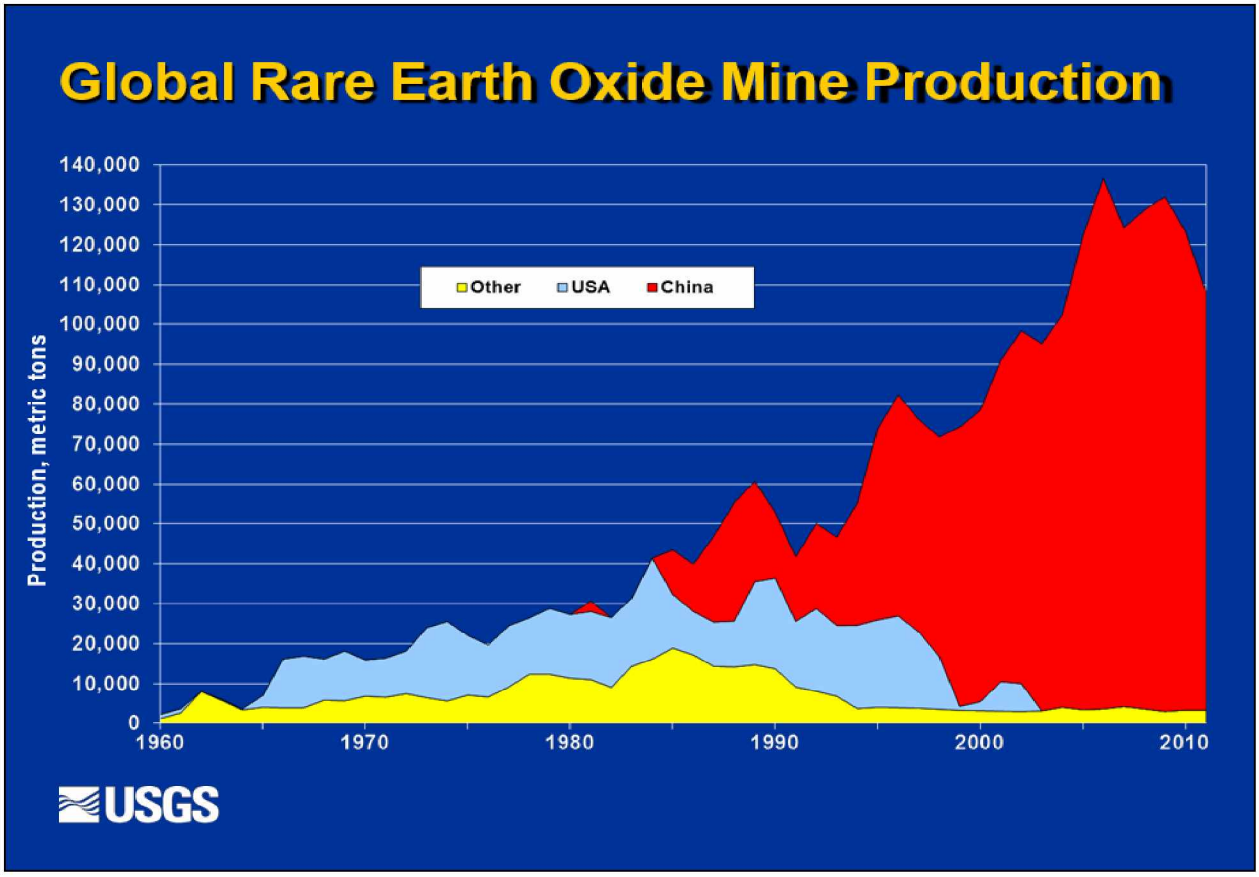

Figure 4. Worldwide production of rare-earth oxides from 1987 to 2010 (U.S. Geological Survey, 2012).

From the beginning of the industry until 1965, the mineral monazite was the major rare earth resource. Thereafter, bastnasite production took over the monazite production. The current trend to shift away from radioactive by-product bearing rare earth ores has led to a considerable decline in monazite bearing mineral sands operations everywhere in the world. Higher concentration of HREEs, abundant supply, and recovery as a low cost by-product, however, ensure a long-term demand for monazite. Until a cost effective and environmentally sound processing technique to dispose of the radioactive waste products is devised, monazite production will remain severely limited. In fact, production of other REE raw-material resources is

also constrained by environmental concerns, including bastnasite production in California and ion adsorption clays in Southern China (Krishnamurthy & Gupta, 2004).

At present, bastnasite is the world's major source of rare earths (Hedrick, 1997, 2000). The declining importance of monazite as a raw material has been due to growing supplies of bastnasite from China and also due to problems associated with the disposal of the radioactive element thorium contained in monazite. The production of Xenotime from the main producer Malaysia has also declined due to increasing reliance on cheap bastnasite from China.

While the world's REE resources are large (Table 4), the availability of individual REEs is highly polarized. The most important REE minerals are enriched with rare earths of low atomic number and depleted with rare earths of higher atomic number, hence making low atomic number REEs more available. Ober in the USGS Mineral Commodity Summaries 2016, estimated China to have the largest REO reserves of any single country, with 42 % of the world's REO reserves. The second largest reserves are in Brazil with 17 % of the estimated total, followed by Australia, India, and the United States.

Table 4. World mine production and reserves (REE Oxides) (Ober, 2016).

(NA-Not Available, *-Included with other countries)

	Mine Production		Reserves
	2014	2015	
United States	5,400	4,100	1,800,000
Australia	8,000	10,000	3,200,000
Brazil	-	-	22,000,000
China	105,000	105000	55,000,000
India	NA	NA	3,100,000
Malaysia	240	200	30,000
Russia	2,500	2,500	*
Thailand	2,100	2,000	NA
Other Countries	NA	NA	41,000,000
World Total(Rounded)	123,000	124,000	130,000,000

In the 1950s, REEs were mined in South Africa, India, and Brazil. China began its large scale REE production in 1990s with cheaper prices, which led to the shutdown of several mines that were not able to compete with lower prices. Mountain Pass mine was also closed in 2002, leaving China as the major producer of REEs. In 2015, China controlled the market with 85 % of the world's mine production (Table 4). Most of China's production comes from REE recovery as a by-product of iron ore mining in Bayan Obo (Krishnamurthy & Gupta, 2004). Australia is the second largest producer with 8 % of the mine production, followed by India, United States and Russia. Other countries produce minor amounts of REEs. In most deposits, REEs are recovered as co-product or by-products of other minerals. The mining and production costs, in most cases, cannot be compensated by the market value of the REEs due to the low concentrations in the reserves. Only in Mountain Pass California were REEs mined as primary products of a bastnasite deposit. Large

amounts of ore have to be processed to achieve small amounts of pure REEs; for example, at Mountain Pass, one metric ton of ore produced 100 gram of Eu_2O_3, and as a by-product 200 g of radioactive thorium (Bünzli, 2000).

The Chinese government has steadily limited its yearly export of REO in recent years due to resource depletion and environmental regulations. The new quota system has evoked new producers to enter the REE market, although they face a lot of challenges: limited technical knowledge outside China, production of radioactive waste, high capital cost of a new processing plant, uncertainty of market price, and uneven demand for individual REEs (Jordens, Cheng & Waters, 2013).

2.6 Abundance

Except promethium, all rare earths occur in nature. The rare earths are relatively abundant in the earth's crust, occurring in over 200 different minerals. It is estimated that the world reserves of REEs are sufficient to cater to the present consumption and can fill the demand for centuries (Jackson & Christiansen, 1993). Calling them "rare" is a misnomer, as the crustal concentration of more abundant REEs is similar to common industrial metals such as copper, zinc, chromium, nickel, molybdenum, tin, tungsten, or lead. Even the least abundant ones (Tm and Lu) are nearly 200 times more plentiful than gold (Figure 5). REEs have very little tendency to become concentrated in commercially exploitable ore deposits and thus are historically termed "rare". Thus, most of the world's supply of REE comes from only a handful of sources (Norman, Zou & Barnett, 2014; Haxel et al., 2002; Humphries, 2012).

Rare earths commonly occur as carbonates, oxides, phosphates and silicates in the ore minerals. While rare earth minerals in most deposits are recovered as co-products or by-products of certain other minerals. However, the rare earths can be recovered as the primary product in large deposits occurring only in a few countries. While the total REE content in world rare earth resources is large, the availability of individual REE is highly unequal and varies from mineral to mineral. The minerals in world rare earth deposits are predominantly enriched with rare earths of lower atomic numbers (LREEs) and highly abated with respect to rare earths of higher atomic numbers (HREEs) (especially dysprosium, europium, neodymium, terbium, and yttrium) (Table 5). The Oddo-Harkins rule also holds true for the abundance of REEs

as REEs with an even atomic number are more common than REEs with an odd atomic number (Harkins, 1917; Oddo, 1914). Additionally, rare earth ore bodies have uranium and thorium associated with them, requiring safe disposal that restricts the exploitation of individual rare earth elements present in them (Kingsnorth, 2011; Krishnamurthy & Gupta, 2004).

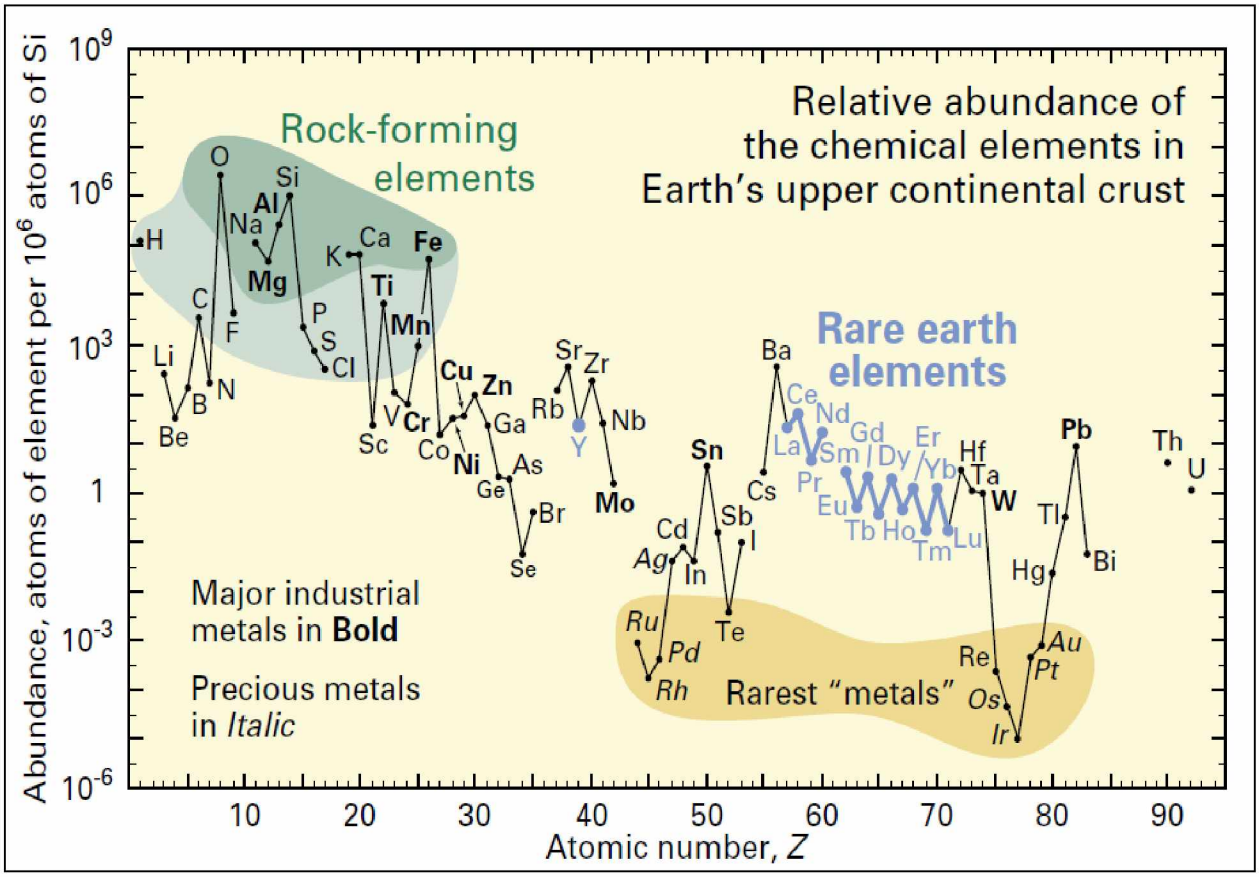

Figure 5. Abundance (atom fraction) of the chemical elements in earth's upper continental crust as a function of atomic number (Haxel et al., 2002).

Table 5. Rare earth element's abundance (mg/kg) in the earth's crust (Krishnamurthy & Gupta, 2004).

Element	Abundance (mg/kg)
Sc	5–22
La	5–39
Ce	20–70
Pr	3.5–9.2
Nd	12–41.5
Sm	4.5–8
Eu	0.14–2.0
Gd	4.5–8.0
Tb	0.7–2.5
Dy	4.5–7.5
Ho	0.7–1.7
Er	2.5–6.5
Tm	0.2–1
Yb	0.33–8
Lu	0.8–1.7
Y	28–70

2.7 Resources

Approximately 95% of all world REE reserves are contained in just three minerals: bastnasite, monazite, and xenotime (Krishnamurthy & Gupta, 2004). Bastnasite is a fluorocarbonate mineral containing approximately 70 % REO, of which the majority are lighter elements. Bastnasite resources include a large deposit in Bayan Obo in China, and at Mountain Pass, California in the U.S. Monazite is a phosphate mineral containing mainly LREEs, 4–12 % of thorium, and a variable amount of uranium (Krishnamurthy & Gupta, 2004; Szumigala & Werdon, 2011). Xenotime is an yttrium phosphate containing approximately 67% REO, of which most are heavier elements. It is usually found with monazite as a minor component, but the concentration of HREEs makes it an important resource. REEs are present as ions in ion-adsorption clays, which is another important HREE source. Several other rare earth minerals have also been used or are in use for REE recovery and have been summarized in Table 6 (Castor & Hedrick, 2006; Krishnamurthy & Gupta, 2004; Szumigala & Werdon, 2011).

Table 6. Minerals that contain REEs and occur in economic or potentially economic deposits (Castor & Hedrick, 2006). (Ln=Lanthanide Element).

Mineral	Chemical Formula	REO Wt.%
Aeschynite	(Ln,Ca,Fe,Th)(Ti,Nb)2(O,OH)6	36
Allanite (orthite)	(Ca,Ln)2(Al,Fe)3(SiO4)3(OH)	30
Anatase	TiO2	3
Ancylite	SrLn(CO3)2(OH)·H2O	46
Apatite	Ca5(PO4)3(F,Cl,OH)	19
Bastnasite	LnCO3F	76
Brannerite	(U,Ca,Ln)(Ti,Fe)2O6	6
Britholite	(Ln,Ca)5(SiO4,PO4)3(OH,F)	62
Cerianite	(Ce,Th)O2	81
Cheralite	(Ln,Ca,Th)(P,Si)O4	5
Churchite	YPO4·2H2O	44
Eudialyte	Na15Ca6(Fe,Mn)3Zr3(Si,Nb)Si25O73(OH,Cl,H2O)5	10
Euxenite	(Ln,Ca,U,Th)(Nb,Ta,Ti)2O6	<40
Fergusonite	Ln(Nb,Ti)O4	47
Florencite	LnAl3(PO4)2(OH)6	32
Gadolinite	LnFeBe2Si2O10	52
Huanghoite	BaLn(CO3)2F	38
Hydroxylbastnasite	LnCO3(OH,F)	75
Kainosite	Ca2(Y,Ln)2Si4O12CO3·H2O	38
Loparite	(Ln,Na,Ca)(Ti,Nb)O3	36
Monazite	(Ln,Th)PO4	71
Mosandrite	(Ca,Na,Ln)12(Ti,Zr)2Si7O31H6F4	<65
Parisite	CaLn2(CO3)3F2	64
Samarskite	(Ln,U,Fe)3(Nb,Ta,Ti)5O16	12
Synchisite	CaLn(CO3)2F	51
Thalenite	Y3Si3O10(OH)	63
Xenotime	YPO4	61
Yttrotantalite	(Y,U,Fe)(Ta,Nb)O4	<24

2.8 Prices

Prices for REE metal and oxides were constant for most of the 1990s into the mid-2000s, until export quotas were implemented by the Chinese government that limited global supply. The export restrictions, monopolistic supply, and strong global demand for rare earth products, created a huge supply-demand deficit that resulted in a significant increase in REE prices. REE prices reached a peak level in 2011 before plummeting down in 2012 and 2013 due to global recession and relaxation in export restrictions. In 2014 prices stabilized, and until the time of this writing, date continue to show resistance to further decline. REE metal and oxide prices from December 2013 to July 2016 are presented in Table 7. Prices for holmium, thulium, ytterbium, and lutetium were not available. Light REEs have the lowest prices, while the heavier ones are more expensive. Scandium has currently the highest price of the presented REEs.

As discussed previously, the United States is largely dependent on imports of REE and derivate products and any variance in the supply-demand equilibrium can prove catastrophic for the American economy. In 2011 disruptions in the Chinese rare earth market led to price fluctuations creating ripple effects across REE-dependent industries (Norman et al., 2014).

Table 7. Rare earth metal and oxide prices (USD kg-1) from December 2013 to July 2016 (HEFA, 2014; MineralPrices, 2016).

Price USD kg-1				
Element and purity	Dec. 2013	May 2014	December 2015	July 2016
La metal ≥ 99%	13	12.5	10	7
La oxide ≥ 99.5%	6.05	5.8	4.8	2
Ce metal ≥ 99%	12	12	10	7
Ce oxide ≥ 99.5%	5.5	5.5	4.4	2
Pr metal ≥ 99%	175	175	175	85
Pr oxide ≥ 99.5%	134	125	105	52
Nd metal≥ 99.5%	94	95	87	60
Nd oxide ≥ 99.5%	69	68	59	42
Sm metal ≥ 99.9%	30	30	20	7
Eu oxide ≥ 99.99%	1,100	980	680	150
Gd metal 99.9%	95	95	95	55
Gd oxide ≥ 99.5%	44	41	39	32
Tb metal ≥ 99.9%	1,900	1,200	810	550
Tb oxide ≥ 99.5%	950	800	600	400
Dy metal ≥ 99%	750	600	470	350
Dy oxide ≥ 99.5%	525	500	340	230
Er metal ≥ 99.9%	225	215	165	95
Er oxide ≥ 99.5%	69	72	77	34
Y metal ≥ 99.9%	75	74	77	35
Y oxide ≥ 99.99%	20	19	15	6
Sc metal 99.9%	15,500	17,500	18,000	15,000
Sc oxide ≥ 99.95%	7,000	7,200	7,200	4,200
Mischmetal ≥ 99%	10	10	8	6

The price of REE derivative products is dependent on the price of REE metal and oxides, which in turn depends on the demand of derivative products in the market. The market price per unit of HREEs is considerably higher than for LREEs provided the relatively strong demand for them along with their relative scarcity. For example, the cost of dysprosium will continue to rise as it will be in constant high demand for applications in the clean energy sector for wind turbines and electric motors. Future pricing is expected to be influenced by global supply and demand trends and an increase in the demand for HREEs is likely unless substitutions are discovered (Bleiwas & Gambogi, 2013).

2.9 REE Resources in Alaska

Alaska has more than 70 known REE mineral occurrences (Figure 6) and millions of acres of surveyed areas with the potential to contain REEs; however, the mineral-asset capability of these occurrences and lands is inadequately understood. Assessment of Alaska's REE potential is curbed by a lack of basic geologic data and compilation of existing data. The Bokan Mountain, Mount Prindle, and Tofty are the most studied sites of REE occurrences in Alaska.

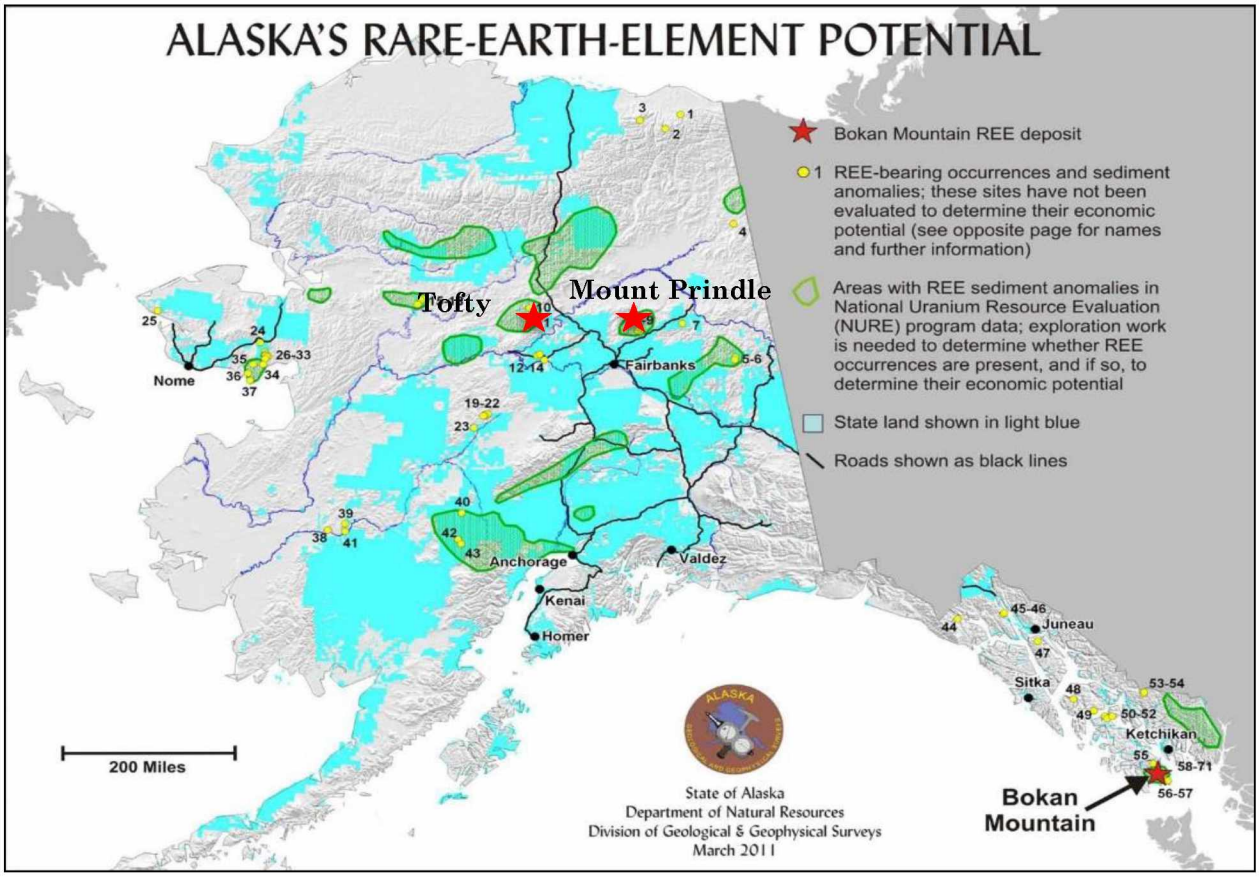

Figure 6. Location map of Alaska rare-earth-element occurrences and anomalies (Modified from Szumigala & Werdon, 2011).

The Bokan Mountain property is one of the most significant REE prospects in the world, located 37 miles southwest of Ketchikan on Prince of Wales Island in Alaska. Preliminary investigations done for the region suggest that the area is the home to the largest REE deposits in North America, with higher enrichment of HREEs. Bokan Mountain is predominantly enriched with HREE's thus making it a valuable resource. It has the fourth largest source of Tb and Y in the world. The uranium, thorium, and REE mineralization is hosted in the Jurassic Bokan Granite Complex, a crudely circular ring dike complex consisting of nine different phases of peralkaline granitic rocks (Thompson, 1997). The valuable minerals are found in irregular cylindrical "pipes," steep shear-zone-localized pods or lenses, and quartz veins. In 2007, Ucore Rare Metals Inc. acquired 100 percent interest in the Bokan Mountain property, and has conducted extensive exploration over the years, including geological mapping, geochemical sampling, aerial and ground geophysical surveys, and drilling. Bentzen III et al. (2013) in the Preliminary Economic Assessment report, outlined a plan for a 1,500 ton/day processing plant for a mine life of 11 years. The mineral resource for the project was estimated to be 5.2 million tons of rare earth ore.

Another major REE occurrence is in an igneous complex near Roy Creek, about 18 miles west of Mount Prindle in interior Alaska (Thompson, 1997). The property currently falls within the White Mountain National Recreation Area and all mining is prohibited in the zone. The Mount Prindle syenite complex was originally investigated for uranium in 1978 by MAPCO Inc. MAPCO sampled and drilled the Roy Creek property and identified several small deposits that are enriched in thorium

and REEs (15%). Mineralization occurs as fissure veins containing allanite, bastnasite, monazite, thorianite, thorite, uraninite, and xenotime with fluorite in a Cretaceous-age granitic igneous complex with five types of granitic-type igneous rocks dominated by syenite.

The Tofty Ridge prospect is near Manley Hot Springs in interior Alaska and the REEs are contained in a Triassic carbonatite sill with a strike length of at least 6 miles. The property has been explored since 1978, and approximately 5,300 feet of core drilling has been done by the U.S. Bureau of Mines and industry. Preliminary exploration from the 30 feet trench rock sampling revealed an average of more than one percent REEs (as cerium and lanthanum) and 0.15% niobium. Portions of the core were geochemically anomalous for niobium, REE, and yttrium. Nearby creeks are suspected to have placer REE resources (Szumigala & Werdon, 2011).

2.10 REE in Coal

2.10.1 Abundance

Coal and coal beds have been found to be significantly enriched with trace metals and can be a potential source for both LREEs and HREEs. Trace elements generally refer to elements present in natural materials at concentrations below 0.1% or 1000 ppm (Swaine, 2013). Coals with high REE concentrations have been discovered in Pavlovka and Rakovka coal deposits in Russia (300–1000 ppm REEs), Appalachian deposits in the U.S. (500–4000 ppm REEs), Sydney Basin in Nova Scotia, Canada (72–483 ppm REEs), Sichuan Basin deposits in China, and others across the globe. These coals are now being actively studied as a new source of REE (Gschneidner Jr, 1964; Seredin, 1991, 1992, 1996; Seredin & Dai, 2012; Wang et al., 2006).

Due to the unstable market conditions, REEs in coal possess substantial economic potential, if REEs are even partially recovered. An REO concentration in the range of 800–900 ppm in the coal combustion ash has been considered as the cut-off grade for beneficial recovery of REEs from coals (Dai et al., 2012; Hower, Ruppert, & Eble, 1999; Seredin & Dai, 2012). Ketris and Yudovich (2009) estimated the REE abundance ratio for coal to coal-ash to be around 0.17. Thus, the cut-off grade of REEs in coal is 115–130 ppm, which indicates that many coal deposits are potential resources, suitable for REE recovery (W. Zhang et al., 2015).

Studies have found that Chinese and Turkish coals contain 101 ppm and 116 ppm REEs, respectively, which is greater than the world concentration average (72 ppm). The REE concentration of DPR Korea and U.S. coals corresponds to the world average level. Seredin (1996) and Zheng, Liu, Chou, Qi & Zhang (2007) estimated that the average content of REEs for world coal is 46 ppm. Seredin and Dai (2012) reported that the average REE abundance in world coal is 69 ppm, and Chinese and U.S. coals contain about 138 ppm and 62 ppm, respectively. A comparison of REE concentration in world coal reserves is summarized in Table 8.

The outlook coefficient (C_{outl}) is used to evaluate the market value of REE-bearing ores. The formula given by Equation 1 calculates the economic potential of REE resources as a ratio of the critical and excessive REE content in ppm of individual elements of the ore.

$$C_{outl} = \frac{(Nd + Eu + Tb + Dy + Er + \frac{Y}{Total\ REE})}{(Ce + Ho + Tm + Yb + \frac{Lu}{Total\ REE})} \quad (1)$$

Obviously, a larger C_{outl} means more critical REEs can be recovered and the resource has higher profitability. Based on the data published by Ketris and Yudovich (2009), the C_{outl} for world coal is 0.64.

Table 8. Comparison of REE concentrations of coals across the globe (Modified from W. Zhang et al., 2015).

	DPR Korea coal	Chinese coal	Turkish coal	U.S. coal	World Coal
La	14.5	18	21.12	12	11
Ce	27.2	35	39.24	21	23
Pr	2.9	3.8	4.71	2.4	3.5
Nd	11.1	15	16.85	9.5	12
Sm	2.3	3	3.18	1.7	2
Eu	0.5	0.65	0.76	0.40	0.47
Gd	1.4	3.4	3.00	1.8	2.7
Tb	0.3	0.52	0.45	0.30	0.32
Dy	2	3.1	2.42	1.9	2.1
Ho	0.4	0.73	0.47	0.35	0.54
Er	1.1	2.1	1.37	1.0	0.93
Tm	0.3	0.34	0.21	0.15	0.31
Yb	1	2	1.35	0.95	1.0
Y	7.2	9	12.76	8.5	8.4
Sc	4.9	4	7.92	4.2	3.9
Lu	ND	0.32	0.21	0.14	0.20
LREE	59.9	78.85	88.86	48.8	54.67
HREE	17.4	22.11	27.16	17.49	17.7
Total	77.3	100.96	116.02	66.29	72.37

2.10.2 Mineralization and Size

REEs are mainly concentrated in coal in the form of accessory phosphates minerals (such as monazite and xenotime), sedimentary minerals (monazite, xenotime, zircon), or clay minerals (kaolinite, illite) (Ekmann, 2012; Finkelman, 1982; Wang et al., 2006; W Zhang et al., 2015). Seredin (1996) suggested that REEs mostly occur in REE enriched coals as crystallized grains of REEs, usually 0.5–5 mm in diameter, deposited during sedimentation and in adsorbed forms on the organic matter or clay minerals.

Hower et al. found that REEs in coal from eastern Kentucky are mainly in the form of REE-rich phosphates, like monazite, which is of authigenic origin judging from the fact that the monazite commonly in-fills cracks in clays and cells in clarain and vitrain. The monazite occurs in very small (<2 mm) irregularly shaped particles (Hower et al., 1999). According to Seredin (1996), most of the REEs in coal (70–80%) are present in the lightest density fraction (<1.40 Specific Gravity).

Based on the hypothesis that REE mineral grains of a few microns are disseminated in the cracks and pores of coal and are enriched in lighter density fractions, gravity separation, accompanied with fine grinding to liberate REE mineral grains, can be used to produce concentrates with relatively higher REE concentrations. The difference in magnetic, electrostatic and physio-chemical characteristics of REE bearing minerals can be exploited for producing REE-enriched concentrates from coal for subsequent extraction for higher profitability provided that some degree of liberation is achieved.

As previously stated, the maximum particle size of rare earth grains contained in coals may not exceed several microns. In such cases, the physical enrichment methods may not be efficient. The magnetic, gravitational, and hydrodynamic forces can be negated by the fine particle size. For fine particles below 74 mm, the entrainment of gangue particles will limit the use of froth flotation (Arol & Aydogan, 2004). Several new techniques, improvements in the preexisting processing methods, and separation devices specifically aimed at fine particle

separation, however have been developed in recent decades to allow ultrafine particle concentration.

2.10.3 Separation

The percentage abundance of valuable elements in an ore determines its feasibility for industrial economic extraction. The cut-off REE grades of traditional rare earth minerals (bastnasite, monazite, etc.) and ion-adsorbed minerals for industrial exploitation are about 1.5%–2.0% and 0.06%–0.15%, respectively, which suggests that any REE deposits containing less than the cut-off grade are not viable for economic extraction irrespective of the size of the reserve. The differences in physical properties such as size, density, surface chemistry, magnetics, and electrostatics, between REEs and gangue minerals have been harnessed to beneficiate considerable amounts of traditional REE minerals. Unlike LREE's, the HREE's are found in ores that are hard to process and thus have a brief history of processing and extraction (GSI, 2016; Jordens et al., 2013; Szumigala & Werdon, 2011; W. Zhang et al., 2015).

Even though the abundance and occurrence of REEs in coal has been known for quite some time and has been well addressed in literature, relatively fewer studies have focused on the enrichment and recovery of REEs from coal and coal combustion products due to the following:

1. The complex nature of the of the occurrence, composition, and distribution of REEs in coal and coal combustion products;

2. The combination of economic and operational limitations along with environmental obligations possessed by the conventional mineral processing techniques (e.g., gravity separation, flotation, magnetic separation, hydrometallurgy) for REE recovery from coal or coal by-products.

2.10.3.1 Physical Beneficiation of REEs

REEs usually are found together in all the minerals with large variations in relative proportions and owing to the chemical similarity, separation of individual REEs from one another is a daunting task. The primary objective of processing of REEs is to supply a sellable concentrate by standard mineral beneficiation and milling techniques. The selection of the most appropriate initial processing steps depends on the characteristics and mineralogy of the ore. The concentrates are eventually leached in acid solutions and the pregnant solution is purified using liquid-liquid extraction to produce final products.

Based on the difference between physical and chemical characteristics of REE-bearing minerals and gangue, gravity separation, magnetic separation, electrostatic separation, and froth flotation have been widely employed for the beneficiation of traditional REE minerals (Fuerstenau & Pradip, 1988; Houot, Cuif, Mottot & Samama, 1991; Jordens et al., 2013; Krishnamurthy & Gupta, 2004; Ren et al., 2000). Table 9 shows the physio-chemical characteristics of common rare earth minerals.

Table 9. Physical properties of common REE bearing minerals (W. Zhang et al., 2015).

Mineral name	Density (g/cm^3)	Magnetic properties	Electrical Conductivity
Bastnasite	3.90–5.20	Paramagnetic	Nonconductive
Monazite	4.98–5.43	Paramagnetic	Nonconductive
Xenotime	4.40–5.10	Paramagnetic	Nonconductive

Magnetic separation is commonly used in REE mineral beneficiation to exploit the variance in magnetic behaviors to eliminate strongly magnetic gangue from the desired paramagnetic REE-bearing minerals (Jordens et al., 2013). Electrostatic separation is generally used for heavy mineral (HM) sands for the enrichment of monazite, zircon, and rutile from gangue minerals. Rutile has a higher conductivity than the other minerals and the gangue, thus electrostatic separation is applied to obtain a rutile concentrate when other separation methods do not suffice (Jordens et al., 2013; Moustafa & Abdelfattah, 2010).

An example of the combination of the gravimetric, electrostatic, and magnetic separation is shown for a heavy mineral sand deposit in Figure 7. Among the beach sand minerals, specific gravity of monazite is the highest. The ore containing 2–5% HMs is first concentrated by gravity separation using cone concentrators to produce a product with 20–30% HMs. This product then passes through a spiral bank, which produces a concentrate of more than 80% HMs. An enrichment of 1600 % is achieved by exploiting the differences in the specific gravity of constituent minerals. Further separation of heavy minerals is then achieved by exploiting small gravimetric

differences or small differences in magnetizability and surface ionization potential. In decreasing order of magnetizability, ilmenite, garnet, xenotime, and monazite, behave as magnetic minerals. Xenotime is more magnetic than monazite and concentrates with ilmenite in magnetic separation. Xenotime, being a poor electrical conductor, is separated electrostatically from ilmenite. Rutile in electrostatic separation behaves as a conducting mineral and is separated from monazite.

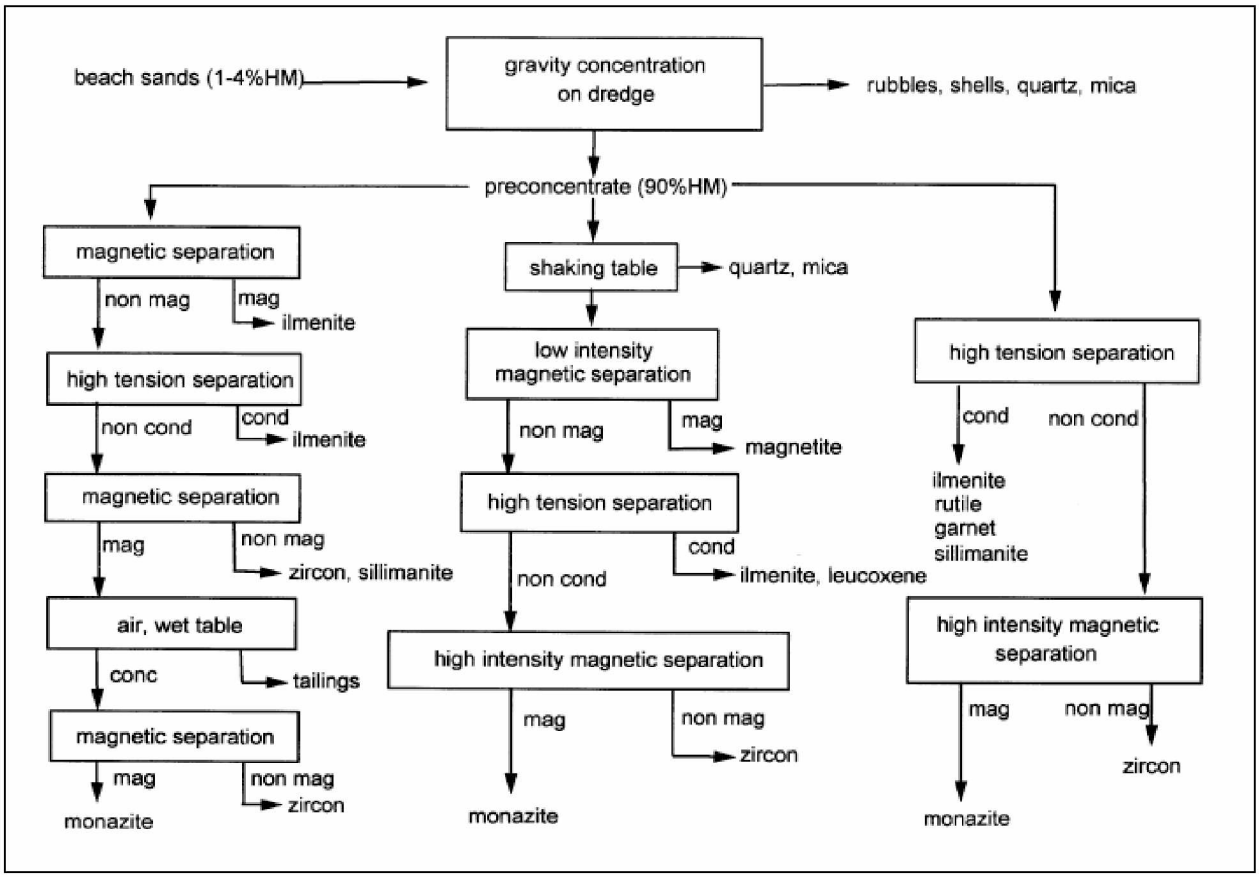

Figure 7. Physical beneficiation of monazite in beach sand minerals (Krishnamurthy & Gupta, 2004).

Flotation has been widely used in the beneficiation of conventional REE ores. The combination of collectors and pH ranges used for froth flotation of REE minerals is summarized in Table 10.

Table 10. Types of collectors used in Floatation of REEs.

Mineral name	Type of collector	Example	Condition
Monazite or Bastnasite	Alkyl carboxylic acid	Fatty acid, oleate, tall oil	pH 6–9
Bastnasite	Alkyl phosphoric acid	Alkyl phosphate Easter P538	pH 4–5
Bastnasite	Hydroxamic acid	Hydroxamate H205	pH 8–8.5
Bastnasite	Aromatic phosphoric acid	Styrene phosphoric acid	pH 6–10
Bastnasite	Aromatic carboxylic acid	O-phthalic acid	pH 5
Bastnasite	Aromatic amide	-	pH 5–6
Monazite or bastnasite	Combination reagent	Mixture of fatty acid and hydroxamate	-

Mountain Pass contains barite, calcite, strontianite, and quartz as the gangue minerals along with Bastnasite ore. A simplified flowsheet for Mountain Pass mine is shown in Figure 8. Prior to rougher flotation, the ore undergoes six different conditioning treatments in large tanks (1800 mm by 2700 mm) with steam being bubbled through the pulp. The reagents are added step-wise in the pulp, which is heated to 70°C to 90°C, and the total conditioning time is about 2 hours. The conditioning process is as follows:

1. In the first stage, soda ash, sodium fluosilicate, and steam is added to the ore slurry.

2. The slurry is then subjected to steam conditioning.
3. In the third stage, ammonium lignin sulfonate is added in the presence of steam.
4. In the fourth stage, the slurry is again subjected to steam conditioning.
5. The fifth stage is the addition of steam-distilled tall oil C-30.
6. In the sixth stage steam is bubbled through the slurry again.

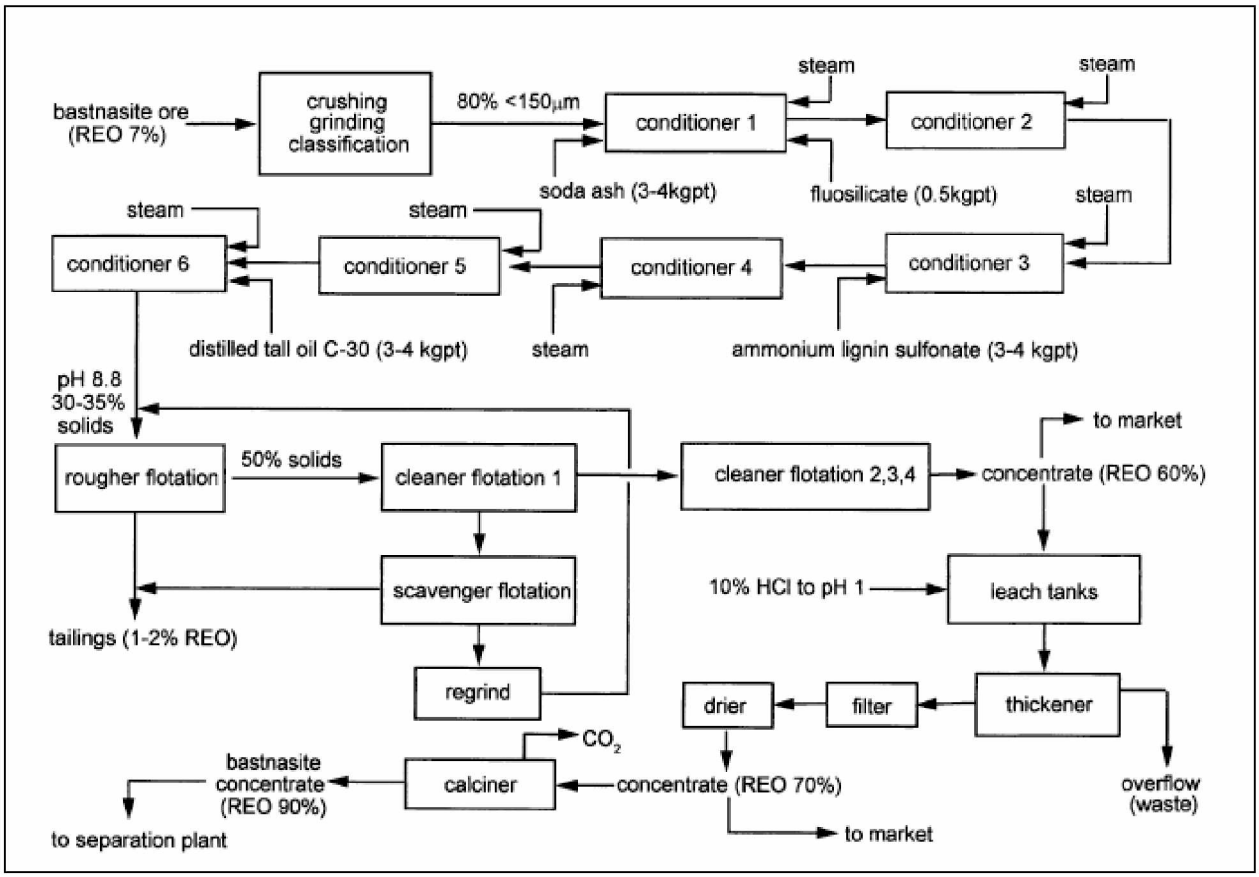

Figure 8. Simplified flowsheet for the recovery of bastnasite at the Mountain Pass Molycorp plant (Aplan, 1989).

The conditioned slurry, with 30–35% solids, is pumped to a rougher flotation circuit. Rougher flotation is carried out in 12 flotation cells (1700 liters) and the tailings from rougher flotation contain an average 1–2% REO. The rougher float concentrate,

which assays approximately 30% REO, is transferred to cleaner cells for four-stage cleaning at 50% solids. Only the tailings from the first cleaner are put through a scavenger flotation circuit and the tailings from other cleaner cells are recirculated in the cleaning circuit. The tailings from the scavenger circuit are combined with rougher tailings and constitute the overall plant tailings which have an average 2% REO concentration. The froth fraction from the scavenger units is reground and reverted back to the rougher cells. After the completion of four-stage cleaning, the final concentrate from the flotation circuit is dewatered and dried. The final dried concentrate of Mountain Pass contains 60% REO and the process has an overall recovery of 65–70% (Pradip & Fuerstnau, 1988).

Three schemes for the processing of REE-Fe-Nb ore from Bayan Obo Mine in Inner Mongolia are shown in Figure 9. The ore is reduced to 90% <74 microns by grinding and initial bulk flotation is carried out after addition of Na_2CO_3 as pH regulator, Na_2SiO_3 as depressant for iron and silicates, and sodium salt of oxidized petroleum (paraffin soap) as collector. The iron minerals, niobium, and silicates are retained in the tailings at the bottom of the flotation cells and are pumped to a separate iron beneficiation and niobium recovery circuit. The floats from the bulk flotation circuit are sent for selective rare earth flotation after removal of surplus fatty acid collector and thickening and desliming at 5 microns. The flotation reagents include: Na2CO3 as pH regulator, Na_2SiO_3 and Na_2SiF_6 as gangue depressants, and hydroxamic acid as collector at a pH between 5 and 6. In selective flotation, the rougher concentrate contains approximately 45% REO assay and depressed calcite, fluorite, and barite

settle as tailings. The floats contains both monazite and bastnasite. The recovery of REEs in the concentrate after selective flotation is about 80%. The two REE bearing minerals are separated by high intensity magnetic separation as the final treatment. The magnetic separation yields two concentrate fractions; the primary product is 68% REO concentrate and a secondary concentrate containing monazite with 36% REO assay. The recoveries for the two products are 25% and 36%, respectively with an overall REE recovery of 61% from the ore (Houot et al., 1991; Jiake & XiangYong, 1985).

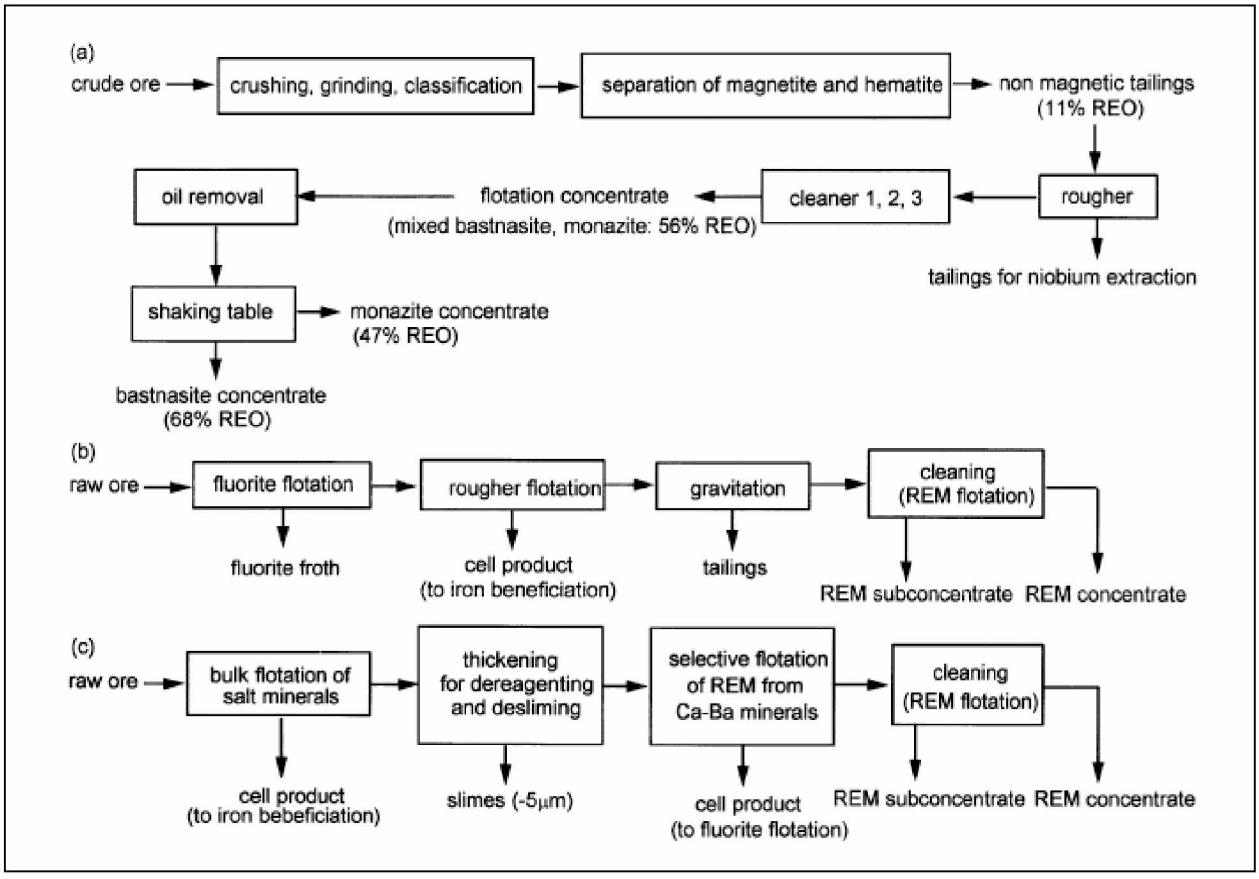

Figure 9. Schemes for the physical beneficiation of Bayan Obo ore (Andresen, 1986; Houot et al., 1991).

It can be concluded from these examples that physical enrichment methods are best suited for pre-concentration stages. Similar techniques can be applied for REEs in coal considering it's mineralogy; however, extensive grinding will be required to liberate finely disseminated REE grains present in the cracks and pores in the coal. No literature references have been found dealing with the application of gravity, electrostatic, magnetic, or flotation for the beneficiation of REEs in coal. Chemical processing techniques, due to their application for extraction of low grade ores like for gold, still appear to be the most appropriate and convenient method for recovering REE from coal.

Research and development of advanced physical separation technologies is necessary, however, to improve the efficiency of REE recovery for particles as small as 1 micron. If successfully done, recovery of REEs from secondary sources can generate revenue, create new job opportunities, and can cut back the U.S. reliance on foreign imports of lanthanoid elements.

2.10.3.2 Chemical Beneficiation of REEs

For REE processing, chemical beneficiation of the concentrate obtained after physical beneficiation generally is performed by hydrometallurgical and sometimes pyro-metallurgical techniques. The REEs are readily soluble in acids, which is attributed to their chemical properties and also permits their easy precipitation. Differences in the basic nature of the REEs also facilitate their chemical separation. With the recent advancements in complex reagents and development in techniques like ion exchange

and solvent extraction, the subtle differences in chemical behaviors of different REEs can be capitalized, upon, to enhance their separation from one another.

In hydrometallurgical processing, leaching techniques have been widely used in the recovery of low-grade ores (Fleming, 1992; Murthy, Kumar & Rao, 2003). Enrichment of REEs using leaching techniques followed by roasting produces extractable REOs and is a key procedure for making commercial REE end products (Krishnamurthy & Gupta, 2004). Industrial enrichment and recovery of trace metals from coal using leaching is widely studied and has even progressed in industrial production stages. Although recovery of any metals from coal through leaching is theoretically possible with suitable leaching reagents, very little work has been cited for extraction of REEs from coal using leaching techniques. As known from the mineralization and size studies, a significant proportion of REEs in coal is in an inorganic form. This proportion can be leached with appropriate reagents, such as sulfuric acid, which reacts well with REE bearing minerals (W. Zhang et al., 2015).

In a nutshell, exploiting REEs from coal can present a potentially significant economic opportunity. Direct treatment of raw coal, however, is not feasible as coal is still one of the most common energy resource. (W. Zhang et al., 2015). As previously stated, most of the REEs in coal have an affinity to be concentrated in the lower density fractions and this preferential partitioning makes the enrichment of REEs possible. Thus, emphasis should be given to concentrating the REEs in the clean-coal product from a coal-preparation plant.

Also, when the fixed carbon is removed from the clean coal, the enrichment ratio of REEs in coal ash is several times higher than the parent coal, thus improving the final value of the resource.

CHAPTER 3 METHODS AND MATERIALS

3.1 Characterizing REEs in Alaskan Coal

3.1.1 Samples and Their Origin

3.1.1.1 Coal Samples

Nearly all coal resources in Alaska are found in Cretaceous and Tertiary rocks distributed in three major coal provinces. Alaskan coal resources have low sulfur content (averaging 0.2–0.4%) compared to the coal in the contiguous United States. The Cretaceous coal resources, generally of bituminous and lignite rank, are mainly distributed in the Northern Alaska-Slope coal province, along with a minor amount of Tertiary coal resources in the area. Most of the Tertiary coal resources, mainly lignite to subbituminous with minor bituminous and semi-anthracite, are found in the Central Alaska-Nenana and Southern Alaska-Cook Inlet coal provinces (Flores, Stricker & Kinney, 2004).

Two previously identified coal samples in this study are from, Healy (Central Nenana) and Wishbone Hill (Southern Alaska-Cook Inlet) regions (Figure 10). The Central Alaska-Nenana coal province is centrally located on the north side of the Alaska Range extending from about 50 miles (80 km) west to 50 miles (80 km) east of the Alaska railroad. It consists of several synclinal basins partly detached from each other by erosion of coal-bearing rocks. More than one-half of the coal mined in Alaska is from this area, and it is the only province in Alaska being currently mined.

Figure 10. Locations of the handpicked sample from Wishbone Hill and the procured sample from Usibelli Coal Mine, Healy (Modified from Google Earth)

The collected coal sample from Healy was from the Suntrana formation, which consists of sandstones, siltstones, mudstones, carbonaceous shales, and coal. Coal beds are interbedded with carbonaceous shales and have a combined thickness ranging from 1.6 to 65 feet (0.5 to 20m) (Flores et al., 2004; Stanley, Flores & Wiley, 1992). The sample was collected as a reduced representative sample from the stockpile of Healy No. 4 seam.

The Wishbone Hill district belongs to the Matanuska field and is in the Southern Alaska-Cook Inlet region. The Matanuska coalfield is the most important Paleocene coalfield in Alaska because it contains high-rank minable coal beds. Wishbone Hill coal district is on the north side of the coalfield between Moose and Granite Creeks. More than 20 coal beds, with thicknesses exceeding 3 feet, are known in the Wishbone Hill coal district (Belowich, 1993). Structures in the Matanuska coalfield are typically complex. The doubly plunging Wishbone Hill syncline has beds that dip up to 40°, and the structure is cut by two sets of transverse faults (Flores et al., 2004). Structural complications on the northwest flank make the coal beds in some structural blocks difficult to mine and preclude meaningful estimation of reserves (Barnes & Payne, 1956). The Wishbone Hill sample used in our test program was from Jonesville coal zone and was handpicked from the exposed oblique-slip fault outcrop and transported in 5 gallon buckets. Both of the samples were mass reduced to about 200 kg.

3.1.1.2 Ash samples from UAF Power Plant

Fly ash (flue-ash) is one of the residues generated in coal combustion and contains very fine particles that rise with the flue gases. Fly ash is captured by electrostatic precipitators and filtration equipment. Alternately, bottom ash is removed from the bottom of the furnace. Depending upon the source and makeup of the coal being burned, the components of fly ash and bottom ash vary considerably. The University of Alaska Fairbanks (UAF) power plant utilizes coal from the Usibelli Coal Mine in Denali Borough, Alaska (Healy Coal Mine); three type of coal by-products, namely fly

ash (FA), bottom ash (BA) and cinders (C, residue left from incomplete combustion of coal), were collected from the power plant for the study.

3.1.2 Size Analysis

The samples were brought to the UAF's mineral processing facility where individual samples were mixed thoroughly and divided using the cone and quartering method. Subsequently, representative samples were crushed by a jaw crusher with a ¾-inch (19 mm) closed-side setting (Figure 11). The product from the jaw crusher was fed into a roll crusher with a ¼-inch (6 mm) closed-side setting (Figure 12) to provide size-reduced representative subsamples for further physical separation and sample characterization in accordance with the standards prescribed in ASTM D4371. All samples were classified separately into the following four size fractions by dry screening for 15 minutes using a set of U.S. mesh sieves and sieve shaker:

- >¼-inch (6 mm)
- ¼-inch to 30 U.S. Mesh (6 mm to 0.6 mm)
- 30 U.S. Mesh to 100 U.S. Mesh (0.6 mm to 0.15 mm)
- <100 U.S. Mesh (0.15 mm).

After homogenization and size reduction, representative samples of the screened fractions of each coal type were subjected to proximate (ASTM D3172) and sulfur (ASTM D4239) analyses. REE content, including yttrium (Y) and scandium (Sc), was analyzed using ICP-AES and ICP-MS at a commercial laboratory utilizing the ME-4ACD81 method. Furthermore, the samples collected from UAF power plant as fly

ash, bottom ash and cinders were further analyzed for their respective REE contents by a commercial laboratory prior to beneficiation.

Figure 11. Single Toggle Jaw Crusher.

Figure 12. Single Smooth Roll Crusher.

3.1.3 Float and Sink Tests

Float-sink tests (Figure 13) were conducted for coarse sizes (>¼-inch and ¼-inch to 30 U.S. Mesh) at specific gravities of 1.30, 1.50, 1.60, 1.70, 1.80 and 2.00 in 20 liter buckets. The test solutions were prepared using anhydrous zinc chloride (99% pure) up to specific gravity of 2.0. LMT (lithium metatungstate) was used for preparation of specific gravity 2.20 at Mineral Industry Research Laboratory (MIRL), UAF. The different specific gravity fractions were thoroughly washed with water to remove all the zinc chloride/LMT and air dried and were subsequently split into subsamples for

proximate (ASTM D3172) and sulfur (ASTM D4239) analyses and for analyses of REE+Y+Sc.

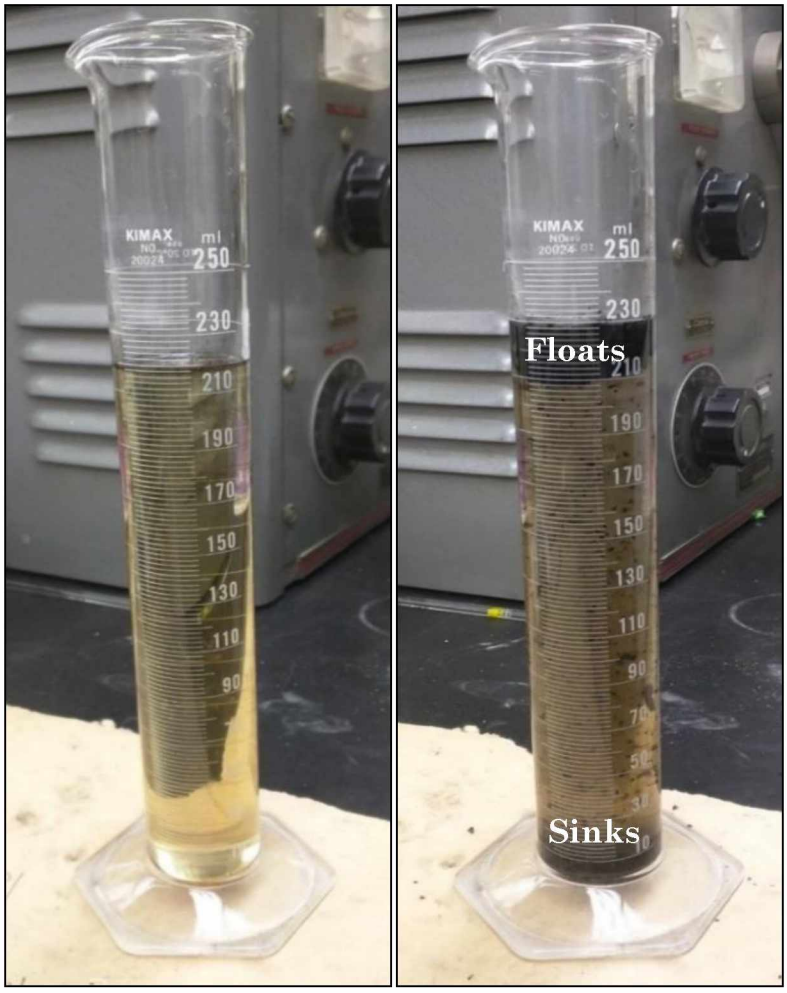

Figure 13. A washability float and sink test for coal.

3.1.4 Magnetic Separation

3.1.4.1 Dry High Intensity Magnetic Separation (Carpco)

Magnetic separation of the <100 Mesh particles was performed using both dry high intensity and wet high intensity Carpco magnetic separators. The highest field strength (3 Amperes) was used at 20 rpm rotor speed and at a splitter blade setting of 4. The dry magnetic separation tests were found to be ineffective, as no distinct

separation was observed for both coal samples even after several iterations. Therefore the dry magnetic separation tests were abandoned.

3.1.4.2 Wet High Intensity Magnetic Separation (Carpco)

A slurry of 20% solids was introduced into the wet magnetic separator at highest field strength of 6.6 Amperes with 6 mm cast iron balls in the casing (Figure 14). The non-magnetic and magnetic slurries were dewatered and air dried and subsequently split into subsamples for proximate, sulfur, and REE+Y+Sc analyses.

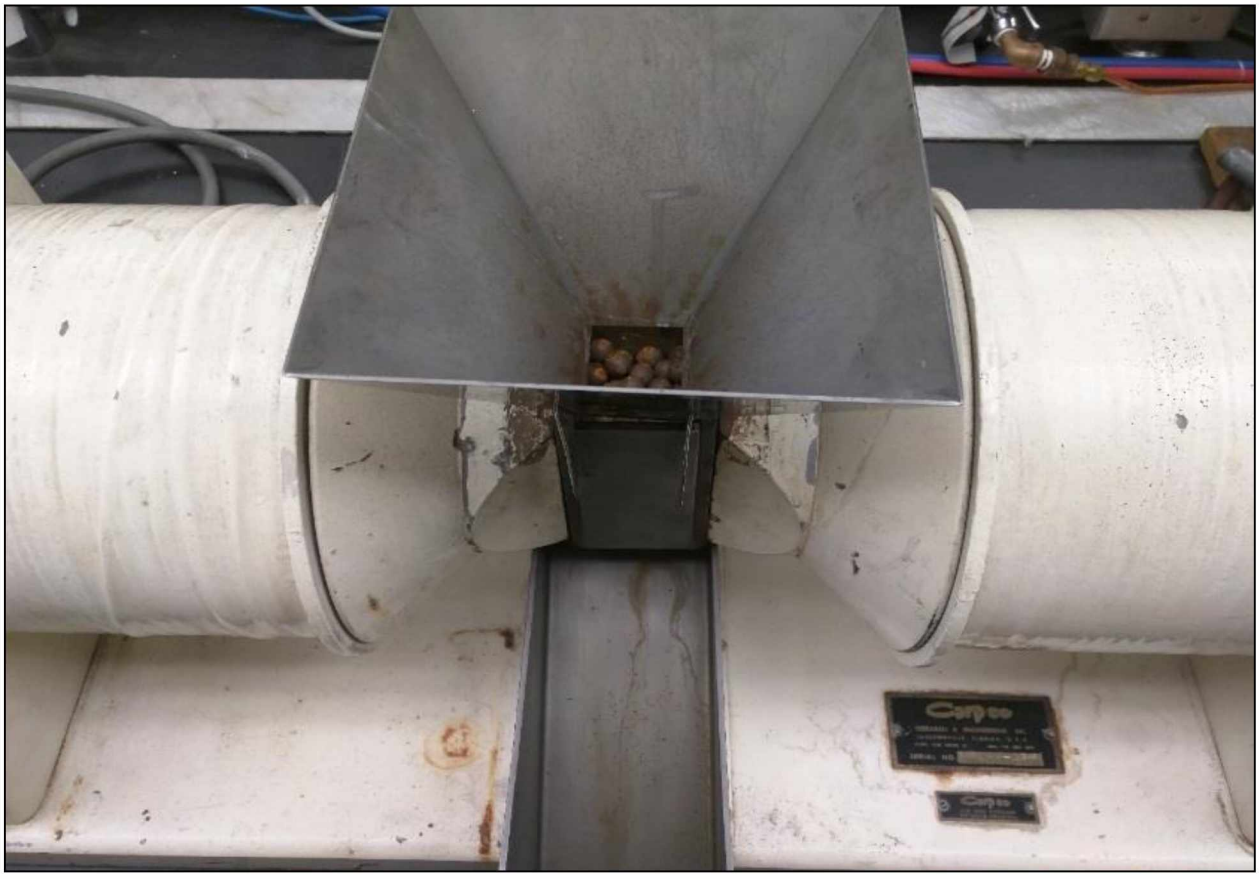

Figure 14. Carpco wet magnetic separator.

3.1.5 Scanning Microscope Analysis

The coal samples from Healy and Wishbone Hill, along with the coal combustion products (bottom ash, fly ash and cinders) from the UAF power plant were subjected to Scanning Electron Microscope analysis to examine the particle size distribution and mineralogical composition using a FEI Quanta 200 Environmental Scanning Electron Microscope (ESEM) at UAF's Advanced Instruments Laboratory (AIL). The information on particle shape, size and composition of the samples is vital in designing the downstream processes for liberation, concentration, and subsequent extraction of REEs.

The Quanta 200 ESEM required that the sample be conductive or properly mounted and coated for conduction (Figure 15). The samples were mounted on a sample holder and coated with Iridium to a thickness of 50 nanometers using Denton Sputter. Iridium coating on non-conducting samples reduces beam penetration and allows for a sharper image. The backscattered electrons and X-rays were captured using the Everhardt-Thornley Detector, which can be used to find the topographical information and elemental composition of the specimen. The elemental composition helps in understanding the strength of the bonds, and the particle size distribution of REEs facilitates the selection of an adequate physical and chemical separation technique.

Figure 15. Sample mount on the Quanta 200 ESEM.

3.1.6 Preliminary Froth Flotation Studies

The fine fraction (<100 Mesh) for both coals was subjected to flotation tests to analyze the potential of physio-chemical separation by exploiting the difference in surface properties of the components. Flotation of the fines for both coal samples was conducted in MIRL Labs at UAF in a laboratory scale Denver 2-liter flotation cell (Figure 16) using fatty acids (fuel oil) (Fuerstenau, 2013; Gupta, Ghosh & Akdogan 2016; Zhang & Edwards, 2012) as collector (0.45kg/t) and Aerofroth 88 as frother (20 ppm) with a pulp density of 7 Wt.% at normal pH. The slurry was subjected to a collector conditioning time of 14 minutes followed by frother conditioning of 1 min.

The batch flotation was initiated by introducing air from the bottom of the flotation cell and was allowed to continue for 3 minutes with collection of the froth every 30 seconds. There were no depressants used. After the tests, the samples were dewatered and air dried (Figure 17), and were subsequently split into subsamples for proximate and sulfur and REE+Y+Sc analyses.

Figure 16. Flotation cell setup at MIRL, UAF.

Figure 17. Sample drying oven.

3.2 Statistically Designed Experimental Program for Froth Flotation

3.2.1 Sample Preparation and Grinding Tests

REEs have been found to be extremely fine-grained in the coal and ash particles (1-10 microns or smaller) (Finkelman, 1988; Scott, Deonarine, Kolker, Adams & Holland, 2015). Therefore, grinding of coal, bottom ash and cinder samples was done by using a tumbling ball mill (Figure 18) at UAF's MIRL labs. REE recovery by flotation of bastnasite ore involves flotation of <74 microns material, so the coal was size reduced to 75 microns (200 U.S. Mesh) for REE concentration analysis using

froth flotation (Krishnamurthy & Gupta, 2004). Fly ash was found to be 90% <75 microns passing as received and thus did not required milling. Wet milling of feed with 50% solids was done with a ball charge of 3.37 kilograms. The cast iron balls were separated and the product was set for wet screening using a 200 U.S. Mesh sieve mounted on a vibratory sieve shaker. The undersize of the 200 Mesh screen was dewatered using a vacuum filter. Wet milling was later abandoned as the produced clays and fines blinded the vacuum filter.

Figure 18. Tumbling ball mill with timer.

Dry milling was done for the specimens with 250 grams of feed with 3.37kg of ball charge. Multiple tests were conducted by varying the milling time and keeping the feed and ball charge constant so as to find the optimum grinding time for reducing the feed to 90% passing the 200 Mesh. Finding the optimum grinding time for the samples is necessary to optimize the power required to liberate the REEs present in the coal and ash matrix. The samples were ground from 15 minutes to 120 minutes at intervals of 15 minutes. Due to the high inherent moisture, the Healy coal sample was dried at 110°C for 30 minutes prior to grinding.

3.2.2 Box-Behnken Design

In mineral processing, multivariate analysis has been applied to optimization of processes such as froth flotation (Azizi, Gharabaghi & Saeedi, 2014; Dube, 2012; Naik et al., 2004; Suresh et al., 2015), dense media separation (Amini, Honaker & Noble, 2016), dry gravity separations (Ghosh, Honaker, Patil, & Parekh, 2014), and spiral concentrators (Honaker, Jain, Parekh & Saracoglu, 2007; Tripathy & Murthy, 2012). A total of 17 experiments based on Box-Behnken test design were conducted in order to optimize the parameters associated with coal flotation (Box & Behnken, 1960). The tests were conducted in random order as delineated by the program so as to reduce systematic experimental error. REE enrichment (Equation 2), REE recovery and REE concentration were measured as responses after completion of the tests. In the Box-Behnken method, significant factors are recognized and then a response surface is predicted based on the quadratic interaction of these significant factors. The levels of variables studied are given in Table 11.

$$REE\ Enrichment = REE\ concentration * REE\ recovery \quad (2)$$

Table 11. Levels of Independent variables and their levels for Box-Behnken design.

				Coded Variable Level		
Parameter	Symbol	Units	Role	-1	0	+1
% Solids	A	%	-	4	7	10
Aero Froth 88	B	ppm	Frother	20	30	40
Fuel Oil	C	lbs/ton	Collector	0.5	0.75	1

Employing an analytical method has advantages, such as reduction in number of experiments, lower reagent consumption, and considerably less lab work; it also allows development of a mathematical model to describe the process by assessing the statistical significance of the factors under study as well as the significance of the interactions between the factors. This also leads to discovering that the optimum conditions, using multivariate analysis as the effect of different levels of variables with each other, cannot be evaluated by analyzing one factor at a time (Ferreira et al., 2007).

The approach of the Box-Behnken statistical design of experiments has been used in this study to establish the best set of variables and their main and interaction effects on the response variable. The input variables of the experimental study are collector dosage (0.5–1.0 lbs/t), frother dosage (20–40 ppm), and % Solids (4-10 %).

The following parameters were held constant at the levels indicated: Impeller Speed=2100 rpm; conditioning time=15 min; and froth collecting time= 3 min. REE

enrichment was estimated using Equation 2. The optimum conditions for maximizing the REE enrichment were determined by means of a three-factor, three-level Box-Behnken experimental design combining response surface modeling and quadratic programming.

3.3 Leaching and Extraction

The proximate, sulfur and REE+Y+Sc analyses for the study were performed by ALS commercial labs. Upon ashing the clean coal, 0.100 grams of ash is mixed with 0.9-1.2 grams of Li-Borate (35.3 % Lithium Tetraborate and 64.7% Lithium Metaborate) and completely fused at 1050°C. This breaks the silicon matrix, or the lattice, and releases the REEs from the glassy matrix. The pearl obtained after this fusion is then added to a three-acid solution (HNO3+HF+HCl 5% volume/volume). The REEs leach out to the pregnant solution with 95% recovery, and this solution is then used for REE analysis using ICP-MS. Lithium Borate fusion followed by three-acid leaching has 10% higher recovery than a conventional four-acid direct leaching, which has a recovery of about 85%. Lithium Borate cannot be recovered from this process (ALS Global, 2014).

Extraction of REEs by ion exchange has been done efficiently for 500 to 3000 ppm of REE concentration in the feed material. Commercial operations in China have used sodium chloride and ammonium sulfate solutions as lixiviants. The REE extraction process can be done in a vessel, heap leaching or in situ. The leach solution can then

be precipitated by the addition of oxalic acid or ammonium bicarbonate (Rozelle et al., 2016).

Joshi et al. (2015) in their patent application for recovery of REEs from coal ash, suggested treatment of the REE bearing coal ash with a mineral acid to form an aqueous mineral acid solution followed by extracting an organic solution containing the rare earth salts from the aqueous mineral acid solution. The organic solution can then be mixed with water to form an aqueous solution from which the rare earth elements can be separated. The flowsheet for the process is shown in Figure 19. The method delineates treating coal ash that includes rare earth elements with 3 Normal (N) nitric acid at 90°C for one hour to get a concentrated mixture. The resultant aqueous mineral acid solution is then mixed with equal or predetermined volume tributyl phosphate and kerosene, and the organic solution containing the rare earth salts is then separated from the aqueous mineral acid solution. The rare earth elements can then be separated by either anion or cation exchange, and the mineral acid can be recovered by distillation.

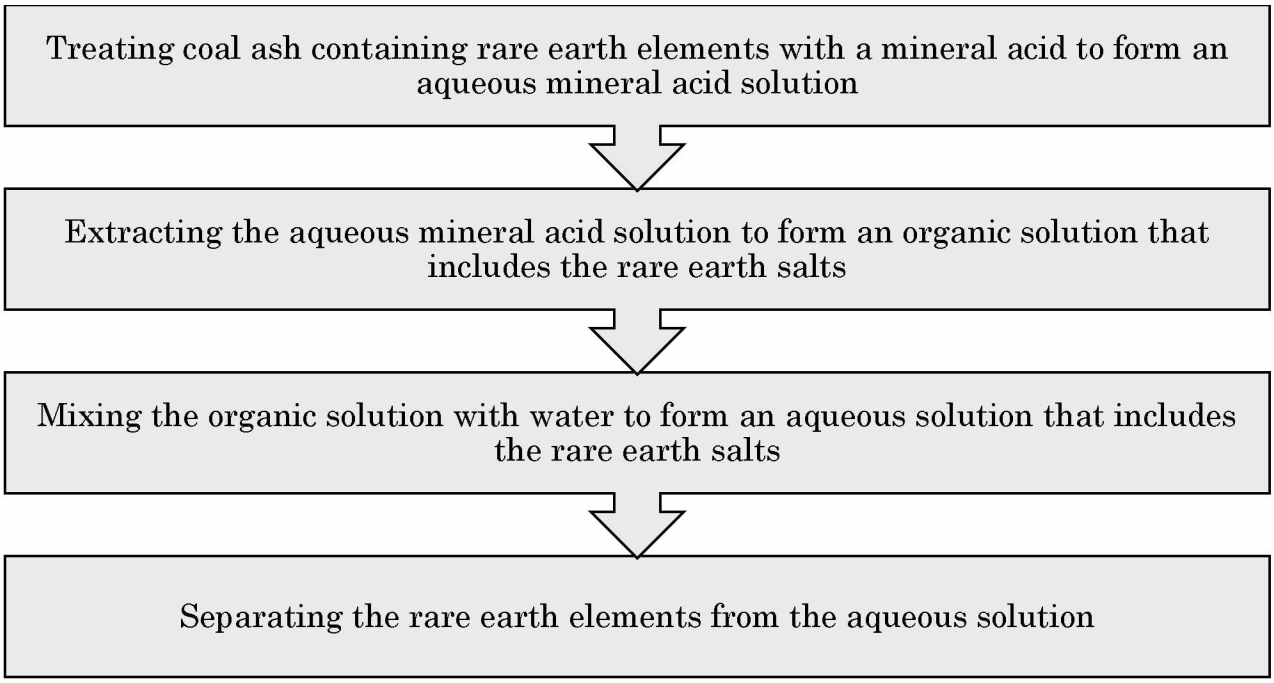

Figure 19. Flowsheet for extraction of REEs from coal ash (Joshi et al., 2015).

An environmentally benign solution for REE extraction from coal ash was proposed from a study conducted at Harvard University in 2016 by Bonificio & Clarke. They demonstrated an alternative, biogenic method based on the adsorption of lanthanide to the bacterium Roseobacter sp. AzwK-3b, immobilized on an assay filter, followed by subsequent desorption as a function of pH.

The Roseobacter sp. AzwK-3b is a Gram-negative marine bacterial strain whose genus has been shown to be a strong metal absorber. The bacteria is immobilized on an assay filter, and a pregnant solution containing the REEs is passed through it. The bacteria bio absorbs the lanthanides with slightly higher preference for middle lanthanides, plucking them out of the solution and fixing them to their surface. Subsequently, the filter is washed with solutions of various pH balances, and each

successive pH wash detaches different rare earths. The findings indicate that more light lanthanides desorbed with higher-pH washes, and more heavy lanthanides desorbed with lower-pH washes. The method can be used for selective extraction of REEs and offers a clean way to produce these valuable elements as the pH of the solution wash is no more acidic than hydrochloric acid. The findings suggest that there is an opportunity to harness the diversity of bacterial surface chemistry to separate and recover technologically important rare-earth metals in an environmentally benign manner (Figure 20) (Bonificio & Clarke, 2016).

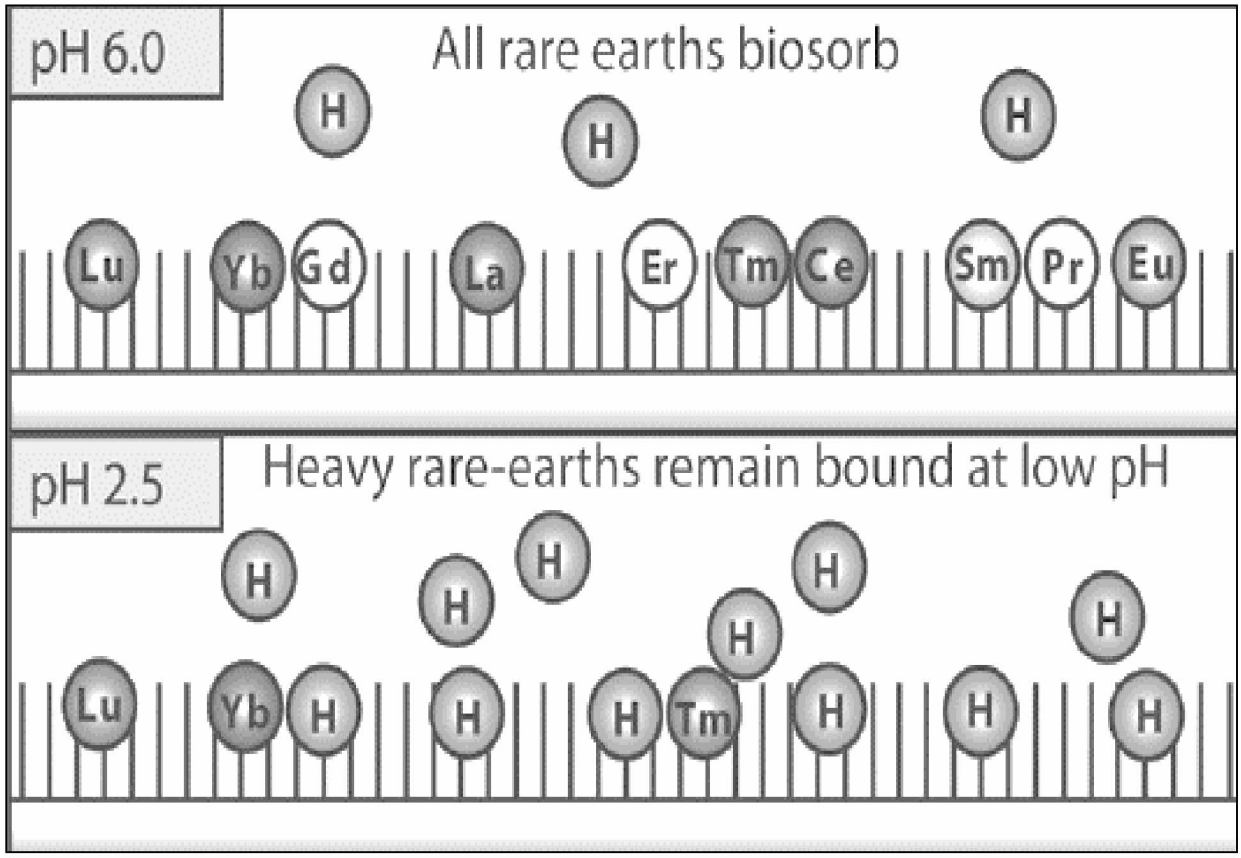

Figure 20. REE extraction using microbial biosorption and desorption as a function of pH (Bonificio & Clarke, 2016).

CHAPTER 4 RESULTS AND DISCUSSION

4.1 Characterizing REEs in Alaskan Coal

4.1.1 Size Analysis

The representative sample characterization provided in Table 12 and Table 13 shows that the majority of the screened sample was greater than 30 Mesh in size for both Healy and Wishbone Hill coal samples. The two-stage crushing resulted in a very small amount of the finer fraction (<100 Mesh), with 2.55% for the Healy and 1.25% for the Wishbone Hill coal samples, respectively. The Healy sample was found to have high inherent moisture content of around 18% with 22% ash on dry basis. The Wishbone Hill sample had very low moisture content of around 4% with high ash content of 46% on dry basis.

Table 12. Size-by-size proximate analysis of the Healy coal sample.

Healy Coal							
U.S. Mesh Size		% Weight	% Moisture	Dry Wt. %	Ash %	Volatile Matter %	Fixed Carbon %
	+1/4 inch	2.39	18.04	2.38	19.21	41.53	21.22
-1/4 inch	+30M	85.72	17.98	85.27	20.55	35.11	26.36
-30M	+100M	9.34	14.52	9.69	29.40	35.98	20.10
-100M		2.55	13.64	2.67	31.33	36.14	18.89
TOTAL		100.00	17.55	100.00	21.62	35.37	25.46

Table 13. Size-by-size proximate analysis of the Wishbone Hill coal sample.

Wishbone Hill Coal							
U.S. Mesh Size		% Weight	% Moisture	Dry Wt. %	Ash %	Volatile Matter %	Fixed Carbon %
	+1/4 inch	9.72	3.9	9.75	49.93	25.00	21.17
-1/4 inch	+30M	80.09	4.2	80.07	44.18	25.49	26.13
-30M	+100M	8.93	4.24	8.93	55.48	25.83	14.45
-100M		1.25	3.7	1.26	60.97	23.29	12.04
TOTAL		100.00	4.17	100.00	45.96	25.45	24.43

The results from the investigation of REE+Y+Sc in the whole sample, shown in Figure 21, revealed that REEs in Wishbone Hill Coal are dominated by Ce, Y, Nd, La and Sc attributing to about 82% of the total available REE concentration, whereas 77% of the total REEs in Healy are Ce, La, Nd and Y. The dark and the light sectors represent lanthanides of odd and even atomic numbers, respectively. Yttrium and Scandium are indicated as shaded regions. The abundance of elements with even atomic numbers in the analyses align with the Oddo-Harkins Rule: that the abundance of elements with an even number of protons is higher than its neighbors with an odd number of protons.

Concentration of REEs in the samples, as shown in Figure 22, indicated that both coals are enriched with higher concentrations of LREEs than HREEs. On a whole sample basis Wishbone Hill coal was found to have higher REE content than Healy coal. Upon ashing, however, the concentration of total REEs in Healy coal was found to be about 524 ppm and about 286 for Wishbone Hill. The upgrade potential of both

LREEs and HREEs for Healy coal was about 4:1 from whole coal to ash basis. Similarly both LREEs and HREEs in Wishbone Hill coal had an upgrade potential of 2:1 from whole coal to ash basis.

Additionally, REEs are higher in the >1/4 inch and <100 Mesh size fractions of Healy, while REEs have higher concentration in particle sizes greater than 30 Mesh in Wishbone Hill (Figure 23 and Figure 24, respectively).

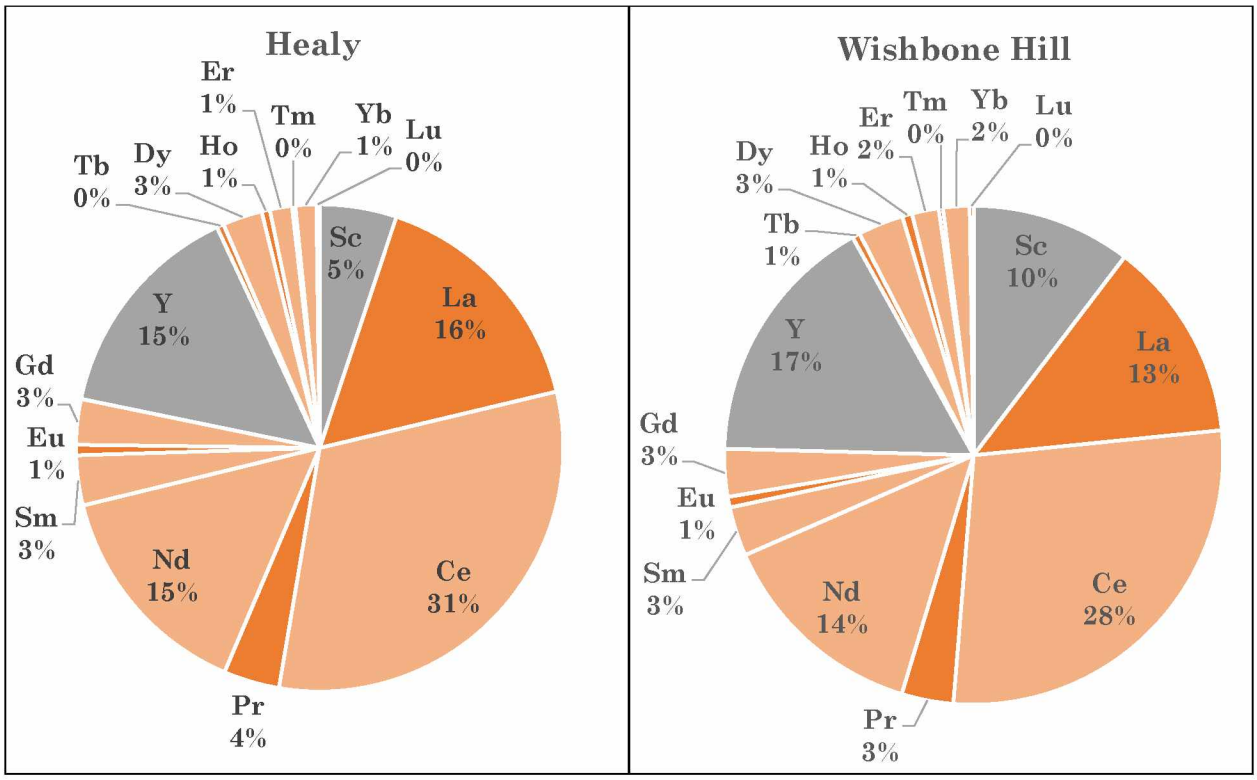

Figure 21. Percentage distribution of individual REEs in the coal samples. Lanthanide elements with odd atomic numbers are in dark sectors while elements with even atomic number are in light sectors. Y and Sc are shown by a different shade.

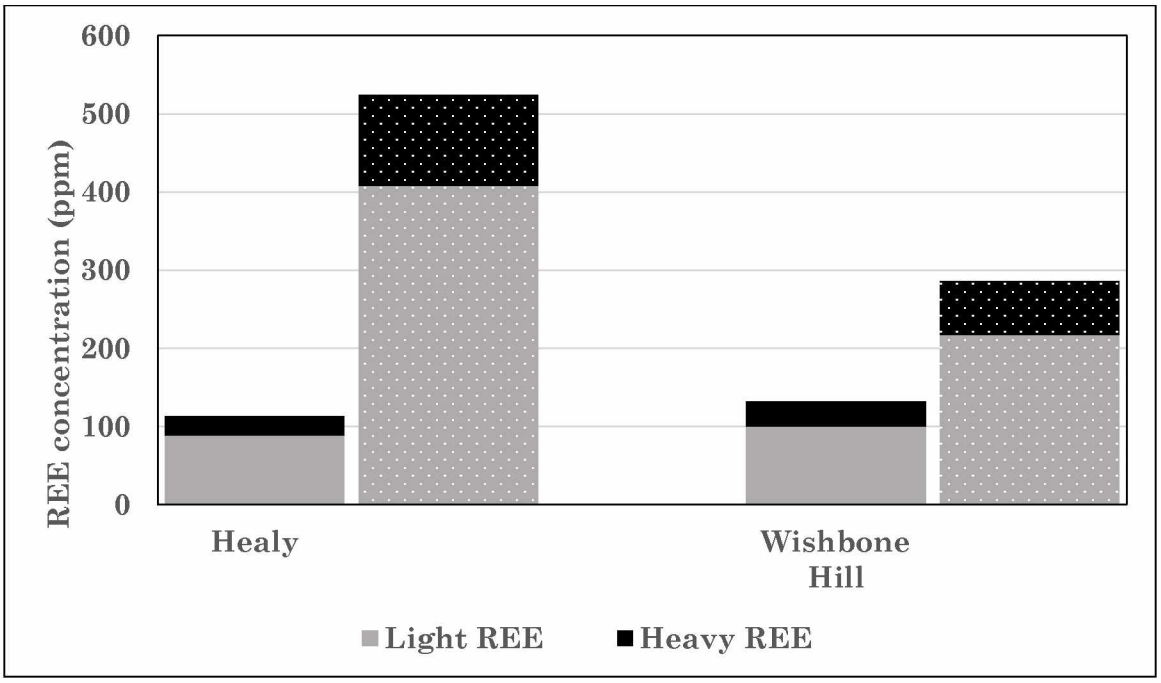

Figure 22. Distribution of HREE and LREE in Healy and Wishbone Hill coal samples. The solid bars are the REE concentrations on whole sample basis and the checkered bars are REE concentrations on ash basis.

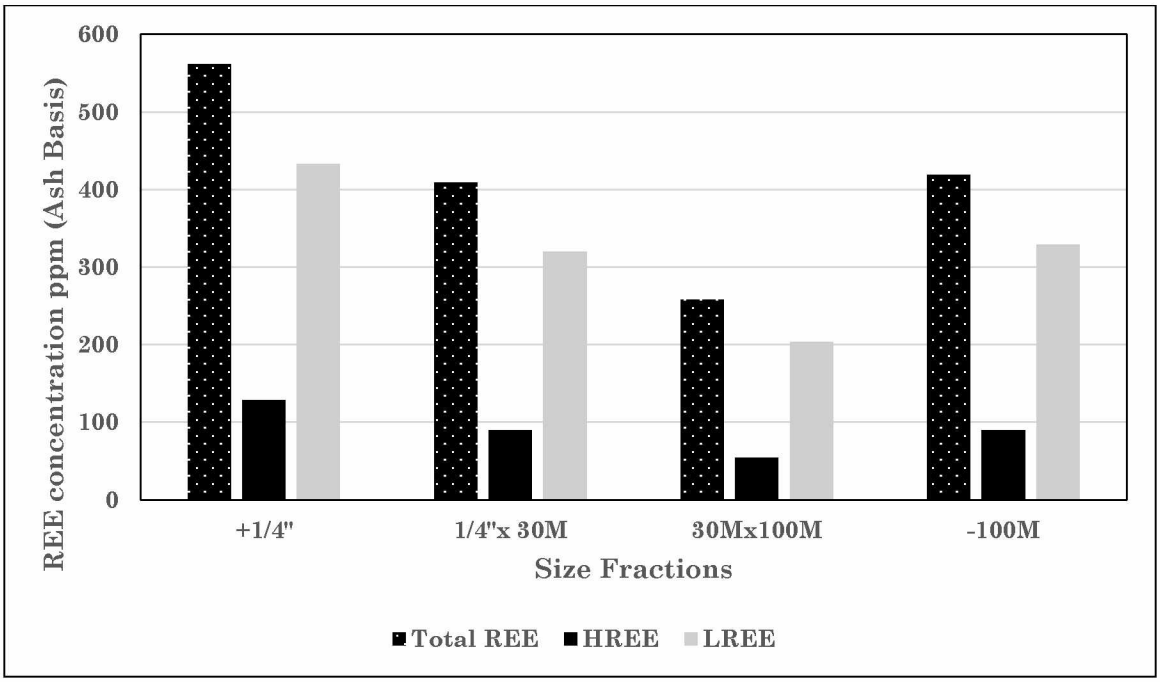

Figure 23. REE distribution on the basis of size for Healy.

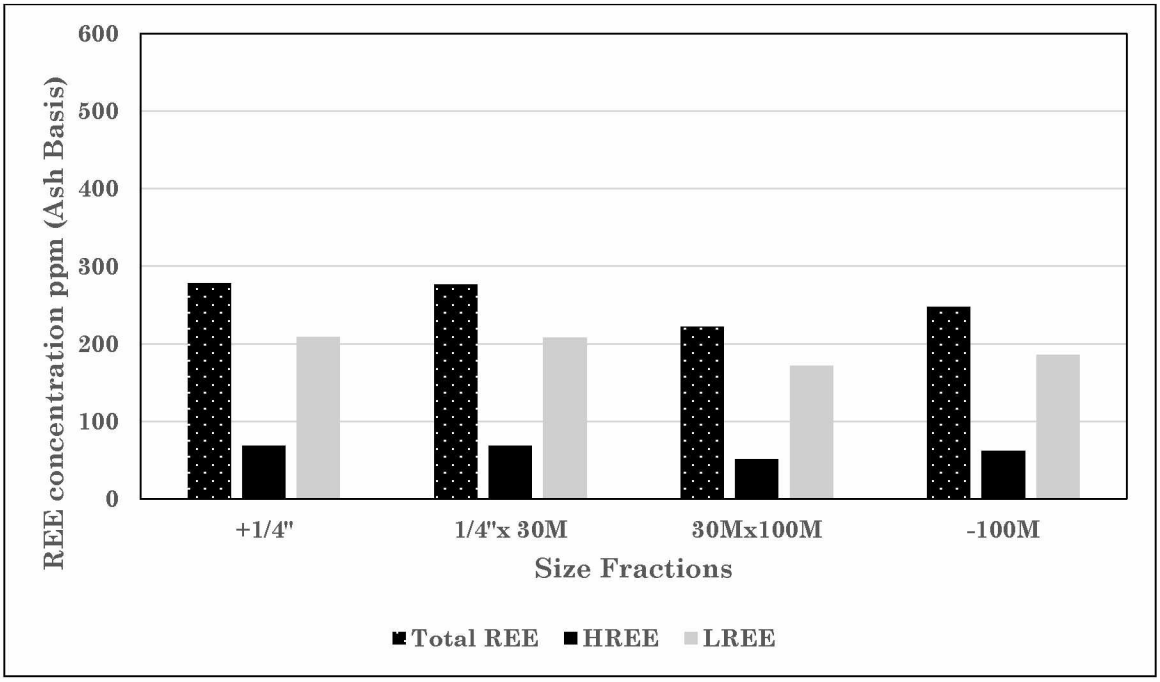

Figure 24. REE distribution on the basis of size for Wishbone Hill.

4.1.2 Float and Sink Tests

The float and sink samples of density fractions ranging from 1.3 to 2.20 specific gravity were analyzed for REE+Y+Sc contents apart from proximate and sulfur analyses (Appendix A, Appendix B, Appendix C, Appendix D and Appendix E). The results for the two coal samples are summarized in Figure 25 and Figure 26. It is observed that all float-sink density fractions for both Healy and Wishbone Hill are predominantly richer in LREEs than HREEs. The trend of the total REEs follows the trend of distribution of LREEs in these samples. The ash contained in the lighter density fractions of Wishbone Hill (i.e., SG less than 1.3), are rich in REEs and have concentrations up to 857 ppm in the <1/4 inch to 30 Mesh Size fraction. The 1.3 floats of Wishbone Hill have an upgrade potential of 16.5:1. Healy has an overall upgrade potential of more than 400% and Wishbone Hill has more than 200% enrichment from whole coal to ash. The washability curves as a results of a series of float and sink tests for both coals are shown in Figure 27 and Figure 28. Washability curves are essential for designing a coal cleaning plant.

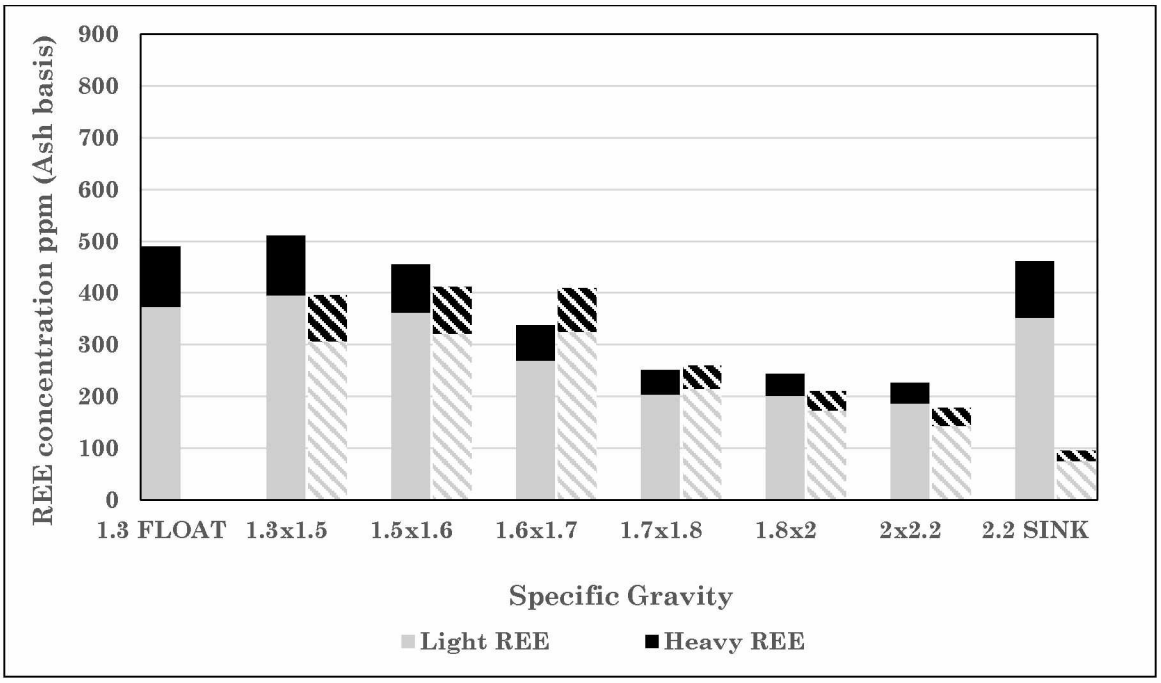

Figure 25 REE distribution on the basis of specific gravity for Healy. The solid bars are the REE concentrations for <1/4 inch to 30 Mesh and the checkered bars are for 30 Mesh to 100 Mesh size fractions.

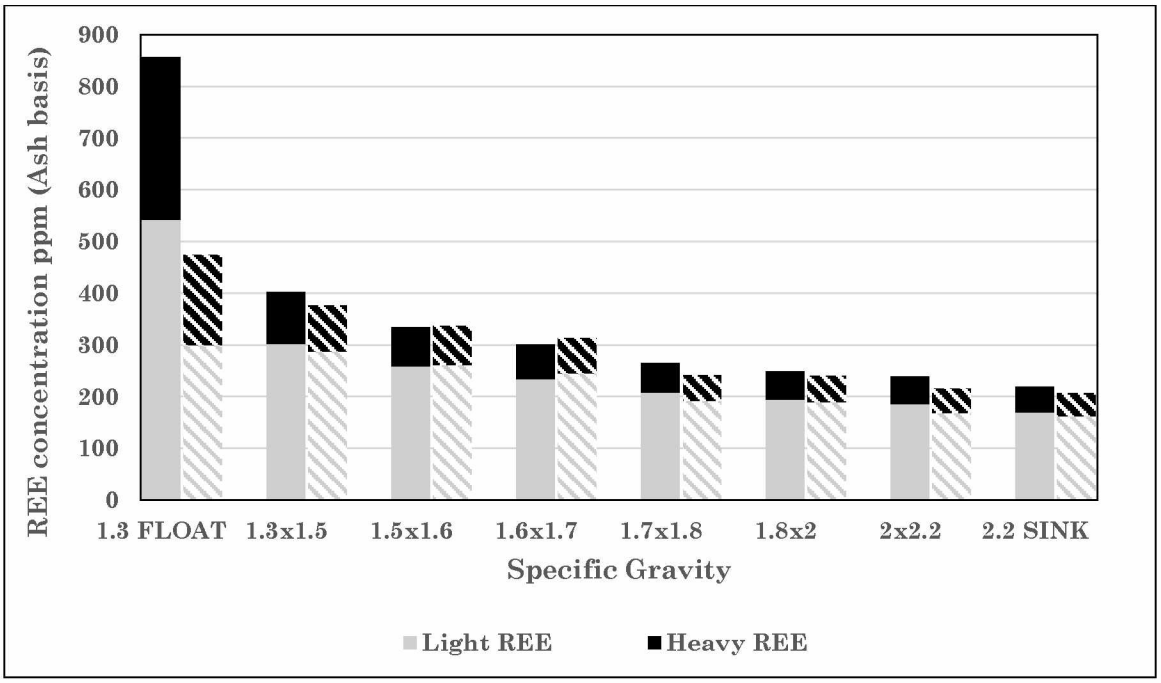

Figure 26. REE distribution on the basis of specific gravity for Wishbone Hill. The solid bars are the REE concentrations for <1/4 inch to 30 Mesh and the checkered bars are for 30 Mesh to 100 Mesh size fractions.

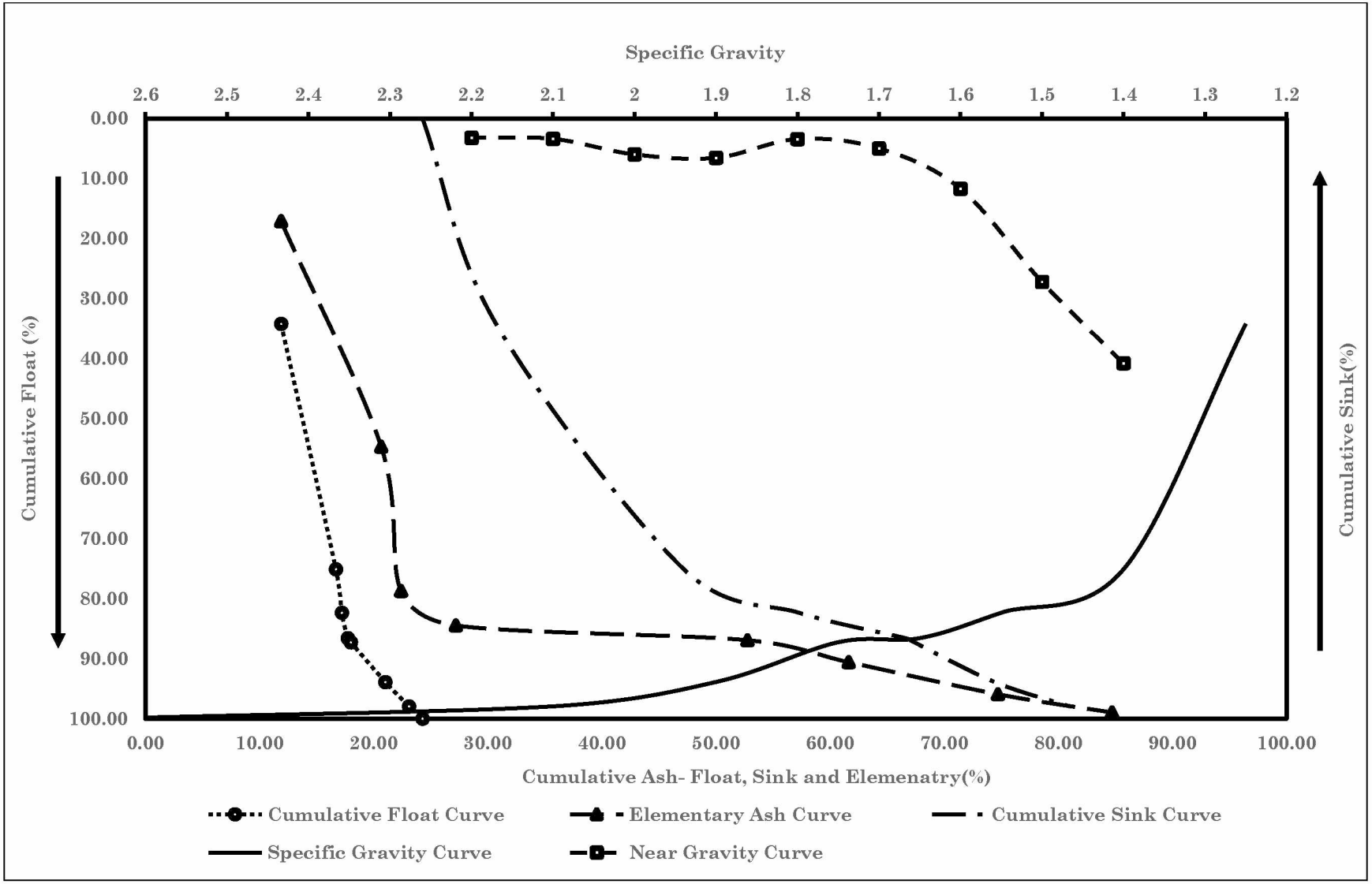

Figure 27. Washability Curves for composite Healy coal sample.

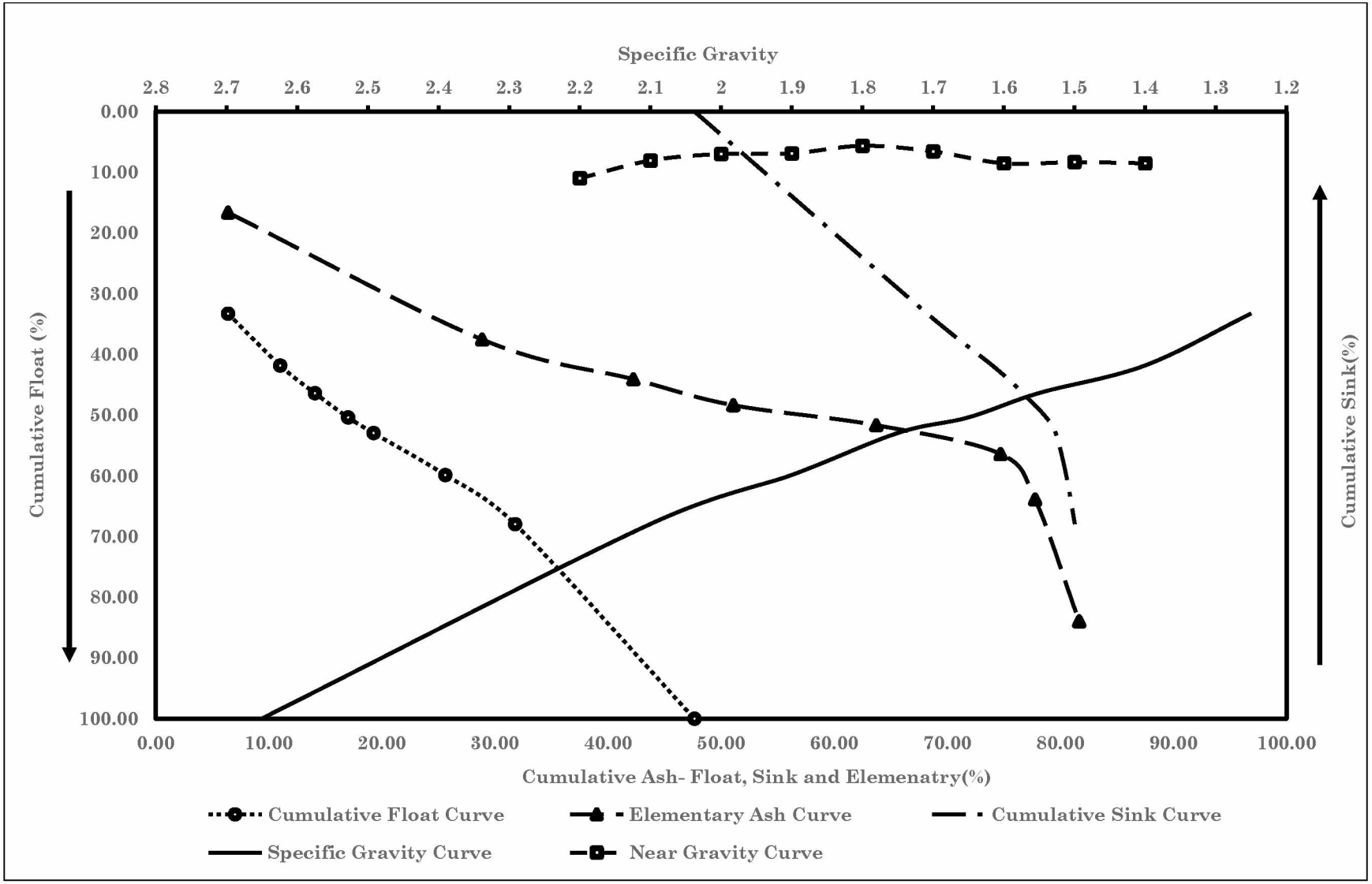

Figure 28. Washability Curves for composite Wishbone Hill coal sample.

4.1.3 Magnetic Separation

From Figure 29, magnetic fractions from both coals appear to be very small compared to non-magnetics (especially for Healy fines, which are around 1%). The Wishbone Hill magnetic fraction is about 12%. For both coals high ash fractions were found to be reporting to magnetics. Conversely sulfur was retained in non-magnetics together with fixed carbon and volatile matter (Appendix F). Wishbone Hill fines contain higher Sc in non-magnetics than that of Healy (Appendix G). LREE are equally distributed between magnetics and non-magnetics for Wishbone Hill fines, except Sc, Sm and Gd, which were richer in magnetics. This trend is similarly observed in Figure 30 for HREE content of the Wishbone Hill. HREE appear to be preferentially reporting to magnetic fractions.

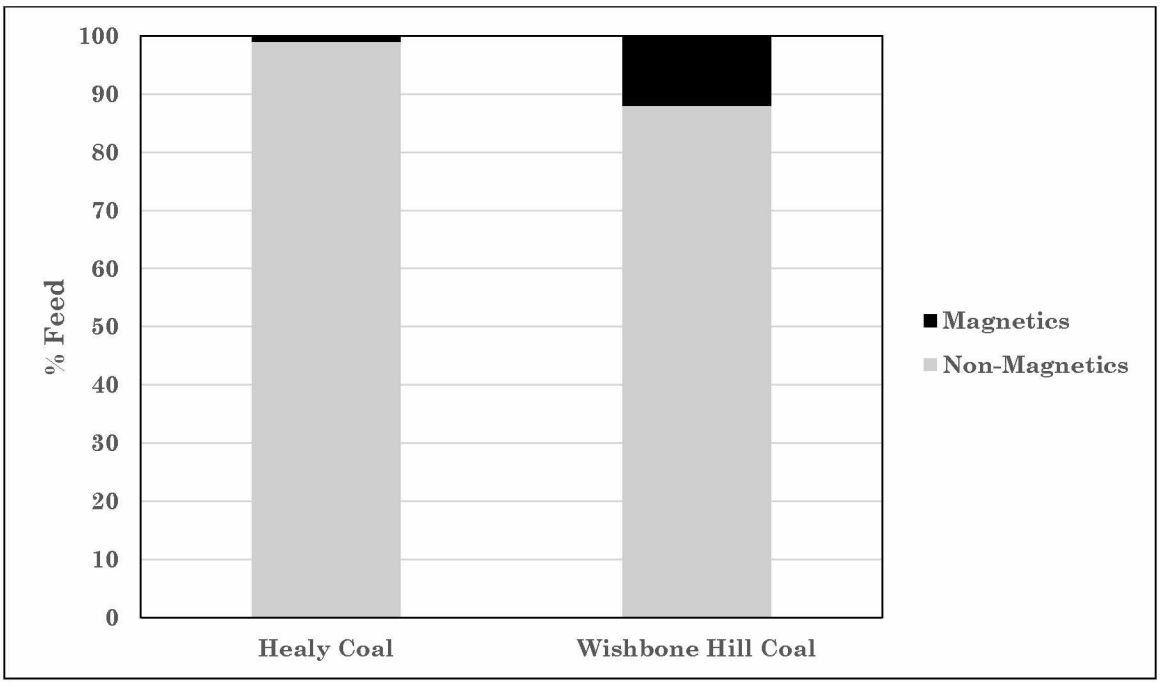

Figure 29. Distribution of magnetic and non-magnetic material in the coal samples of Healy and Wishbone Hill.

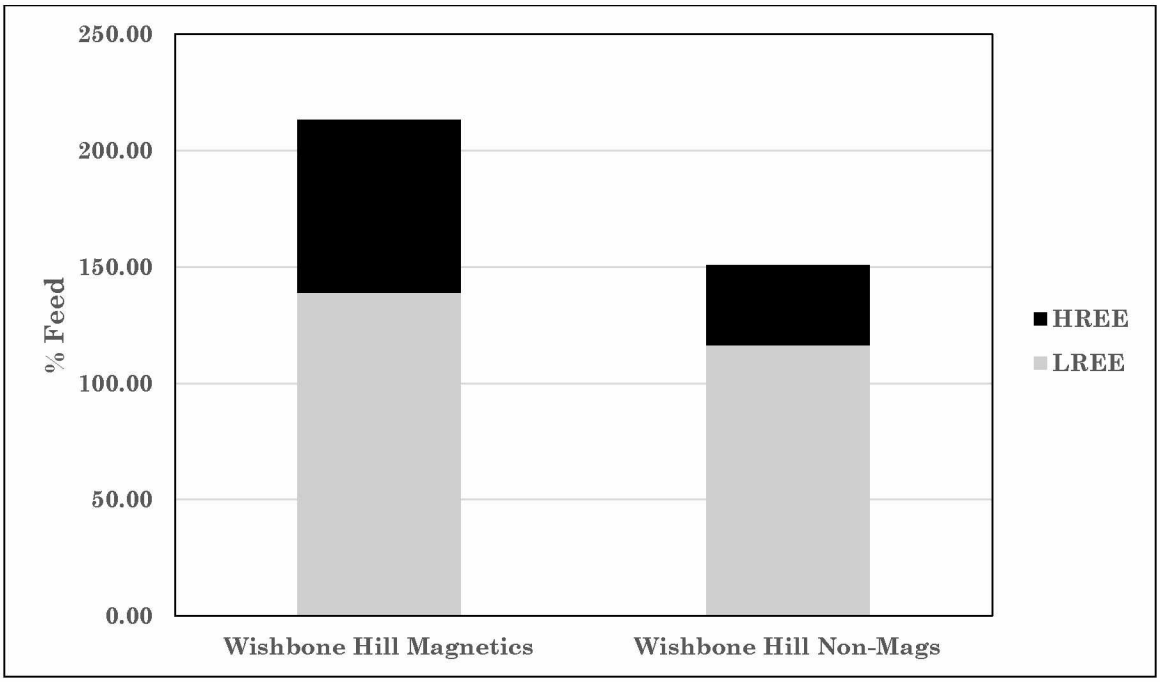

Figure 30. Distribution of LREE and HREE in magnetics and non-magnetics of Wishbone Hill Coal.

4.1.4 Scanning Electron Microscope Analysis

The elemental composition of the coal and ash samples was studied using SEM and the sample composition is presented in Table 14. The composition of Wishbone Hill coal showed lower amounts of calcium and its oxides as compared to Healy. Wishbone Hill coal inorganics had higher silica content than Healy. Inorganic parts of coal were comprised primarily of SiO_2, Al_2O_3, and Fe_2O_3. Titanium and potassium were detected in trace amounts for both coals. In coal combustion products, magnesium, titanium, potassium and sulfur were detected in trace amounts. Post-combustion fly ash retained more calcium originating from the source while aluminum was concentrated in bottom ash. The silicon-to-aluminum ratio for the coal combustion products (BA=0.61,

FA=0.44 and Cinders =1.25) was lower than the parent Healy coal (1.75), indicating formation of lower strength bonds of Al-O-Al or Al-O-Si than strong bonds of Si-O-Si.

Table 14. Mineralogical composition analysis of the samples.

	Healy	Wishbone Hill	Cinders	Fly Ash	Bottom Ash
Component	% wt. in ash	%wt. in ash	% wt.	% wt.	% wt.
MgO	-	-	3.25	5.89	0.95
Al2O3	27.27	31.64	23.15	29.08	46.95
SiO2	47.78	59.56	29.13	12.86	28.73
SO3	-	-	4.17	12.09	2.78
K2O	2.47	3.13	0.84	3.03	1
CaO	10.54	0.39	25.36	27.25	10.25
TiO2	2.44	1.46	0.78	1.42	2.91
Fe2O3	9.49	3.81	13.33	8.36	6.44
Total	100	100	100	100	100

Solid spheres were seen in cinder and fly ash samples when viewed under an SEM. These hollow spheres are the results of ash fusion in the boilers of the power plant due to high temperatures. Porous particles and spheres of sizes ranging from a few microns to 500 microns do not have a smooth texture (Figure 31 and Figure 32). Bottom ash particles exhibit a glassy matrix with elements intricately fused together (Figure 33). The pulverized coal particles ranged from a few microns to 100 microns and were of irregular shape (Figure 34). It is evident from the images that the samples were 90% passing the 200 Mesh (75 microns). The black background of the images is attributed to the carbon tape on which the particles were glued for imaging.

(a)

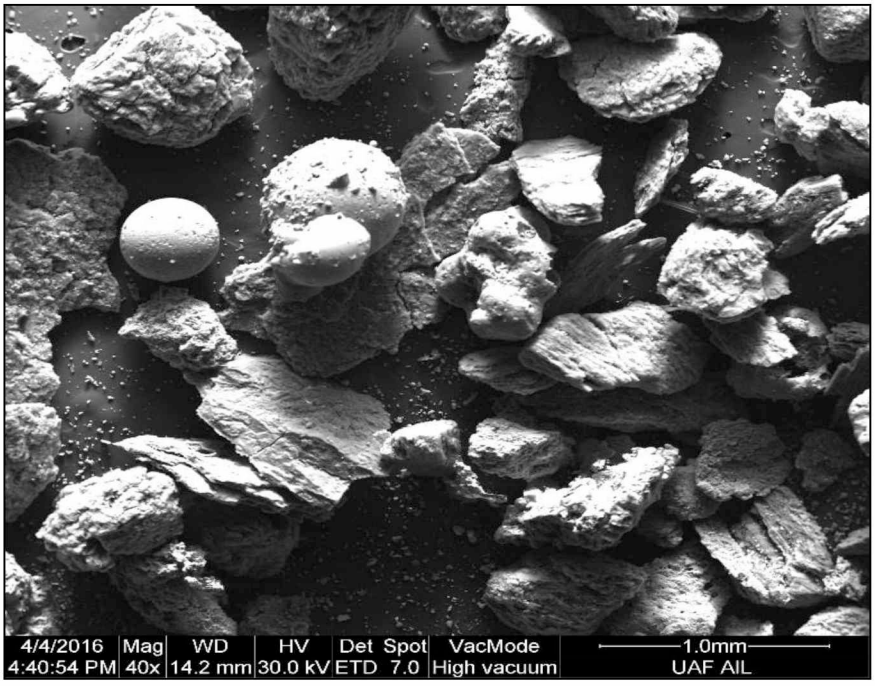

(b)

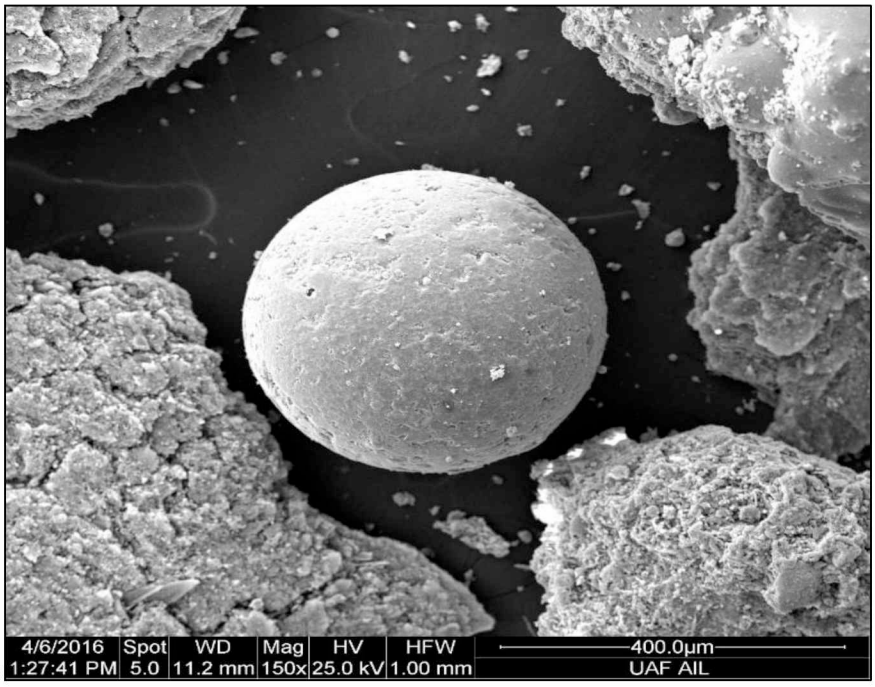

Figure 31. SEM images of Cinders with Quanta 200 ESEM with (a) lower and (b) higher magnification.

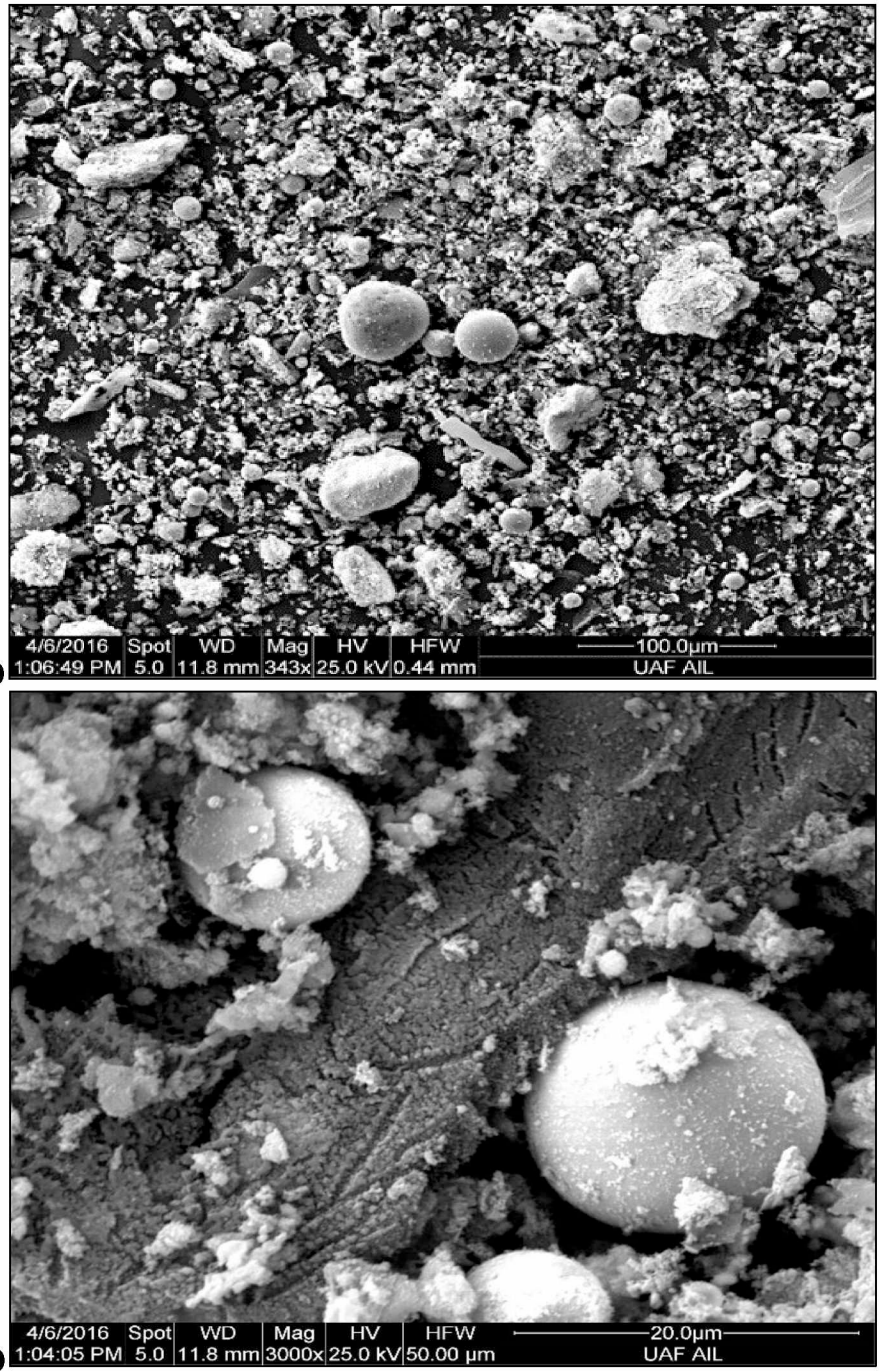

(a)

(b)

Figure 32. SEM images of Fly Ash with Quanta 200 ESEM with (a) lower and (b) higher magnification.

(a)

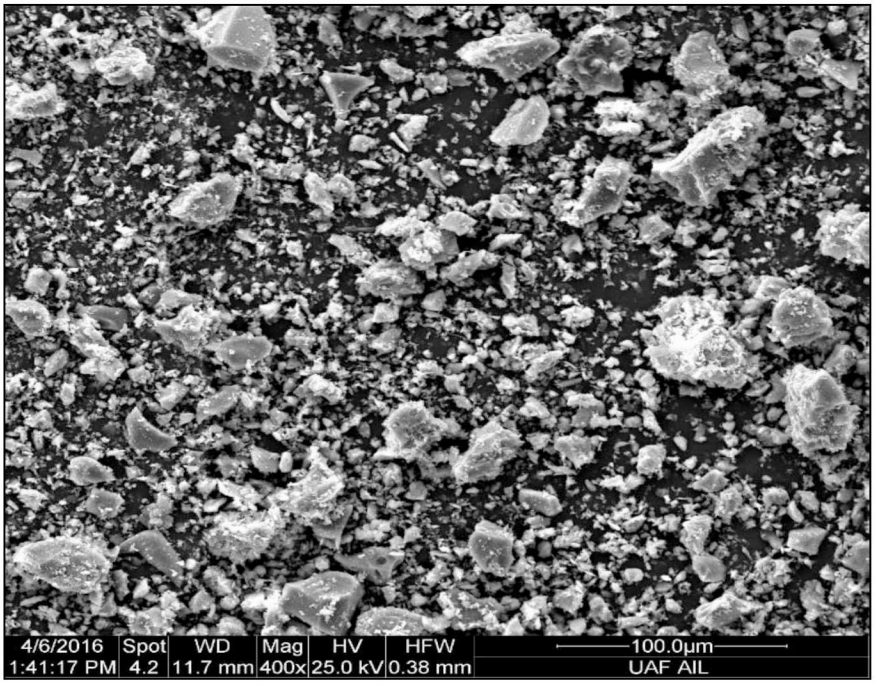

(b)

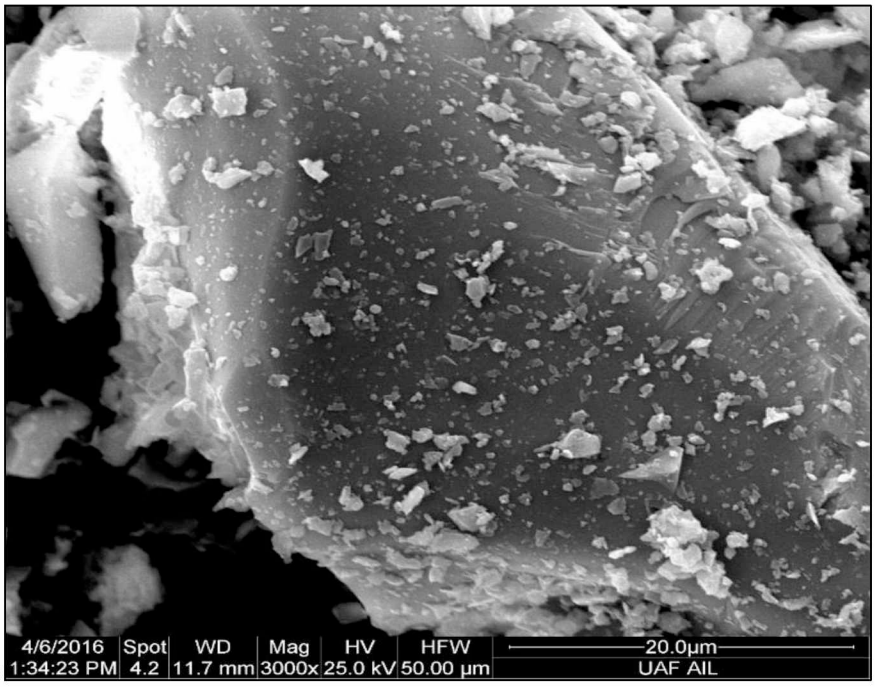

Figure 33. SEM images of Bottom Ash with Quanta 200 ESEM with (a) lower and (b) higher magnification.

(a)

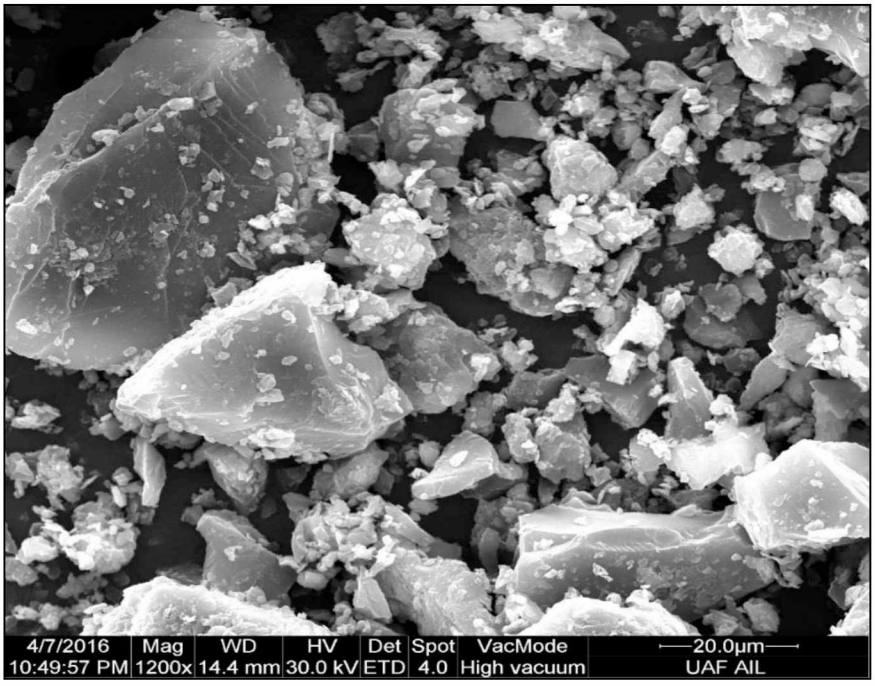

(b)

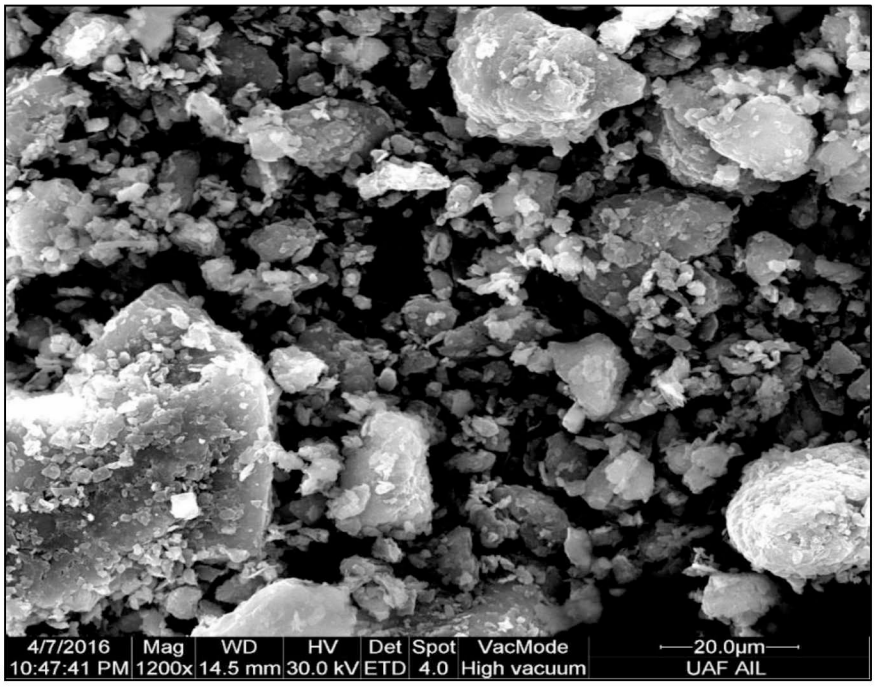

Figure 34. SEM images of (a) Healy and (b) Wishbone Hill Coal samples with Quanta 200 ESEM.

4.1.5 Preliminary Froth Flotation Studies

Figure 35 and Figure 36 show the distribution of total REEs, LREEs and HREEs in the floats and tailing fractions of the Healy and Wishbone Hill fines after froth flotation. The float fraction yield values of Healy and Wishbone Hill coals were 26% and 30%, respectively. The tailings displayed much higher ash content, especially Wishbone Hill tailings, with about 75% of ash content and reduced volatile matter and fixed carbon (Appendix H). Proximate analysis of Healy flotation products revealed that sulfur and volatiles were equally distributed between tailings and floats. Furthermore, a relatively small difference was observed in the ash content between the tailings and floats as compared to Wishbone Hill fines. The percentage distribution of individual REEs remained almost the same in the floats and the tailings for both Healy and Wishbone Hill samples (Appendix I). Both LREE and HREEs were concentrated more in the float fractions than tailings on ash basis. This correlated well with the findings of the float and sink tests. The findings indicated that the ash residues of lower specific gravities of Alaskan coals are much richer in REEs than the higher density counterparts.

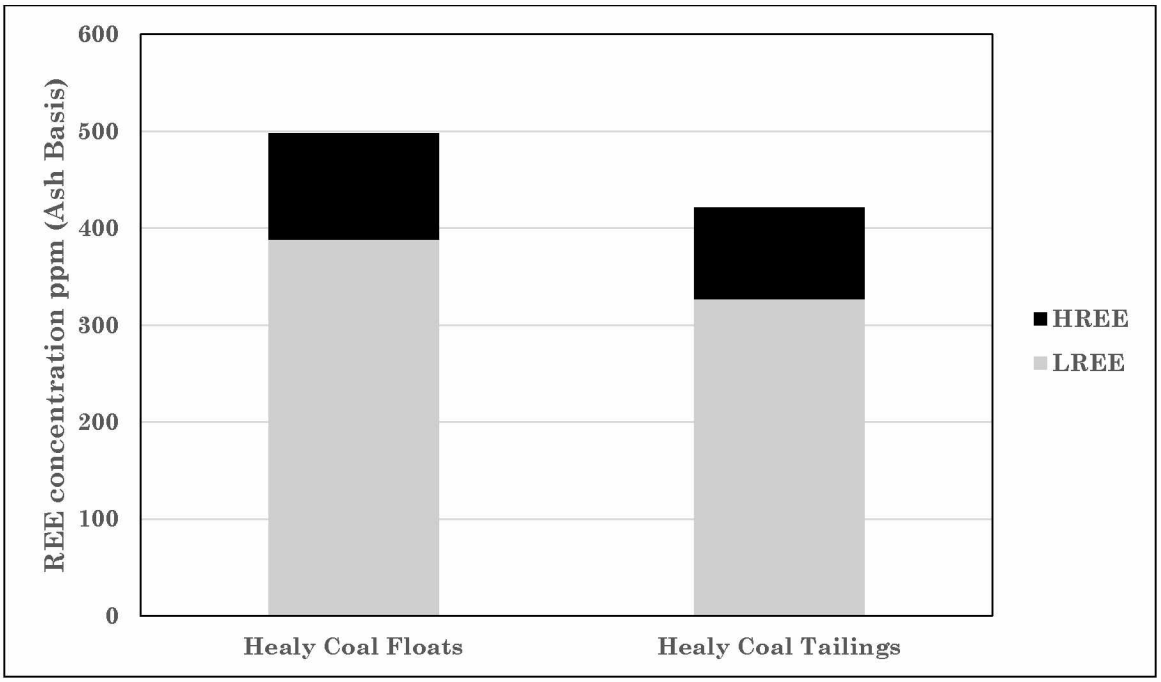

Figure 35. Total HREE and LREE distribution in the flotation products of Healy.

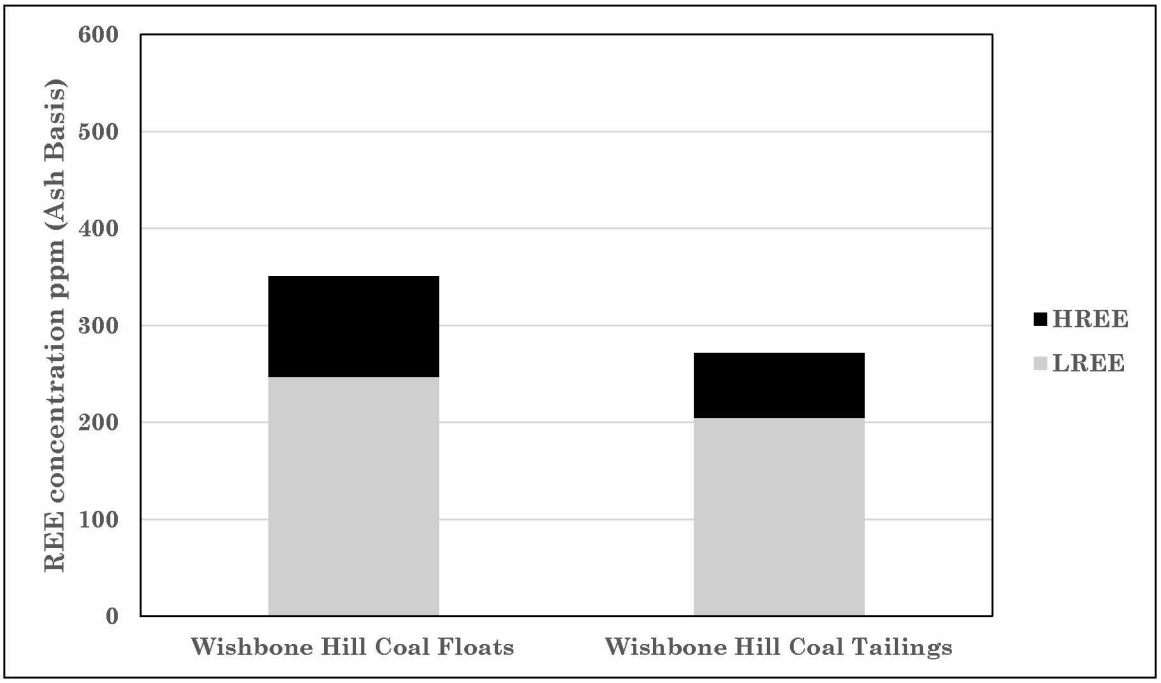

Figure 36. Total HREE and LREE distribution in the flotation products of Wishbone Hill.

4.1.6 REE Content in Ash Samples from UAF Power Plant

Incomplete combustion residue (i.e., cinders (C)), expectedly contained large amounts of fixed carbon and volatiles with around 67% ash product as found in proximate and sulfur analysis. Fly-ash had also retained some carbon and volatile matter with high concentrations of sulfur. Conversely, bottom ash had very small amounts of volatile matter and sulfur, around 99% ash with no carbon in it. In trends of REE contents of the power plant products, percentage distribution of individual REEs were found to be the same for all three samples (Figure 37). Also, Figure 38 revealed that all three byproducts have almost the same REE concentration on ash basis. The differences in concentrations distributed between the products were relatively low and preferential enrichment of individual REEs was not observed.

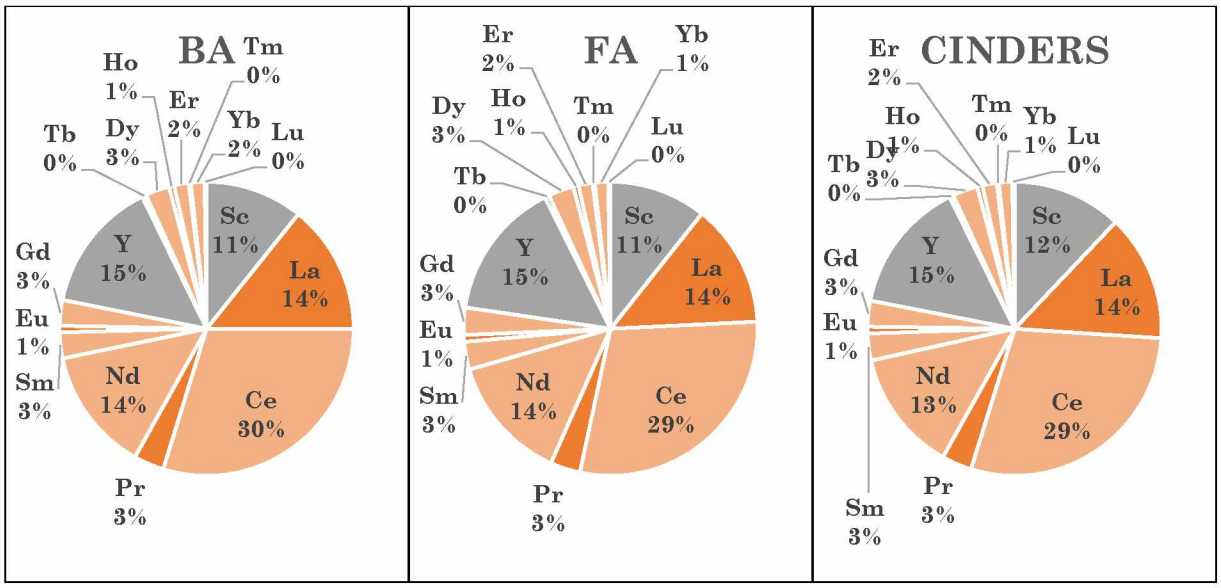

Figure 37. Distribution of individual REEs in coal combustion products.

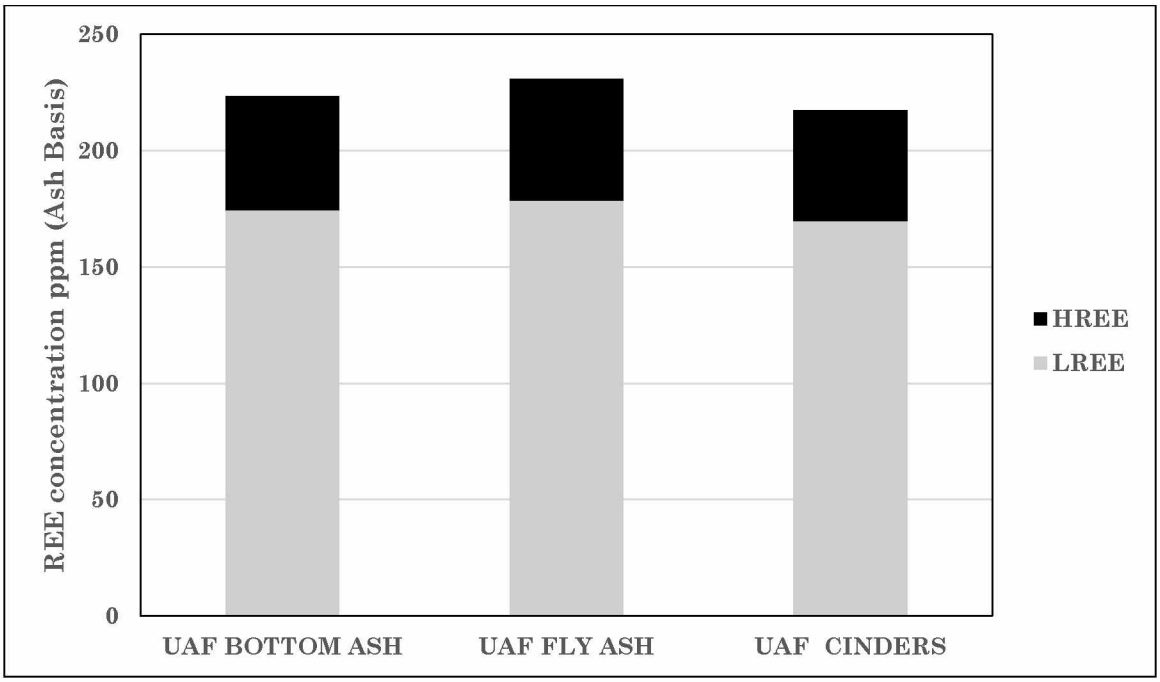

Figure 38. REE distributions of UAF power plant products.

4.2 Statistically Designed Experimental Program for Froth Flotation

4.2.1 Sample Preparation and Grinding Tests

The grinding test results shown in Figure 39 revealed that the optimum batch grinding times for Wishbone Hill and Healy are 40 and 120 minutes, respectively. For flotation tests samples are ground to 90% 200 Mesh (75 Microns). Furthermore, grinding time for coal combustion products was found to be less than the parent coal. The data obtained by SEM analysis is cross validated by the results of grindability tests. The silicon-to-aluminum ratio for coal byproducts was found to be less than parent coal, which attributes to lesser grinding time for bottom ash and cinders as compared to their parent, Healy coal.

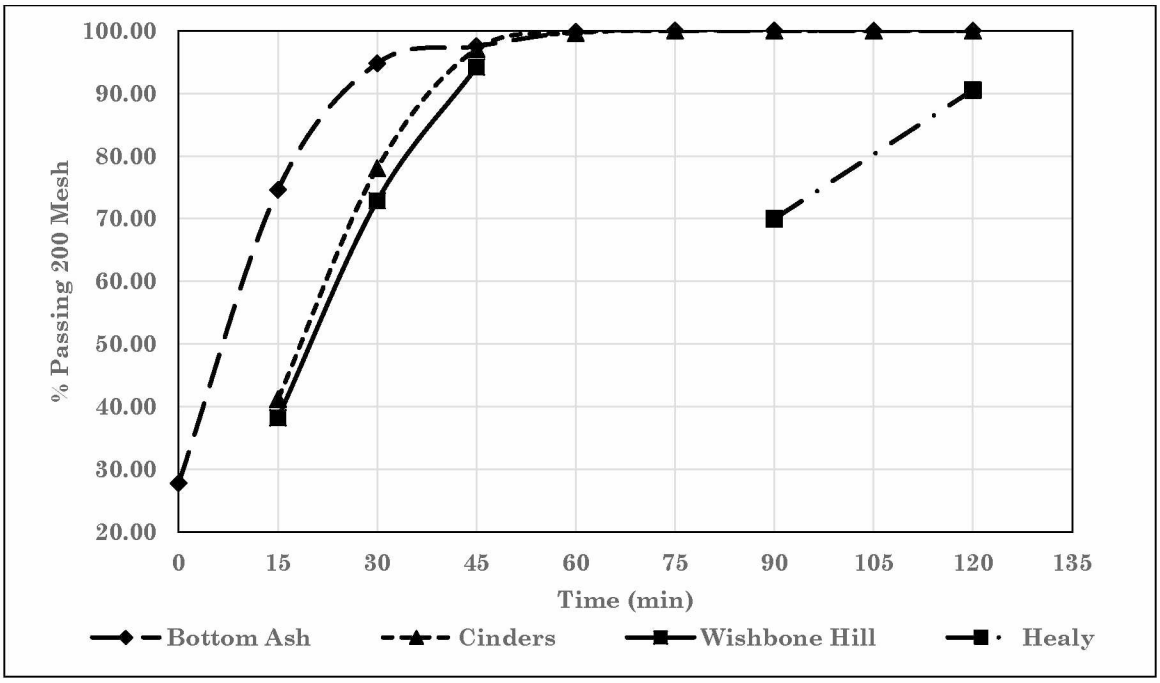

Figure 39. Optimum grinding time for the coal and ash samples.

4.2.2 Box-Behnken Design

From the characterization studies it was established that REEs are predominantly concentrated in the ash residues of clean coal. It was also previously established in Chapter 2 that REEs in coal are present in the 1-10 microns size fraction. Thus, liberating REEs by grinding and concentrating clean coal by froth flotation seemed to be a viable option. A parametric experimental test was designed using a three-factor, three-level Box-Behnken design in order to investigate the individual and interaction effects of three operational parameters (frother dosage, collector dosage and pulp density).

A total of 17 experiments were conducted so as to optimize the parameters associated with froth flotation of REE rich coals. The tests were done in a random run-order so as to reduce systematic experimental error. REE Enrichment, REE Recovery and

REE Concentration were measured as responses. The results from flotation tests for Healy and Wishbone Hill are shown in Table 15 and Table 16. The results were used to develop empirical models that describe the parameter and parameter interaction effects on the response variables.

The significance of the empirical model was tested based on the p-values obtained from the Analysis of Variance (ANOVA). ANOVA is one of the most organized and logical approaches for analysis of a factorial design test to obtain vital information for understanding the process behavior. Empirical equations were built to predict the response based on the individual and combined effects of the controllable variables. The significance of each parameter and their interactions were tested against the null hypothesis that the coefficient for the variable is null. The terms that obtain a p-value less than 0.10 in an overall F-test were considered significant. All insignificant parameters were removed by backward elimination. High adjusted R^2 value was used as a measure to determine the efficacy of the best-fit model to the data. Additionally, the models were tested against the following regression assumptions:

1. Residual errors for the selected models were found to be independent;
2. Residual errors for the selected models were found to be distributed normally with a mean value of zero;
3. The variance of errors for the selected models was found to be constant across all the observations.

Table 15. Parameter values and the results for Healy coal flotation achieved from an experimental program conducted using three-level Box-Behnken design where three factors are: A – % solids, B – frother dosage in ppm, C – collector dosage in lbs/ton.

		Factor 1	Factor 2	Factor 3	Response 1	Response 2	Response 3
Std.	Run	A:	B:	C:	REE Enrichment	REE Recovery	REE Concentration
		%	ppm	lbs/ton		%	ppm
10	1	7	40	0.5	250.2	50.2	498.5
12	2	7	40	1	243.2	50.7	479.6
17	3	7	30	0.75	271.5	55.0	494.0
16	4	7	30	0.75	308.9	63.0	490.4
9	5	7	20	0.5	69.2	15.4	449.1
3	6	4	40	0.75	340.1	67.0	508.0
14	7	7	30	0.75	329.2	66.1	498.3
4	8	10	40	0.75	298.1	59.6	500.3
15	9	7	30	0.75	318.1	64.5	493.3
7	10	4	30	1	383.6	75.0	511.6
13	11	7	30	0.75	336.1	67.1	500.7
5	12	4	30	0.5	390.5	78.4	498.4
1	13	4	20	0.75	137.5	29.3	469.2
6	14	10	30	0.5	308.2	66.5	463.7
2	15	10	20	0.75	87.0	23.4	371.1
11	16	7	20	1	91.3	20.2	452.4
8	17	10	30	1	284.4	61.8	460.5

Table 16. Parameter values and the results for Wishbone Hill Coal flotation achieved from an experimental program conducted using three-level Box-Behnken design where three factors are: A – % solids, B – frother dosage in ppm, C – collector dosage in lbs/ton.

		Factor 1	Factor 2	Factor 3	Response 1	Response 2	Response 3
Std.	Run	A	B	C	REE Enrichment	REE Recovery	REE Concentration
		%	ppm	lbs/ton		%	ppm
10	1	7	40	0.5	235.2	72.1	326.1
12	2	7	40	1	254.4	78.9	322.4
17	3	7	30	0.75	236.7	72.9	324.7
16	4	7	30	0.75	237.4	75.3	315.3
9	5	7	20	0.5	60.0	15.2	334.5
3	6	4	40	0.75	211.8	60.4	350.8
14	7	7	30	0.75	213.5	62.9	339.6
4	8	10	40	0.75	222.9	65.5	340.4
15	9	7	30	0.75	224.6	65.5	342.8
7	10	4	30	1	238.5	69.1	345.3
13	11	7	30	0.75	225.4	65.0	346.8
5	12	4	30	0.5	224.8	65.6	342.9
1	13	4	20	0.75	174.4	40.3	432.5
6	14	10	30	0.5	219.8	65.6	335.1
2	15	10	20	0.75	45.0	16.1	248.9
11	16	7	20	1	54.4	16.6	328.3
8	17	10	30	1	216.8	59.9	362.0

A quadratic model was found significant for REE Enrichment for Healy as shown in Table 17. The model selected was found to be highly significant with a model p-value of less than 0.0001 and also with an adjusted R^2 value of 0.96; it could be said that selected model predicted the actual results quite accurately. Lack of fit for this model was found insignificant, which implies that there is 76.26% probability that a "Lack of fit F-value" this large could occur due to error.

Table 17. ANOVA table for REE Enrichment model for Healy.

Analysis of variance table [Partial sum of squares - Type III]						
Source	Sum of Squares	Df.	Mean Square	F Value	p-value Prob. > F	
Model	1.642E+005	4	41049.28	89.15	< 0.0001	significant
A-% Solids	9396.60	1	9396.60	20.41	0.0007	
B-Frother Dosage	69677.50	1	69677.50	151.33	< 0.0001	
A^2	6734.44	1	6734.44	14.63	0.0024	
B^2	80716.37	1	80716.37	175.30	< 0.0001	
Residual	5525.22	12	460.44			
Lack of Fit	2967.91	8	370.99	0.58	0.7626	not significant
Pure Error	2557.31	4	639.33			
Cor. Total	1.697E+005	16				
R-Squared	0.97					
Adj. R-Squared	0.96					

The empirical model for predicting REE Enrichment for Healy can be expressed as Equation 3, where % solids and frother dosage represent the absolute value of each.

$$\boldsymbol{REE\ Enrichment = -919.09 - 73.55 * \%\,Solids + 92.29 * Frother\ Dosage + 4.44 * \%\,Solids^2 - 1.38 * Frother\ Dosage^2} \quad \textbf{(3)}$$

It was evident from the empirical equation that REE enrichment was dependent on % solids and frother dosage and their higher orders and was independent of collector dosage. The second degree interaction terms for the two variables were found to be statistically insignificant and thus were eliminated. REE Enrichment is found to be negatively associated with % solids and positively associated with frother dosage; however, the response variable is found to have inverse relationships with the second order terms of the parameters.

To compare the effect of individual parameters and higher order terms on the response variables, a series of 3-dimensional response surfaces were created. Figure 40 shows that REE Enrichment has a strong positive correlation with frother dosage and a negative correlation with % solids. There seems to be no slope in the diagonal direction of the response surface suggesting absence of interaction effect of the two variables. The maximum enrichment was observed for frother dosage in the range of 35 ppm to 37 ppm at 4% solids in slurry using the optimization tool. It was noticed that the REE Enrichment improved with an increase in collector dosage until 35-37 ppm and dropped upon further increase in frother concentration. At lower % solids and higher frother dosage, higher values for REE Recovery and REE Concentration were observed and the two response variables were found to have an interaction effect of the two parameters. Whenever frother dosage was decreased or solids concentration in the pulp was increased, there was a decrease in the response variables as seen in Figure 41 and Figure 42.

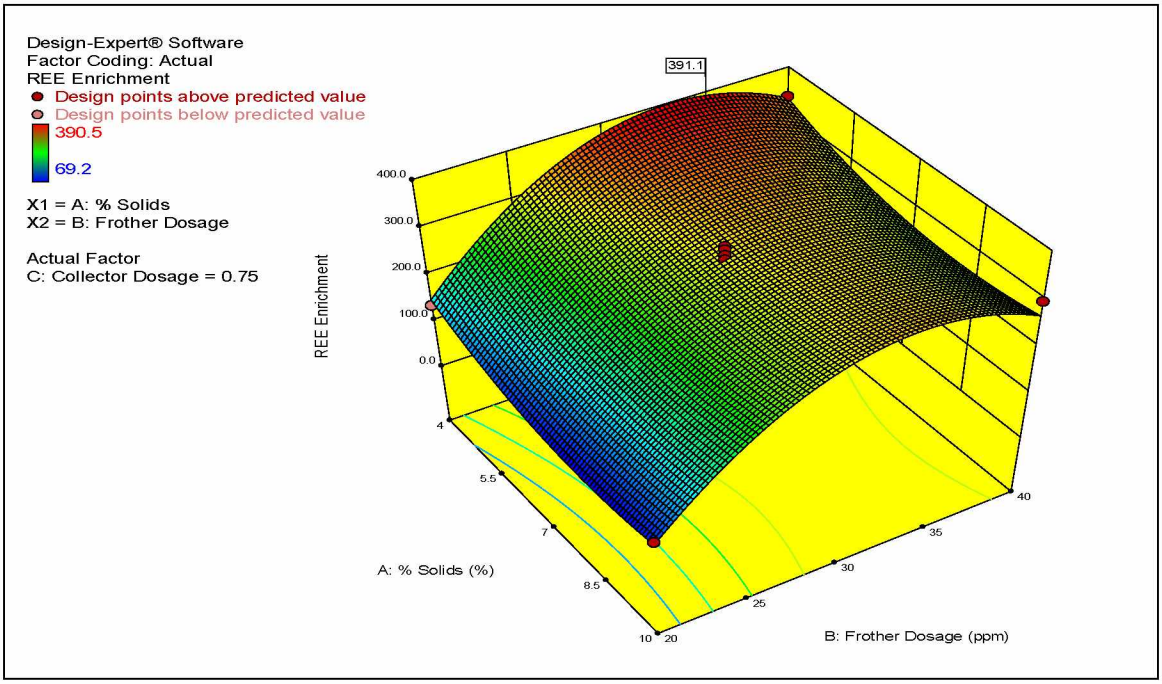

Figure 40. Response surface for maximizing REE enrichment for Healy as a function of pulp density (% Solids) and frother dosage (ppm).

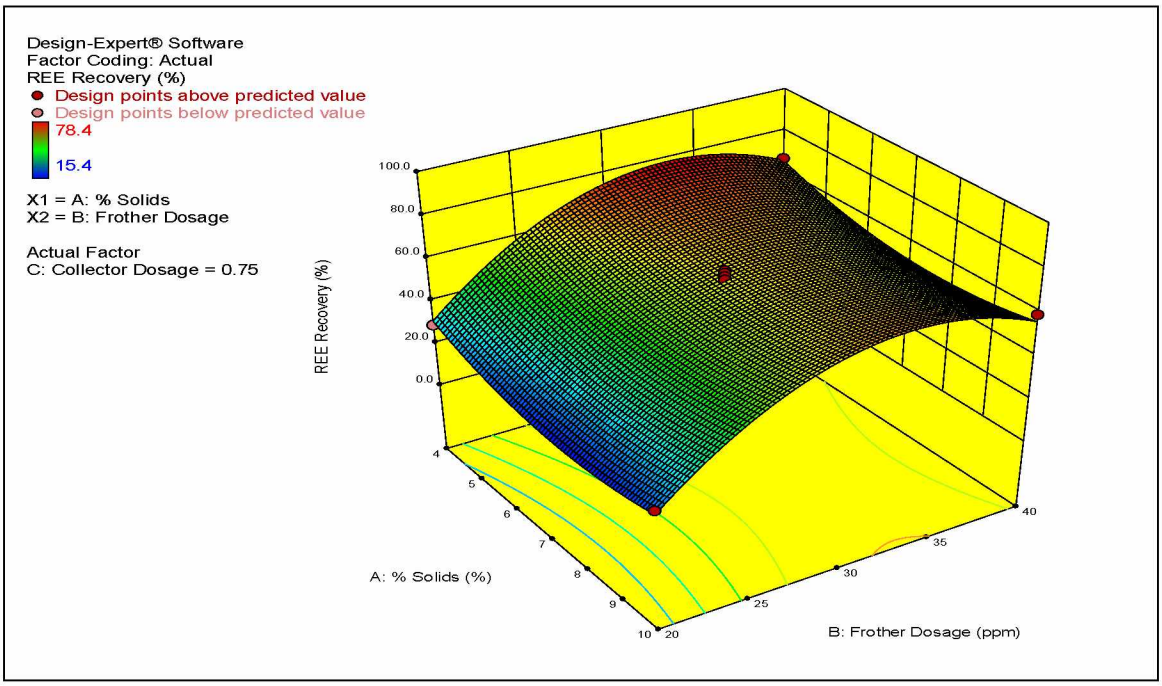

Figure 41. Response surface for REE recovery for Healy as a function of pulp density (% Solids) and frother dosage (ppm).

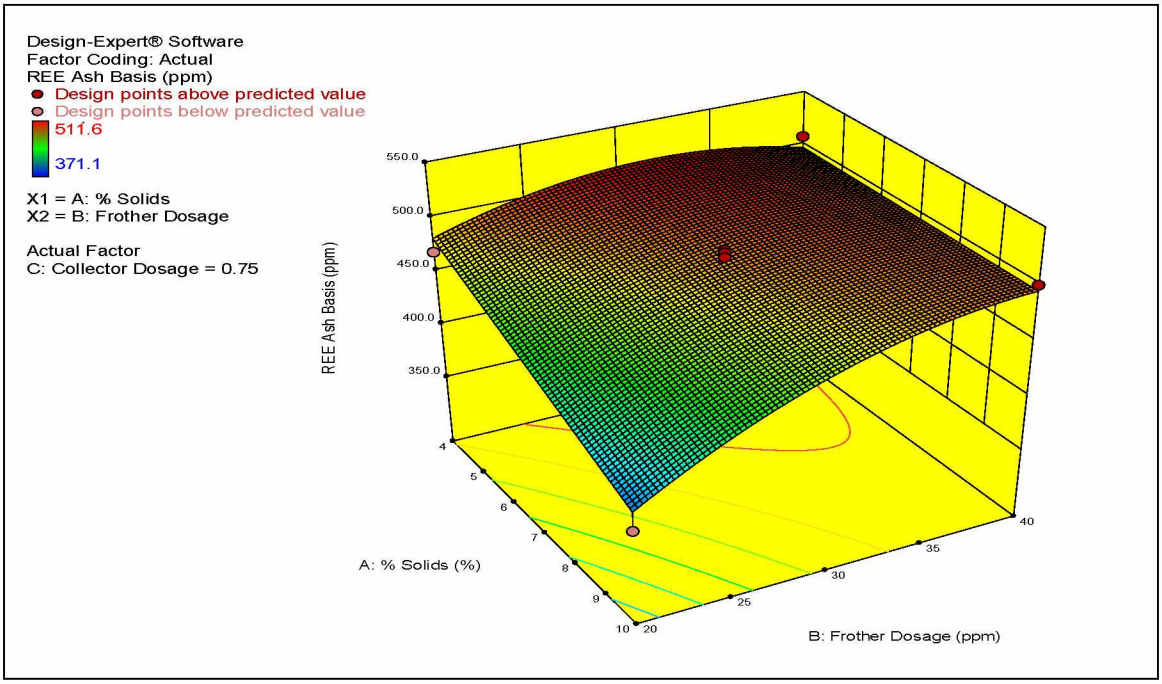

Figure 42. Response surface for REE concentration for Healy as a function of pulp density (% Solids) and frother dosage (ppm).

The same model selection procedure was employed for the response variables for Wishbone Hill. The quadratic model was found to be significant for REE Enrichment as shown in Table 18. The model selected was found to be highly significant with a model p-value of less than 0.1062 and also with an adjusted R^2 value of 0.91. Lack of fit for this model was found significant, and can be attributed to an outlier from Run No. 15 where hardly any coal yield was obtained in the froth fraction. All model assumptions were verified for this model and residual errors for this model were found to have a zero mean value with a constant variance and independent of any parameters involved in model.

Table 18. ANOVA table for REE Enrichment model for Wishbone Hill.

Analysis of variance table [Partial sum of squares - Type III]						
Source	Sum of Squares	Df.	Mean Square	F Value	p-value Prob. > F	
Model	71373.18	4	17843.30	40.73	< 0.0001	significant
A-% Solids	2625.20	1	2625.20	5.99	0.0307	
B-Frother Dosage	43575.56	1	43575.56	99.47	< 0.0001	
AB	4931.98	1	4931.98	11.26	0.0057	
B^2	20240.44	1	20240.44	46.21	< 0.0001	
Residual	5256.69	12	438.06			
Lack of Fit	4866.63	8	608.33	6.24	0.0473	significant
Pure Error	390.06	4	97.51			
Cor. Total	76629.87	16				
R-Squared	0.93					
Adj. R-Squared	0.91					

The empirical model for predicting REE Enrichment for Wishbone Hill can be expressed as Equation 4, where % solids and frother dosage represent the absolute value of each:

$$\boldsymbol{REE\ Enrichment} = -329.13 - 41.15 * \%\,\boldsymbol{Solids} + 40.66 * \boldsymbol{Frother\ Dosage} + 1.17 * \%\,\mathbf{Solids} * \mathbf{Frother\ Dosage} - 0.69 * \boldsymbol{Frother\ Dosage}^2 \quad \textbf{(4)}$$

The REE Enrichment model for Wishbone Hill exhibited a similar trend as for Healy, as the response variable was found to be independent of collector dosage and dependent only on % solids and frother dosage, their interaction, and second order terms. All second order terms with collector dosage were found to be statistically insignificant. Percent solids was found to be negatively associated with REE

Enrichment while a positive correlation with frother dosage was seen. A positive slope in the diagonal direction in Figure 43 suggests a positive relationship of REE Enrichment with the interaction of the two variables. From Figure 44 it can be seen that REE recovery decreases with an increase in % solids but is the highest at 10% solids with 35 ppm-37 ppm of frother dosage. This increase in the response with the decrease of one variable can be attributed to the interaction between the input variables. The absence of curvature in Figure 45 suggests the absence of second order terms in determining REE concentration. It is seen that REE concentration on ash basis is the minimum at the highest value of % solids and lowest value of frother dosage.

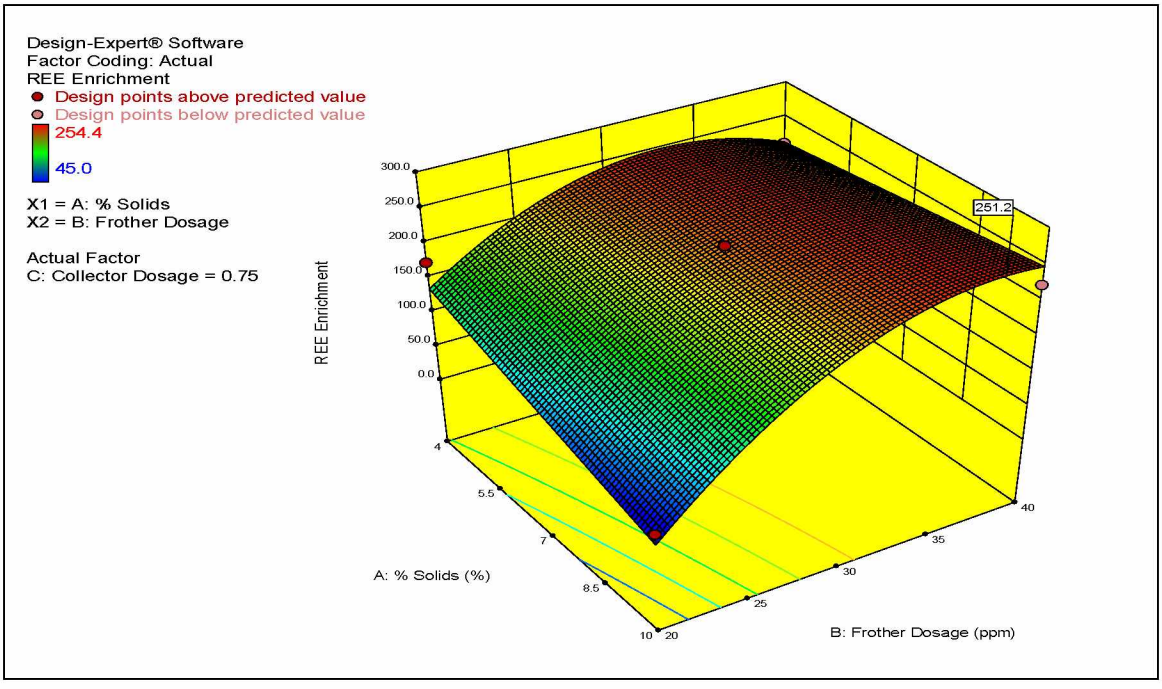

Figure 43. Response surface for Maximizing REE enrichment for Wishbone Hill as a function of pulp density (% Solids) and frother dosage (ppm).

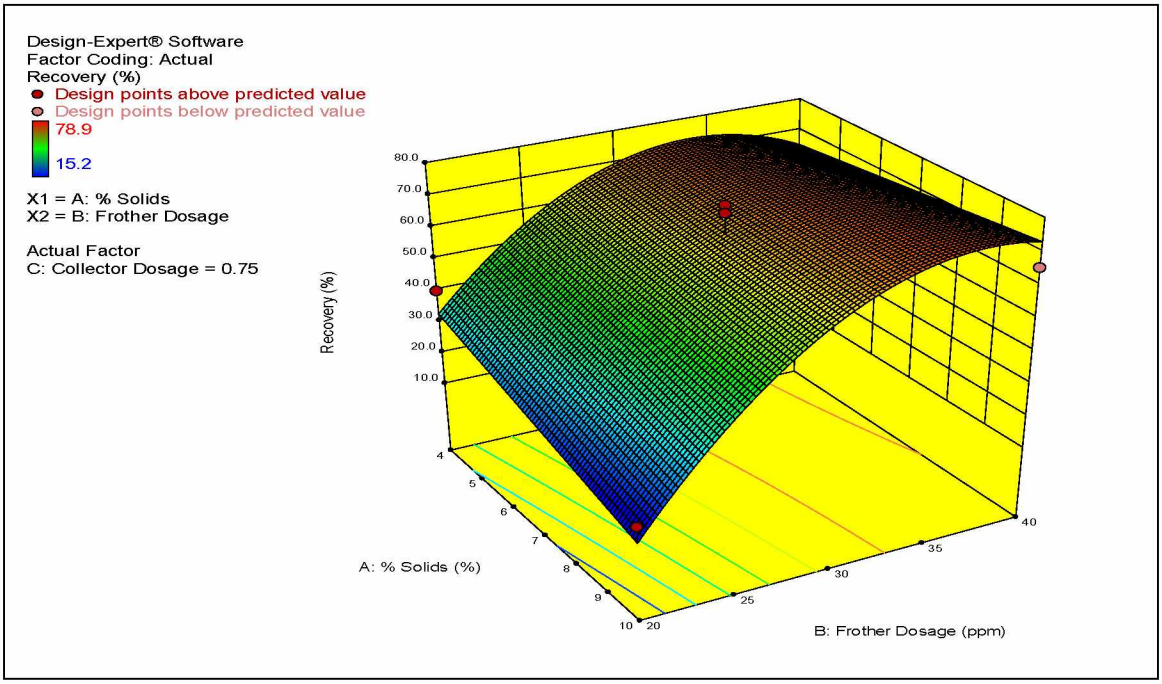

Figure 44. Response surface for REE recovery for Wishbone Hill as a function of pulp density (% Solids) and frother dosage (ppm).

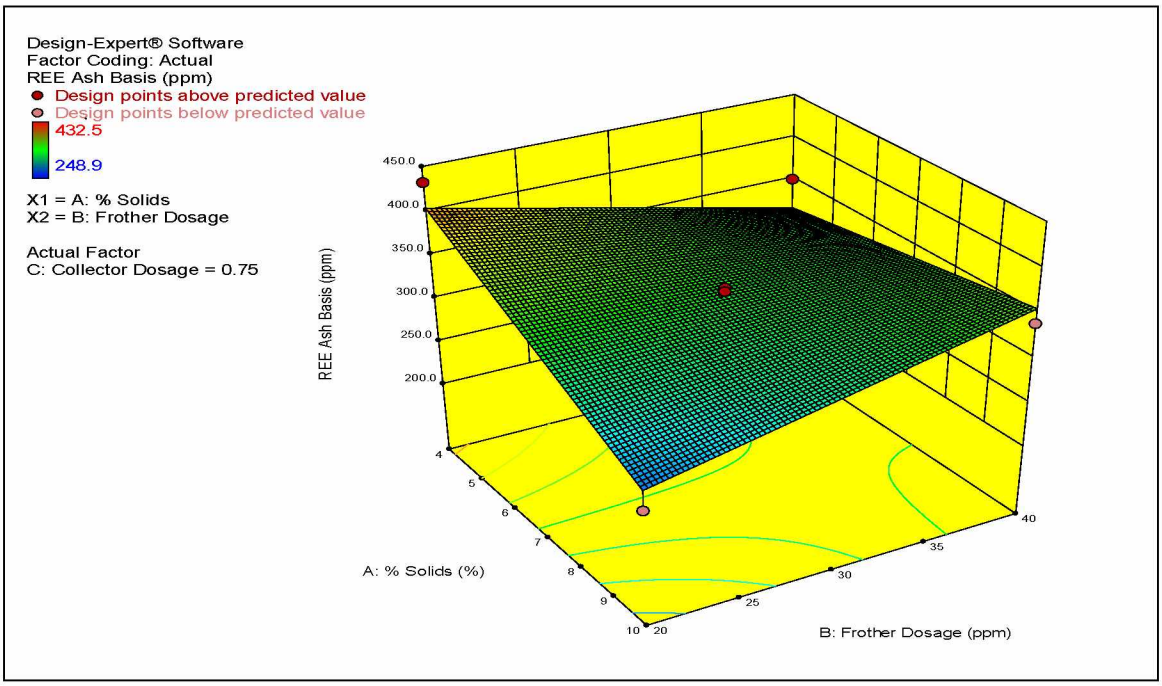

Figure 45. Response surface for REE concentration for Wishbone Hill as a function of pulp density (% Solids) and frother dosage (ppm).

From the results it can be deduced that the two coal samples have good flotation characteristics, which can be attributed to their surface hydrophobicity. Therefore the samples float without any addition of collector. Increasing the pulp density increases the amount of solids in the pulp, thus hindering coal attachment to the bubbles and subsequent flotation. Increasing the frother dosage up to the optimum ensures froth stability and good clean coal generation. Higher addition of frother causes more froth, thus entraining more tailings into the froth phase and hindering process performance.

Upon keeping % solids (4%-10%) and frother dosage (20 ppm-40 ppm) in ranges given and investigating maximizing the REE enrichment, a product with REE enrichment of 251.1 is achievable for the optimal values of the test variables as % solids=10% and frother dosage=37.9 ppm for Wishbone Hill. The total REE concentration for the optimum set of reagent dosage is 348 ppm on ash basis with 74.5% REE recovery. For Healy the optimum set of variables for maximizing REE enrichment can be obtained at % solids=4.2% and frother dosage=32.7 ppm to get a highest REE enrichment of 391. The best set of reagent dosage yields a total REE concentration of 506 ppm on ash basis with 77.3% REE recovery in froth fraction from parent coal.

The results obtained from parametric Box-Behnken design provided some significant conclusions. It was found that frother dosage plays an important role while floating REE-rich Alaskan coals. The REE concentration and REE recovery in the froth with conditions for maximum REE enrichment for the Healy and Wishbone Hill samples are given in Table 19.

Table 19. Set of optimum parameters from the Box-Behnken Design to maximize REE enrichment and the value of other output variables on the optimum conditions.

Sample	Pulp Density (% Solids)	Frother Dosage (ppm)	Max REE Enrichment	REE Concentration (ppm)	REE Recovery (%)
Healy	4.2	32.7	391	506	77.3
Wishbone Hill	10	37.9	251.1	348	74.5

CHAPTER 5 FLOWHEET AND ECONOMIC ANALYSIS

5.1 Flowsheet

Based on the results obtained from the physical and physio-chemical processing tests, the flowsheet for extraction of REEs from Alaskan coals is proposed in Figure 46. The run off mine (ROM) coal obtained from drilling and blasting, is transported to the processing unit, where it is size-reduced by crushing. A jaw crusher with closed side setting of 19mm and a reduction ratio of 20:1 is used as a primary crusher. The size reduced coal is subsequently crushed by a smooth single roll secondary crusher with closed side setting of 6mm and a reduction ratio of 4:1.

The product from the size reduction is transferred on to a 20° inclined vibrating screen which classifies the incoming feed into oversize and undersize. The oversize of the screen, with an aperture of 6mm, constitutes the feed for the dense media circuit while the undersize is sent for further size reduction into a ball mill classifying cyclone circuit. Coal >6mm is mixed with dense medium prepared from suspending fine magnetite in slurry to achieve a pulp density of 1.55. A dense medium cyclone separates the feed slurry based on the specific gravity into overflow and underflow. The overflow of the dense medium cyclone is the clean coal with an average specific gravity of 1.31 and 14.1% ash content for Wishbone Hill and a specific gravity of 1.35 and 17.2% ash content for Healy. The underflow product is at 2.22 specific gravity and 57.8% ash for Healy and 2.97 specific gravity and 77.0% ash for Wishbone Hill.

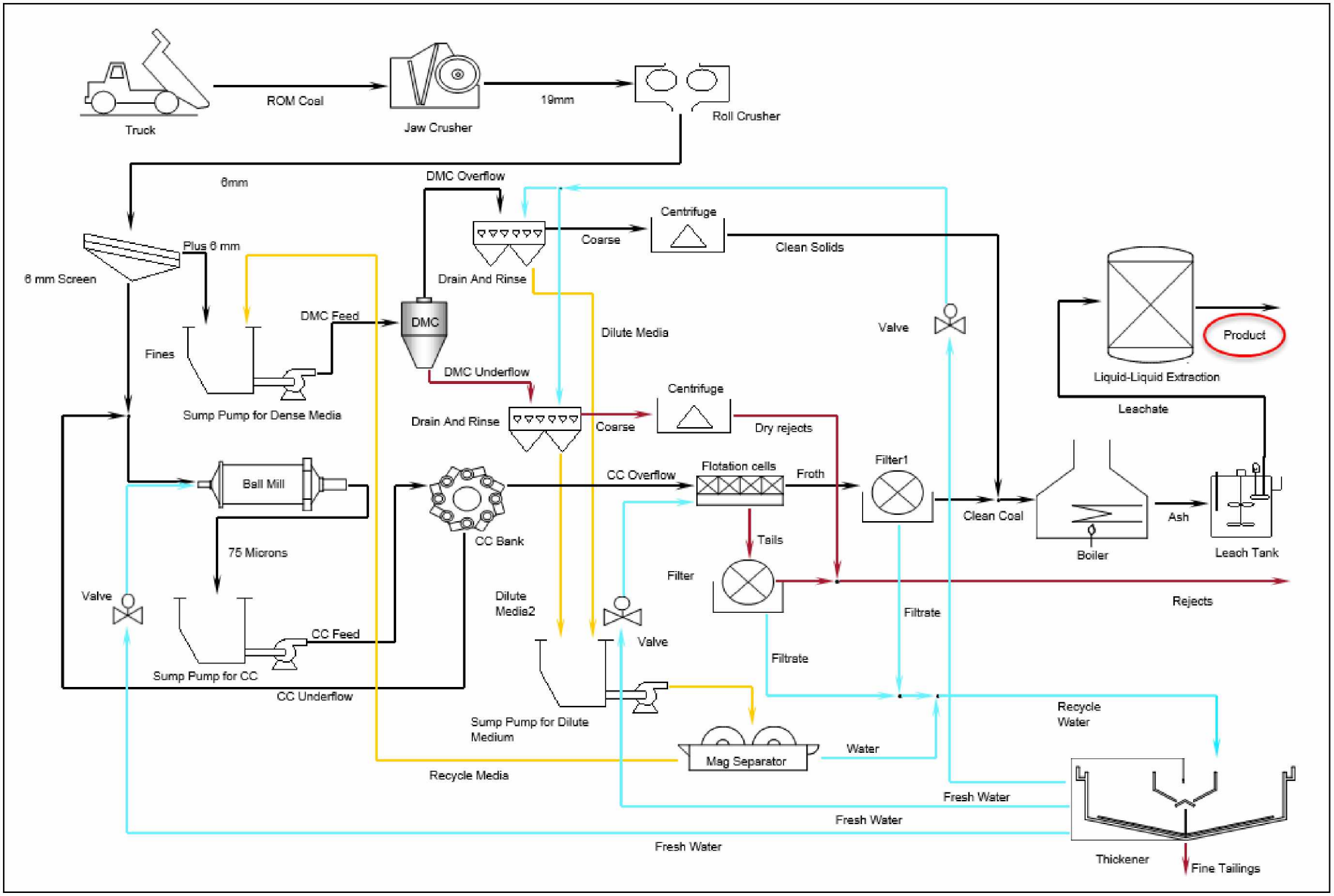

Figure 46. Schematic Flowsheet for commercial extraction of REEs from Alaskan coals.

The total REE recovery in the clean coal for the dense medium circuit is 73% and 26% for Healy and Wishbone Hill, respectively. Two drain and rinse screens with basket centrifuge are deployed for draining the dense medium and dewatering the coal in product streams. The REE concentration achieved in the clean coal is 518 ppm on ash basis thus having a REE upgrade potential of 7.2:1 for Wishbone Hill. For Healy the upgrade potential is 5.8:1 and the cumulative REE concentration is 500 ppm in clean coal.

The undersize from the screen (<6mm) is sent to the ball mill for further size reduction. Water is added to the ball mill via control valves to maintain the optimum percent solids in the mill. Controlling the % solids in the ball mill is one of the essential parameters to optimize the power drawn for the communition process. The ball mill has a retention time of 40 minutes for Wishbone Hill and 120 minutes for the Healy sample. The product from the ball mill is sent for size classification into the classifying cyclone bank. The classifying clone separates the incoming feed at a cut size of 75-80 microns and the overflow containing the fines are sent to the froth flotation unit. The underflow of the classifying clone bank with particles larger than 75 microns are recirculated into the ball mill.

In the froth flotation process, the slurry of 10% solids and 4.2% solids for Wishbone Hill and Healy, respectively, report to the conditioning tank with mean conditioning time of 1 minute after frother addition at room temperature and neutral pH. Clean coal in the froth phase is dewatered using disc filters. The REE recovery and REE

concentration in the process is 74.5% with 348ppm for Wishbone Hill and 77.3% and 506 ppm for Healy, respectively. The overall recovery of the processing plant is summarized in Table 20.

Table 20. Overall REE Recovery from the processing plant.

	Healy	Wishbone Hill
REE Recovery DMC	72.68	25.98
REE Recovery Flotation	77.3	74.5
Total Recovery	75.9	59.6

The fine clean coal is added to the clean coal product from the dense medium cyclone circuit and sent for downstream processing. The tailings from the froth flotation process are mixed with the underflow product of the dense medium circuit and can be used to extract any carbonaceous material as secondary product. The clean coal is ashed in the boiler and sent for leaching and extraction in the tanks. The leaching process with Lithium Borate fusion and 3-acid digestion recovers 95% of the REEs in ash. The pregnant solution from REE leaching is then sent for extraction of individual REEs by the biogenic method based on the adsorption of lanthanide to the bacterium Roseobacter sp. AzwK-3b. This process separates the REEs from the solution by successive acid washes of varying acidic strengths.

The flow sheet of the process defines the basic circuits required for establishing the coal preparation plant. The fine circuit (<75 microns) constitute 70% of the total feed and therefore decides the overall REE enrichment and recovery. The clean coal product is sold separately as thermal coal while middlings can be extracted before discarding the tailings and can be supplied as low grade thermal coal. The plant is designed for 20% higher capacity, therefore the feed can be increased after an event of an unexpected shutdown.

5.2 Economic Analysis

Economic evaluations of mining and mineral processing ventures incorporate the detailed examination and assessment of the technical, financial, social and political perspectives of the setting in which the mineral deposit is situated. Therefore, the current investigation outlines the essential technical inputs that form the foundation for financial evaluation of a project. These include estimation of mineable ore, the rate of production, evaluation of the performance of production, capital and operating costs and the revenue. Estimation of these parameters requires consideration of a number of technical factors such as the ore characteristics, available mining and extraction technologies and the market supply-demand scenario. In a basic economic project model, the estimated costs and revenues, indicate possible cash flows over the period of development and operation. The economic model can reflect the actual value of the ore, provided all input costs, revenues, inflation, and taxes. This might be an adequate end-point for the internal evaluation of a project.

The studied Alaskan coals possess huge monetary potential as they contain REEs worth many million USD every year as seen from Table 21. The total proven coal reserves for Wishbone Hill and Healy are 17 M tons and 250 M tons, respectively. The coals are rich in scandium, which is of most noteworthy value. The economic valuation is accomplished for the five most prominent REEs present in Alaskan coals and is based on REE metal prices from July 2016. The annual production of Healy coal mine is 2 M tons and will be 0.5 M tons when Wishbone Hill comes to life. Together, the coals contain REEs worth about 325 million USD per year if the resource is utilized as a possible source of REE extraction in the near future.

Table 21. Economic potential of the REEs in Alaskan coal samples based on REE metal prices from July 2016.

	Wishbone Hill	Healy
Total Coal Reserves (M Tons)	17	250
Annual Production (M Tons)	0.5	2
Ash (%)	45.96	21.62
REE Concentration(ppm)	277	525
Sc (%)	11	6
La (%)	13	15
Ce (%)	28	31
Nd (%)	14	14
Y (%)	16	15
REE Reserves(tons)	63.65	227.01
Sc ($)	$ 103,587,549	$ 216,821,715
La ($)	$ 56,432	$ 241,604
Ce ($)	$ 124,823	$ 498,168
Nd ($)	$ 538,792	$ 1,939,204
Y ($)	$ 355,784	$ 1,198,224
Annual REE Value ($)	$ 104,663,380	$ 220,698,915

The financial aspect of equipment selection is based primarily on the utility and size of the unit operation. The best available option is for equipment selected, which has the desired performance with low running and maintenance costs. The objective is also to minimize floor space requirements. Thus optimum size of the unit is chosen to ensure minimum floor space usage. The installation and running costs per hour of various equipment are given in Table 22. Supplementary costs are assessed as fractional expenditure of the total equipment installation cost and have been condensed in Table 23.

Table 22. Installation and hourly operation cost of the equipment used.

Equipment	No.	Installation Cost	Hourly Operating Cost	Power Required	Total Installation Cost
Jaw Crusher	1	$ 36,600	$ 15.01	125	$ 136,600
Roll Crusher	1	$ 80,300	$ 6.54	50	$ 80,300
Single Deck Screen	1	$ 23,985	$ 1.23	20	$ 23,985
Dense Media Cyclone	1	$ 200,000	$ 0.14	20	$ 200,000
Ball Mill	1	$1,070,000	$ 63.19	2000	$ 1,070,000
Classifying Cyclone	4	$ 20,000	$0.26	NA	$80,000
Flotation Circuit	5	$38,000	$1.04	30	$ 190,000
Drain and Rinse Screens	2	$16,900	$0.78	NA	$ 33,800
Basket centrifuge	2	$120,000	$15.26	NA	$ 240,000
Sump Pump	3	$20,000	$1.35	60	$60,000
Disc Filters	2	$183,700	$7.40	30	$ 367,400
Leach Tank	1	$16,900	$ 0.37	NA	$16,900
Extraction Tank	1	$16,900	$ 0.37	NA	$ 16,900
Mag Separators	1	$40,100	$1.41	10	$40,100
Thickener	1	$930,000	$55.70	25	$930,000
Total		$ 2,913,385	$170.05		$3,485,985

Table 23. Supplementary costs.

Other Expenses	Fractional Cost of Total Investment	Total Cost
Civil Work	0.6	$2,091,591
Structural Work	0.5	$1,742,993
Electrical Instrumentation	0.5	$1,568,693
Pipework	0.2	$522,898
Erection Work	0.5	$1,568,693
Design Work	0.3	$871,496
Payroll Cost	0.1	$348,599
Total Overall Cost		$8,714,963

The contrast between the predicted and actual outcome of a project in terms of the capacity of production, time, and revenue will depend on design errors, changes in the ore characteristics, component failures, cost escalation, changes in future demand and up-gradation to novel low-cost technologies. The assessment for the current flowsheet was done in order to come up with the best estimate value. Items that will be identified later are omitted. The conditions and assumptions for the operation of the flowsheet are given in Table 24. The project seems promising as the plant reaches the break-even point in the seventh year of operation at 9% internal rate of revenue (IRR). Even after estimation of the bulk of the detailed design, however, it is still necessary that estimation of the whole project be undertaken before a project go-ahead is given.

Table 24. Technical, financial, and operational project parameters.

Technical Parameters	
Cutoff Grade (g REE/ton on whole coal basis)	130
Reserve Level at Cutoff (million tons)	267
Contained Value (kg REE)	34,710,000
Ore Production Rate (t/d)	7,000
Mill Recovery	73%
Operating days/year	350
Project Life (year)	7
Financial Parameters	
Current REE Price ($/g)	1.00
Transportation and Shipping Cost ($/t)	3.50
Mill Operating Cost ($/t)	14.00
Total Operating Cost ($/t)	17.50
Additional Capital Cost ($ 000)	50
Mill Capital Cost ($ 000)	12,200
Total Capital Cost ($ 000)	12,250
Working Capital ($ 000)	13,000
Depletion Allowance (%)	15%
Royalty (% Net Smelter Return)	5%
Income Tax Rate (%)	46%
Salvage Value (% of Capital Costs)	10%
Real Risk-adjusted Discount Rate (%)	10%
Inflation (%)	3%
Operational Parameters	
Total number of working days/year	350
No of shifts/day	3
No. of hours/shift	8
Mill recovery (%)	73
Refinery Charges (%)	80

CHAPTER 6 CONCLUSIONS AND RECOMMENDATIONS

6.1 Conclusions

The United States has been the world leader and a source of encouragement for other countries in its commitment for conservation of natural resources and development of clean and environmentally benign technologies. The promotion of extracting valuable REEs from alternative sources instead of conventional mining is one such example of sustainable approach to development.

A comprehensive study was performed to identify and quantify the presence of REEs for two coal samples from Alaskan coal deposits. The coal samples, one each from Central Alaska-Nenana and Southern Alaska-Cook Inlet coal provinces, were studied to determine their mineralogical composition by Scanning Electron Microscopy and the effect of density and size on the concentration and distribution of REEs. Additionally, froth flotation experiments were conducted using a three-level three-factor Box Behnken design for modelling and optimization of the independent variables for maximizing REE enrichment in Alaskan Coal samples. The results were then subjected to ANOVA analysis to determine the significant factors to evaluate their main and interaction effects on the enrichment of REEs into float fraction of fine coal. An optimization algorithm was used to predict the set of optimum conditions for flotation of coal to achieve high REE enrichment in the froth phase.

Healy and Wishbone Hill samples have an overall concentration of 524 ppm and 286 ppm, respectively, of REEs on ash basis. On whole coal basis both samples have

higher concentration of REEs as compared to the amounts present in world coals (Figure 47). The coals are found to possess the potential to be used as an REE resource under favorable socio-economic and geo-political scenarios. REE enrichment can be achieved by processing coarser size particles by dense medium separation and finer sizes by froth flotation.

Other salient conclusions that can be drawn from the study are listed below:

1. The representative sample characterization showed that the majority of the screened sample, about 88.11% and 89.81%, is over 30 Mesh in size for Healy and Wishbone Hill coals, respectively. The proximate analysis of the samples reveal that the Healy sample had a high inherent moisture content of around 18% with around 22% dry ash content. The Wishbone Hill sample had very low moisture content of 4% with 46% dry ash content
2. Analysis of the samples for REE+Y+Sc content with ICP-AES and ICP-MS demonstrated that, on whole coal basis, the REE content of the Wishbone Hill coal is higher than that of Healy coal. HREE and LREE report to lower density fractions (1.7 and lower). Also the coals are comparatively richer in LREE content as compared to HREE. The concentrations can reach up to 857 ppm and 504 ppm on ash basis for selected density fractions in Wishbone Hill and Healy, respectively.

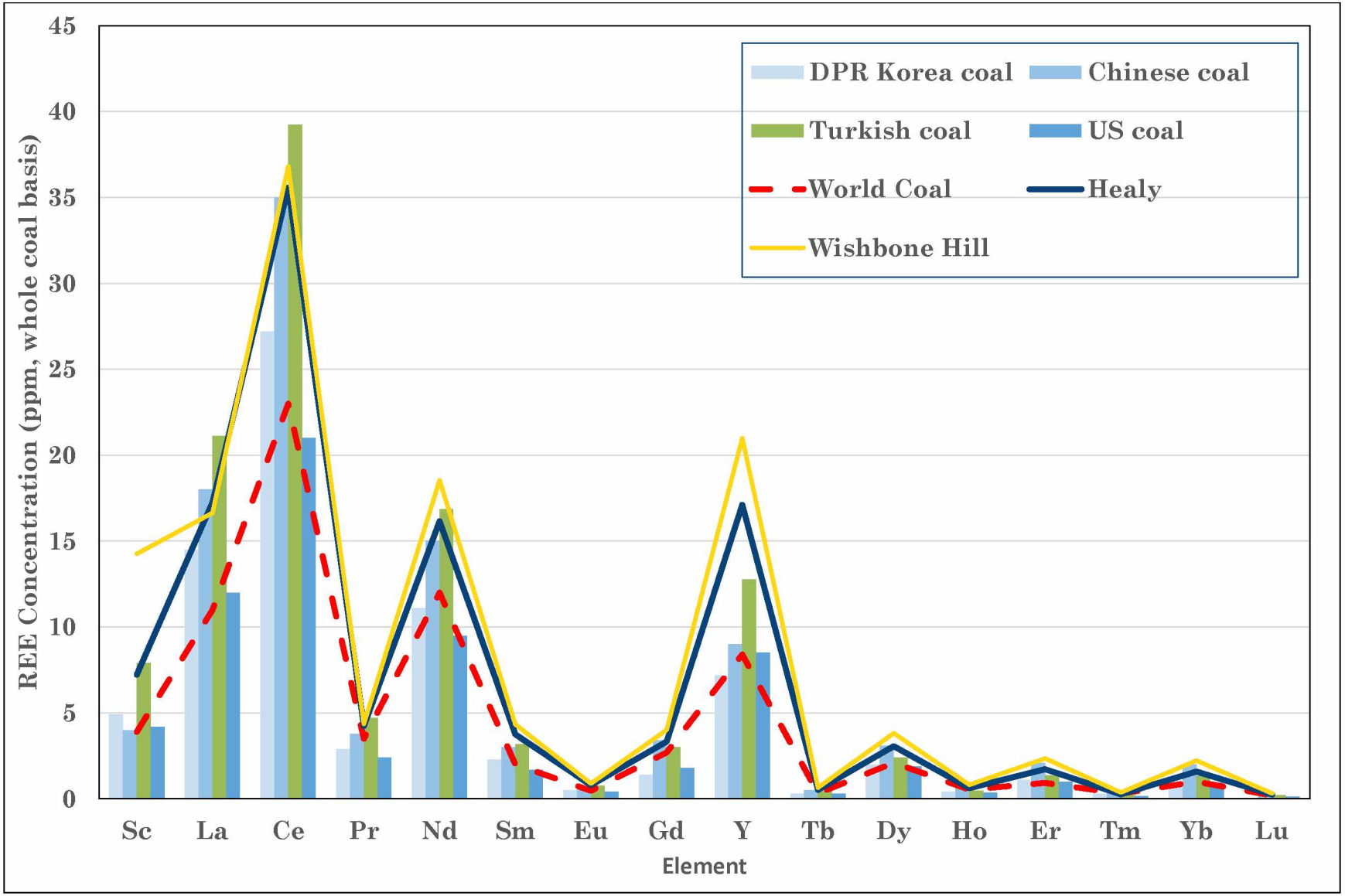

Figure 47. Comparison of REE concentrations in Alaskan coals to world coals.

3. Wet high intensity magnetic separation tests on <100 Mesh fractions showed that Wishbone Hill fines contain higher Sc in non-magnetics than that of Healy. LREEs are similarly distributed between magnetics and non-magnetics for Wishbone Hill fines except Sc, Sm and Gd, which were richer in magnetics. This trend is also valid for HREE content of the Wishbone Hill, where HREE elements appear to be preferentially reporting to magnetic fractions.
4. Flotation tests on <100 Mesh fines reveal that both LREE and HREE are concentrated more in float fractions than tailings on ash basis. This finding is more pronounced for Wishbone Hill fines.
5. Fly ash is found to have relatively higher contents of both LREE and HREE than bottom ash and cinders on ash basis. The differences in concentrations distributed between the coal combustion products are seemingly low.
6. The SEM analysis of the coal samples and the by-products revealed that Healy has higher presence of calcium and its oxides while Wishbone Hill has higher silica. Both coals are low in sulfur content and titanium (Ti) and potassium (K) are detected as trace elements in the inorganic fractions of both coals.
7. The presence of a glassy silica matrix in the coal byproducts necessitate ultrafine grinding for liberation of the finely disseminated REE minerals in submicron sizes ranges.
8. From the statistical experimental design, it was found that flotation performance of both coals is independent of the collector dosage and requires only a frother for efficient flotation. The majority of the REEs concentrated in

the clean coal in the 17 experimental tests. High adjusted R^2 values for both models suggests a good relationship between the observed and estimated values. It was found that maximum REE enrichment for Wishbone Hill coal can be achieved at optimum frother dosage of 37.9 ppm and 10% feed solids. For a high REE enrichment of 391 in Healy coal, the optimum frother dosage is 32.7 ppm and 4.2% solids by weight in the feed slurry.

9. The optimum set of reagent dosage and pulp density yields a total REE concentration of 506 ppm and 348 ppm on ash basis with 77.3% and 74.5% REE recovery in froth fraction for Healy and Wishbone Hill samples, respectively.
10. The overall REE recovery for Healy and Wishbone Hill samples from the proposed processing plant is 76% and 60%, respectively. The processing plant breaks even in the seventh year.

6.2 Recommendations

Based on the results from the current study, further research in the following areas is recommended:

1. Since high concentrations of REEs were detected for coal combustion products, detailed studies concerning exploitation of REEs from them should be conducted. The cost of such a process should be evaluated and compared with the current flowsheet proposed to come up with the most economically feasible process.

2. The results from this study showed that a conventional flotation cell was able to achieve higher REE recoveries. A detailed study for froth flotation should be conducted using column flotation cells to understand the effect of mechanical and design parameters on enrichment of REEs as wash water in column flotation inhibits the entrainment of clay particles. This can lead to higher concentrations of REEs in the product.
3. Recently, significant interest has developed for leaching and extraction of REEs and other heavy elements by eco-friendly bacteria so as to minimize the negative environmental impacts. Such environmentally benign studies combining interdisciplinary collaboration can result in minimizing the use of harmful acids and reagents, and production of toxic tailings.

REFERENCES

Alonso, E., Sherman, A. M., Wallington, T. J., Everson, M. P., Field, F. R., Roth, R., & Kirchain, R. E. (2012). Evaluating rare earth element availability: A case with revolutionary demand from clean technologies. Environmental Science & Technology, 46(6), 3406-3414.

ALS Global. (2014). Geochemical Procedure ME-MS81 Lithium Metaborate fusion-ICP-MS Multi-element Method. ALS Global.

Amini, S. H., Honaker, R., & Noble, A. (2016). Performance evaluation of a dense-medium cyclone using alternative silica-based media. Powder Technology, 297, 392-400.

Andresen, L. (1986). Occurrence and processing of rare earth minerals. Erzmetall, 39(4), 152-157.

Aplan, F. (1989). The Processing of Rare Earth Minerals. In Rare Earths: Extraction, Preparation and Applications, (pp 15-34). Las Vegas.

Arol, A., & Aydogan, A. (2004). Recovery enhancement of magnetite fines in magnetic separation. Colloids and Surfaces A: Physicochemical and Engineering Aspects, 232(2), 151-154.

ASTM D4371. (2012). Standard Test Method for Determining the Washability Characteristics of Coal, ASTM International. https://www.astm.org/Standards/D4371.htm.

ASTM D3172. (2013). Standard Practice for Proximate Analysis of Coal and Coke, ASTM International. https://www.astm.org/Standards/D3172.htm.

ASTM D4239. (2011). Standard Test Method for Sulfur in the Analysis Sample of Coal and Coke Using High-Temperature Tube Furnace Combustion, ASTM International. https://www.astm.org/Standards/D4239.htm.

Azizi, D., Gharabaghi, M., & Saeedi, N. (2014). Optimization of the coal flotation procedure using the Plackett–Burman design methodology and kinetic analysis. Fuel Processing Technology, 128, 111-118.

Barnes, F. F., & Payne, T. G. (1956). The Wishbone Hill District, Matanuska coal field, Alaska (No. 1016). U.S. Geological Survey.

Belowich, M. A. (1993). Geology, mine development, and marketing for Evan Jones coal. Procedings from Focus on Alaska coal, 132-139. Anchorage, Alaska.

Bentzen III E. H., Ghaffari, H., Eng, P., Galbraith, L., Hammen, R. F., Robinson, R. J., Hafez, S. A., & Srikant Annavarapu, R. M. (2013) Preliminary Economic Assessment On the Bokan Mountain Rare Earth Element Project, Near Ketchikan, Alaska. Document No. 1196000100-REP-R0001-02. Tetra tech. 800-555 West Hastings Street, Vancouver, BC, Canada.

Binnemans, K., Jones, P. T., Blanpain, B., Van Gerven, T., Yang, Y., Walton, A., & Buchert, M. (2013). Recycling of rare earths: a critical review. Journal of Cleaner Production, 51, 1-22.

Bleiwas, D. I., & Gambogi, J. (2013). Preliminary estimates of the quantities of rare-earth elements contained in selected products and in imports of semi manufactured products to the United States, 2010 (No. 2013-1072). US Geological Survey.

Bonificio, W. D., & Clarke, D. R. (2016). Rare-earth separation using bacteria. Environmental Science & Technology Letters, 3(4), 180-184.

Box, G. E., & Behnken, D. W. (1960). Some new three level designs for the study of quantitative variables. Technometrics, 2(4), 455-475.

Bunzli, J. C. G. (2000). Lanthanides Kirk-Othmer Encyclopedia of Chemical Technology: John Wiley & Sons, Inc.

Castor, S. B., & Hedrick, J. B. (2006). Rare earth elements. Industrial minerals volume, 7th edition: Society for mining, metallurgy, and exploration, Littleton, Colorado, 769-792.

Cordier, D. J., & Hedrick, J. B. (2011). Rare Earths. US Geological Survey, Mineral Commodity Summaries.

Dai, S., Jiang, Y., Ward, C. R., Gu, L., Seredin, V. V., Liu, H., Zou, J. (2012). Mineralogical and geochemical compositions of the coal in the Guanbanwusu Mine, Inner Mongolia, China: further evidence for the existence of an Al (Ga and REE) ore deposit in the Jungar Coalfield. International Journal of Coal Geology, 98, 10-40.

Dai, S., Li, D., Chou, C. L., Zhao, L., Zhang, Y., Ren, D., Sun, Y. (2008). Mineralogy and geochemistry of boehmite-rich coals: new insights from the Haerwusu Surface Mine, Jungar Coalfield, Inner Mongolia, China. International Journal of Coal Geology, 74(3), 185-202.

Department of Energy, U. S. (2011). Critical Materials Strategy. US Department of Energy, Washington DC, USA, 14-25.

Dube, R. M. (2012). Collectors for Enabling Flotation of Oxidized Coal (Masters Thesis). Retrieved from uknowledge.uky.edu.

Ekmann, J.M. (2012), Rare Earth Elements in Coal Deposits – a Prospectivity Analysis, Search and Discovery Article #80270, Adapted from poster presentation given at AAPG Eastern Section meeting, Cleveland, Ohio, 22-26 September 2012.

European Commission, (2010). Critical Raw Materials for The EU. Report of the ad-hoc working group on defining critical raw materials. Brussels.

Falconnet, P. G. (1988). Rare Earths Production and Marketing Opportunities. In Materials Science Forum (Vol. 30, pp. 1-12). Trans Tech Publications.

Ferreira, S. C., Bruns, R., Ferreira, H., Matos, G., David, J., Brandao, G., Souza, A. (2007). Box-Behnken design: an alternative for the optimization of analytical methods. Analytica chimica acta, 597(2), 179-186.

Finkelman, R. (1988). The Inorganic geochemistry of coal - A scanning electron-microscopy view. Scanning Microscopy, 2(1), 97-105.

Finkelman, R. B. (1982). Modes of occurrence of trace elements and minerals in coal: an analytical approach. In Atomic and Nuclear Methods in Fossil Energy Research (pp. 141-149): Springer US.

Fleming, C. (1992). Hydrometallurgy of precious metals recovery. Hydrometallurgy, 30(1), 127-162.

Flores, R. M., Stricker, G. D., & Kinney, S. A. (2004). Alaska Coal Geology, Resources, And Coalbed Methane Potential. United States Geological Survey (United States). United States Department of the Interior.

Fuerstenau, D. (2013). Design and development of novel flotation reagents for the beneficiation of Mountain Pass rare-earth ore. Minerals & Metallurgical Processing, 30(1).

Fuerstenau, D. W., & Pradip, P. (1988). Alkyl hydroxamates as collectors for the flotation of bastnaesite rare-earth ores. In Journal of Metals (Vol. 40, No. 11, pp. 14-15). 420 Commonwealth Dr, Warrendale, PA 15086: Minerals Metals Materials Society.

Gambogi, J. (2013). Rare Earths—Mineral Commodity Summaries. United States Geological Survey. Retrieved January, 7, 2013.

Ghosh, T., Honaker, R., Patil, D., & Parekh, B. (2014). Upgrading low-rank coal using a dry, density-based separator technology. International Journal of Coal Preparation and Utilization, 34(3-4), 198-209.

Greinacher, E. (1980). History of rare earth applications, rare earth market today: overview. Industrial Applications of Rare Earth Elements, 3-17.

Gschneidner Jr, K. A. (1964). Rare earths: the fraternal fifteen. US Atomic Energy Commission, Division of Technical Information.

Gschneidner, K., & Daane, A. (1988). Physical metallurgy. Handbook on the Physics and Chemistry of Rare Earths, 11, 409-484.

GSI. (2016, April 15). A note on Rare Earth Elements. Retrieved from http://www.portal.gsi.gov.in/portal/page?_pageid=127,719655&_dad=portal&_schema=PORTAL

Gupta, T., Ghosh, T, & Akdogan, G. (2016). Characterizing REEs in Alaskan Coal and Ash. Paper presented at the SME Annual Conference and Expo (ACE) 2016, Phoenix, Arizona.

Harkins, W. D. (1917). The evolution of the elements and the stability of complex atoms. I. A new periodic system which shows a relation between the abundance of the elements and the structure of the nuclei of atoms. Journal of the American Chemical Society, 39(5), 856-879.

Haxel, G. B., Hedrick, J. B., Orris, G. J., Stauffer, P. H., & Hendley II, J. W. (2002). Rare Earth Elements: Critical Resources for High Technology (2327-6932). United States Geological Survey.

Hedrick, J. (1999). Rare Earths: US Geological Survey Minerals Yearbook. Metals and Minerals, 1, 61-1. United States Geological Survey.

Hedrick, J. B. (1997). Rare-earth metal prices in the USA ca. 1960 to 1994. Journal of alloys and compounds, 250(1), 471-481.

Hedrick, J. B. (2000). Rare Earths: US Geological Survey Minerals Yearbook. Metals and Minerals, 1, 61-1. United States Geological Survey. Vol. 1, 11.

HEFA. (2014). Rare Earth Metal and Oxide Prices. Retrieved from http://www.baotou-rareearth.com/.

Honaker, R., Jain, M., Parekh, B., & Saracoglu, M. (2007). Ultrafine coal cleaning using spiral concentrators. Minerals Engineering, 20(14), 1315-1319.

Houot, R., Cuif, J. P., Mottot, Y., & Samama, J. C. (1991). Recovery of rare earth minerals, with emphasis on flotation process. In Materials Science Forum (Vol. 70, pp. 301-324). Trans Tech Publications.

Hower, J. C., Ruppert, L. F., & Eble, C. F. (1999). Lanthanide, yttrium, and zirconium anomalies in the Fire Clay coal bed, Eastern Kentucky. International Journal of Coal Geology, 39(1), 141-153.

Humphries, M. (2012). Rare earth elements: The global supply chain. Congressional Research Service, 2011, 7-5700.

Jackson, W. D., & Christiansen, G. (1993). International strategic minerals inventory summary report; rare-earth oxides (No. 930-N). US Dept. of the Interior, Geological Survey.

Jiake, L., & XiangYong, C. (1985) A new development of mineral processing flowsheet for the treatment of a complex ore containing Fe, rare earths, Nb and F. XVth ZMPC, Vol. 3, pp.474-485, Cannes, France.

Jordens, A., Cheng, Y. P., & Waters, K. E. (2013). A review of the beneficiation of rare earth element bearing minerals. Minerals Engineering, 41, 97-114.

Joshi, P. B., Preda, D. V., Skyler, D. A., Tsinberg, A., Green, B. D., & Marinelli, W. J. (2015). Recovery of Rare Earth Elements and Compounds from Coal Ash, U.S. Patent No. 8,968,688. Washington, DC: U.S. Patent and Trademark Office.

Ketris, M., & Yudovich, Y. E. (2009). Estimations of Clarkes for Carbonaceous biolithes: World averages for trace element contents in black shales and coals. International Journal of Coal Geology, 78(2), 135-148.

Kilbourn, B. T. (1993). A Lanthanide Lanthology: Part 1, A-L. New York, New York, Molycorp, Incorporated.

Kingsnorth, D. J. (2011). Rare Earth Opportunities, Real or Imaginary. Melbourne, Australia, Industrial Minerals Company of Australia Pty Ltd.

Kremers, H. E. (1961). Rare earth metals. In Hampel, C.A. (ed.), Rare Metals Handbook, 2nd Editon, pp. 393-417, Reinhold, New York.

Krishnamurthy, N., & Gupta, C. K. (2004). Extractive Metallurgy Of Rare Earths. Boca Raton, Florida.CRC press.

Martin, B. M. (2010). Rare Earth Materials in the Defense Supply Chain. Washington DC, DIANE Publishing Company. United States Government Accountability Office.

McGill, I. (2012). Rare Earth Elements, In Ullmann's Encyclopedia Of Industrial Chemistry: Wiley-VCH Verlag GmbH & Co. KGaA, Weinheim.

MineralPrices. (2016). Rare earth metal and oxide prices. Retrieved from http://mineralprices.com/.

Moldoveanu, G. A., & Papangelakis, V. G. (2013). Recovery of rare earth elements adsorbed on clay minerals: II. Leaching with ammonium sulfate. Hydrometallurgy, 131, 158-166.

Moustafa, M. I., & Abdelfattah, N. A. (2010). Physical and chemical beneficiation of the Egyptian beach monazite. Resource Geology, 60(3), 288-299.

Murthy, D., Kumar, V., & Rao, K. (2003). Extraction of gold from an Indian low-grade refractory gold ore through physical beneficiation and thiourea leaching. Hydrometallurgy, 68(1), 125-130.

Naik, P. K., Reddy, P., & Misra, V. N. (2004). Optimization of coal flotation using statistical technique. Fuel Processing Technology, 85(13), 1473-1485.

Norman, A., Zou, X., & Barnett, J. (2014). Critical minerals: Rare earths and the US Economy. National Center for Policy Analysis.

Ober, J. A. (2016). Mineral commodity summaries 2016. US Geological Survey.

Oddo, G. (1914). Die molekularstruktur der Radioaktiven atome. Zeitschrift für anorganische Chemie, 87(1), 253-268.

Peramaki, S. (2014). Method development for determination and recovery of rare earth elements from industrial fly ash (Post Doctoral Thesis). Retrieved from http://urn.fi/URN:ISBN:978-951-39-6001-8.

Polinares. (2012). EU Policy on Natural Resources, "Fact Sheet: Rare Earths Oxides (REO)," Polinares working paper no. 37, March 2012. Retrieved from http://www.polinares.eu/docs/d21/polinares_wp2_annex2_factsheet3_v1_10.pdf.

Pradip, C., & Fuerstnau, D (1988). Alkyl hydroxamates as collectors for the flotation of bastnaesite rare-earth ores. In Journal of Metals (Vol. 40, No. 11, pp. 14-15). 420 Commonwealth Dr, Warrendale, PA 15086: Minerals Metals Materials Society.

Ren, J., Song, S., Lopez-Valdivieso, A., & Lu, S. (2000). Selective flotation of bastnaesite from monazite in rare earth concentrates using potassium alum as depressant. International Journal of Mineral Processing, 59(3), 237-245.

Rozelle, P. L., Khadilkar, A. B., Pulati, N., Soundarrajan, N., Klima, M. S., Mosser, M. M., Pisupati, S. V. (2016). A Study on Removal of Rare Earth Elements from US Coal Byproducts by Ion Exchange. Metallurgical and Materials Transactions E, 3(1), 6-17.

Scott, C., Deonarine, A., Kolker, A., Adams, M., & Holland, J. (2015). Size Distribution of Rare Earth Elements in Coal Ash. In World of Coal Ash Conference, Nashville, TN May (Vol. 5, No. 7).

Seredin, V. (1996). Rare earth element-bearing coals from the Russian Far East deposits. International Journal of Coal Geology, 30(1), 101-129.

Seredin, V. V. (1991). About the new type of rare earth element mineralization in the Cenozoic coal-bearing basins. USSR Acad. Sci., 320(6), 1446-1450.

Seredin, V. V. (1992). Ashes of coals - new potential source of Y and HREE. 29th International Geological Congress,Kyoto, 3:785.

Seredin, V. V., & Dai, S. (2012). Coal deposits as potential alternative sources for lanthanides and yttrium. International Journal of Coal Geology, 94, 67-93. doi:http://dx.doi.org/10.1016/j.coal.2011.11.001.

Stanley, R. G., Flores, R. M., & Wiley, T. J. (1992). Fluvial facies architecture in the Tertiary Usibelli Group of Suntrana, central Alaska. Geologic Studies in Alaska by the US Geological Survey. pp.204-211.

Suresh, A., Lingam, R., Sriramoju, S., Bodewar, A., Ray, T., & Dash, P. (2015). Pilot scale demineralization study on coal flotation tailings and optimization of the operational parameters with modeling. International Journal of Mineral Processing, 145, 23-31.

Swaine, D. J. (2013). Trace elemen.ts in coal:Courier International Limited, tiptree, Essex, Great Britain. Butterworth-Heinemann.

Swift T.K., Moore G.M., Glowacki H.R.R. and Sanchez E. (2014). Rare earth Technology Alliace: The Economic Benefits of the North American Rare Earths Industry. Economics & Statistics Department American Chemistry Council

Szumigala, D.J. & Werdon, M.B. (2011). Rare-Earth Elements: A brief overview including uses, worldwide resources, and known occurrences in Alaska: Alaska Division of Geological & Geophysical Surveys Information Circular 61, 12 p. http://doi.org/10.14509/22262

Thompson, T. (1997). Uranium, thorium, and rare metal deposits of Alaska. Economic Geology, Monograph, 9, 466-482.

Tripathy, S. K., & Murthy, Y. R. (2012). Modeling and optimization of spiral concentrator for separation of ultrafine chromite. Powder Technology, 221, 387-394.

U.S. Geological Survey. (2010). Mineral Commodity Summaries 2010: U.S. Geological Survey, 193 p.

U.S. Geological Survey. (2015). Mineral Commodity Summaries 2015: U.S. Geological Survey.

U.S. Geological Survey. (2002). USGS Geological Survey Fact Sheet 087-02. USGS.

U.S. Geological Survey. (2012). Global Rare Earth Oxide (REO) Production Trends. Retrieved from http://minerals.usgs.gov/minerals/pubs/commodity/rare_earths/.

Virta, R. L. (2011). U.S. Geological Survey, 2011, Mineral commodity summaries 2011. U.S. Geological Survey.

Wallace, D. N. (1981). The Use of Rare Earth Elements in Zeolite Cracking Catalysts. In Industrial Applications of Rare Earth Elements, Chapter 6, pp 101–116. Columbia, W. R. Grace & Company, Davison Chemical Division.

Wang, W., Qin, Y., Wei, C., Li, Z., Guo, Y., & Zhu, Y. (2006). Partitioning of elements and macerals during preparation of Antaibao coal. International Journal of Coal Geology, 68(3–4), 223-232. doi:http://dx.doi.org/10.1016/j.coal.2006.02.006

Zhang, J., & Edwards, C. (2012). A review of rare earth mineral processing technology. In 44th Annual Meeting of the Canadian Mineral Processors. CIM, Ottawa (Vol. 79).

Zhang, W., Rezaee, M., Bhagavatula, A., Li, Y., Groppo, J., & Honaker, R. (2015). A review of the occurrence and promising recovery methods of rare earth elements from coal and coal by-products. International Journal of Coal Preparation and Utilization, 35(6), 295-330.

Zheng, L., Liu, G., Chou, C.-L., Qi, C., & Zhang, Y. (2007). Geochemistry of rare earth elements in Permian coals from the Huaibei Coalfield, China. Journal of Asian Earth Sciences, 31(2), 167-176.

APPENDICES

Appendix A. Float-Sink data of the Healy coal sample.

Healy <1/4inch to 30Mesh											
Washability		% Weight	% moisture	% Dry Weight	Ash %	Volatile Matter %	Fixed Carbon %	Total Sulfur %	Cum. Dry Wt	Cum Ash	Cum Sulfur
SINK	FLOAT										
FLOAT	1.3	38.26	9.18	38.38	11.89	41.85	37.08	0.43	38.38	11.89	0.43
1.3	1.5	44.17	10.22	43.80	21.09	38.39	30.30	0.56	82.18	16.82	0.50
1.5	1.6	3.81	13.98	3.62	28.47	35.49	22.06	0.39	85.80	17.33	0.49
1.6	1.7	1.91	7.61	1.95	38.24	31.90	22.25	0.32	87.75	17.79	0.49
1.7	1.8	0.64	7.83	0.65	52.70	26.16	13.31	0.15	88.40	18.04	0.49
1.8	2	6.79	8.65	6.85	62.00	20.91	8.44	0.10	95.25	21.16	0.46
2	2.2	3.73	2.74	4.01	77.47	14.95	4.84	0.06	99.26	23.28	0.45
2.2	Sink	0.69	2.60	0.74	88.19	9.21	0.00	0.03	100.00	**23.72**	0.44
Total		100.00	9.46	100.00	**23.72**	37.14	29.67	0.44			
Healy <30Mesh to100Mesh											
Washability		% Weight	% moisture	% Dry Weight	Ash %	Volatile Matter %	Fixed Carbon %	Total Sulfur %	Cum. Dry Wt	Cum Ash	Cum Sulfur
SINK	FLOAT										
FLOAT	1.3	0.14	10.05	0.14	10.27	45.40	34.28	0.45	0.14	10.27	0.45
1.3	1.5	19.15	13.58	19.11	13.09	45.78	27.55	0.24	19.26	13.07	0.24
1.5	1.6	35.39	13.23	35.46	17.58	43.18	26.01	0.30	54.71	15.99	0.28
1.6	1.7	23.84	19.40	22.19	20.76	40.72	19.12	0.27	76.90	17.44	0.28
1.7	1.8	0.82	9.80	0.86	53.08	26.56	10.56	0.20	77.76	17.81	0.28
1.8	2	5.05	9.51	5.28	58.08	28.55	3.86	0.12	83.04	20.22	0.27
2	2.2	4.77	8.33	5.04	59.50	30.99	1.18	0.09	88.09	22.32	0.26
2.2	Sink	10.84	4.80	11.91	83.11	12.09	0.00	0.03	100.00	**28.91**	0.23
Total		100.00	13.40	100.00	**28.91**	38.27	19.43	0.23			
Composite Sample Washability											
Healy 1/4 inch to 0											
Washability		% Weight	% moisture	% Dry Weight	Ash %	Volatile Matter %	Fixed Carbon %	Total Sulfur %	Cum. Dry Wt	Cum Ash	Cum Sulfur
SINK	FLOAT										
FLOAT	1.3	33.95	9.18	34.23	11.89	41.85	37.08	0.43	34.23	11.89	0.43
1.3	1.5	41.11	10.40	40.89	20.66	38.79	30.15	0.54	75.12	16.69	0.49
1.5	1.6	7.54	13.56	7.24	22.40	39.78	24.26	0.34	82.36	17.21	0.48
1.6	1.7	4.49	15.06	4.23	27.20	37.47	20.27	0.29	86.59	17.73	0.47
1.7	1.8	0.67	8.16	0.69	52.76	26.23	12.85	0.16	87.28	18.00	0.47
1.8	2	6.54	8.73	6.63	61.63	21.63	8.01	0.10	93.90	21.02	0.44
2	2.2	3.79	3.60	4.06	74.71	17.41	4.28	0.06	97.96	23.10	0.43
2.2	Sink	1.92	4.11	2.04	84.71	11.18	0.00	0.03	100.00	**24.28**	0.42
Total		100.00	9.93	100.00	**24.28**	37.30	28.49	0.42			

Appendix B. Float-Sink data of the Wishbone Hill coal sample.

Wishbone Hill <1/4 inch to 30Mesh											
Washability		% Weight	% moisture	% Dry Weight	Ash %	Volatile Matter %	Fixed Carbon %	Total Sulfur %	Cum. Dry Wt	Cum Ash	Cum Sulfur
SINK	FLOAT										
FLOAT	1.3	34.65	2.81	34.61	6.09	36.93	54.17	0.50	34.61	6.09	0.50
1.3	1.5	9.36	3.98	9.24	28.81	30.96	36.25	0.38	43.85	10.92	0.47
1.5	1.6	5.05	3.64	5.01	42.23	26.56	27.57	0.29	48.86	14.15	0.46
1.6	1.7	4.40	3.41	4.37	51.08	23.90	21.61	0.23	53.23	17.19	0.44
1.7	1.8	2.59	2.56	2.60	62.51	19.76	15.17	0.15	55.82	19.28	0.42
1.8	2	7.57	2.47	7.59	74.73	16.20	6.60	0.08	63.41	25.88	0.38
2	2.2	8.12	2.26	8.16	78.38	14.41	4.95	0.06	71.57	31.82	0.35
2.2	Sink	28.26	2.13	28.43	81.33	14.01	2.53	0.04	100.00	**45.81**	0.26
Total		100.00	2.72	100.00	**45.81**	24.95	26.51	0.26			

Wishbone Hill <30Mesh to 100Mesh											
Washability		% Weight	% moisture	% Dry Weight	Ash %	Volatile Matter %	Fixed Carbon %	Total Sulfur %	Cum. Dry Wt.	Cum Ash	Cum Sulfur
SINK	FLOAT										
FLOAT	1.3	28.10	9.28	26.78	9.52	31.29	49.91	0.34	26.78	9.52	0.34
1.3	1.5	2.16	5.06	2.15	30.81	29.19	34.94	0.37	28.93	11.04	0.34
1.5	1.6	0.31	3.92	0.31	43.84	25.47	26.77	0.32	29.24	11.37	0.34
1.6	1.7	0.68	4.15	0.69	50.74	23.92	21.19	0.26	29.92	12.23	0.34
1.7	1.8	2.35	2.85	2.39	75.51	14.48	7.16	0.09	32.32	16.65	0.32
1.8	2	0.51	2.98	0.52	72.37	15.18	9.47	0.11	32.84	17.48	0.32
2	2.2	7.19	7.29	7.01	71.64	17.19	3.88	0.05	39.84	26.92	0.27
2.2	Sink	58.70	2.44	60.16	83.11	12.09	2.36	0.03	100.00	**59.90**	0.13
Total		100.00	4.80	100.00	**59.90**	18.41	16.89	0.13			

Composite Sample Washability											
Wishbone Hill 1/4 inch to 0											
Washability		% Weight	% moisture	% Dry Weight	Ash %	Volatile Matter %	Fixed Carbon %	Total Sulfur %	Cum. Dry Wt	Cum Ash	Cum Sulfur
SINK	FLOAT										
FLOAT	1.3	33.44	3.36	33.29	6.38	36.45	53.81	0.49	33.29	6.38	0.49
1.3	1.5	8.64	4.01	8.55	28.86	30.92	36.22	0.38	41.83	11.00	0.46
1.5	1.6	4.58	3.64	4.54	42.24	26.55	27.56	0.29	46.38	14.06	0.45
1.6	1.7	4.03	3.42	4.01	51.07	23.90	21.60	0.23	50.38	17.00	0.43
1.7	1.8	2.57	2.59	2.58	63.72	19.27	14.43	0.14	52.96	19.26	0.42
1.8	2	6.88	2.47	6.91	74.71	16.19	6.62	0.08	59.87	25.60	0.38
2	2.2	8.06	2.72	8.08	77.77	14.66	4.85	0.06	67.96	31.77	0.34
2.2	Sink	31.80	2.19	32.04	81.66	13.65	2.50	0.04	100.00	**47.64**	0.24
Total		100.00	2.93	100.00	**47.64**	24.17	25.27	0.24			

Appendix C. REE analysis of the Healy coal sample with size and density fractions (data reported on "Whole Coal" basis).

Healy Coal																	
U.S. Mesh Size		Sc	La	Ce	Pr	Nd	Sm	Eu	Gd	Y	Tb	Dy	Ho	Er	Tm	Yb	Lu
		ppm	ppm	ppm	ppm	ppm	ppm	ppm	ppm	ppm	ppm	ppm	ppm	ppm	ppm	ppm	ppm
	+1/4 inch	5.70	16.55	34.06	4.10	15.80	3.68	0.84	3.42	16.82	0.53	3.12	0.64	1.79	0.24	1.63	0.24
-1/4 inch	+30M	7.17	17.00	35.20	4.20	15.99	3.73	0.80	3.31	17.03	0.52	3.04	0.62	1.69	0.26	1.58	0.24
-30M	+100M	7.69	18.70	37.58	4.46	16.99	3.88	0.77	3.43	17.41	0.51	3.11	0.63	1.92	0.27	1.63	0.24
-100M		8.58	20.63	41.59	4.92	18.65	4.10	0.93	3.70	18.98	0.58	3.53	0.70	1.91	0.27	1.83	0.25
TOTAL		7.23	17.25	35.57	4.24	16.16	3.76	0.80	3.33	17.11	0.52	3.06	0.62	1.72	0.26	1.59	0.24
Healy -1/4inch +30Mesh																	
Washability		Sc	La	Ce	Pr	Nd	Sm	Eu	Gd	Y	Tb	Dy	Ho	Er	Tm	Yb	Lu
SINK	FLOAT	ppm	ppm	ppm	ppm	ppm	ppm	ppm	ppm	ppm	ppm	ppm	ppm	ppm	ppm	ppm	ppm
FLOAT	1.3	3.40	8.57	17.30	2.01	8.55	2.06	0.44	1.96	9.71	0.29	1.60	0.33	0.92	0.13	0.81	0.12
1.3	1.5	4.61	16.80	33.81	4.02	16.19	3.70	0.77	3.42	16.63	0.54	2.99	0.60	1.62	0.25	1.56	0.24
1.5	1.6	5.43	21.61	42.40	4.85	19.81	4.14	0.94	3.78	18.01	0.57	3.26	0.65	1.85	0.29	1.64	0.26
1.6	1.7	5.09	22.47	42.27	4.90	19.33	4.12	0.92	3.78	17.81	0.59	3.09	0.70	1.77	0.28	1.87	0.25
1.7	1.8	6.49	24.88	44.05	4.97	19.16	3.97	0.81	3.17	16.45	0.50	2.95	0.61	1.73	0.28	1.79	0.25
1.8	2	9.80	28.64	49.72	5.92	21.92	4.35	0.85	3.49	17.30	0.49	3.15	0.69	1.92	0.28	1.88	0.31
2	2.2	13.00	32.34	58.33	6.91	24.70	4.65	0.95	3.72	19.91	0.63	3.60	0.80	2.16	0.35	2.33	0.37
2.2	Sink	11.20	53.87	130.71	16.62	66.66	15.78	1.85	14.19	64.61	2.43	13.49	2.53	6.47	0.97	4.81	0.56
Total		4.94	15.68	30.81	3.64	14.58	3.27	0.68	2.97	14.58	0.46	2.58	0.53	1.44	0.22	1.36	0.21
Healy -30Mesh+100Mesh																	
Washability		Sc	La	Ce	Pr	Nd	Sm	Eu	Gd	Y	Tb	Dy	Ho	Er	Tm	Yb	Lu
SINK	FLOAT	ppm	ppm	ppm	ppm	ppm	ppm	ppm	ppm	ppm	ppm	ppm	ppm	ppm	ppm	ppm	ppm
FLOAT	1.3	NSS	NSS	NSS	NSS	NSS	NSS	NSS	NSS	NSS	NSS	NSS	NSS	NSS	NSS	NSS	NSS
1.3	1.5	2.16	9.15	15.44	1.84	7.59	1.83	0.39	1.72	8.12	0.25	1.39	0.28	0.74	0.12	0.70	0.10
1.5	1.6	4.39	13.43	20.75	2.42	10.27	2.42	0.52	2.26	10.91	0.33	1.87	0.41	1.07	0.16	0.96	0.15
1.6	1.7	4.03	15.69	26.26	3.05	12.50	2.70	0.63	2.56	11.77	0.37	2.24	0.45	1.26	0.20	1.11	0.17
1.7	1.8	5.99	29.31	45.26	5.10	19.78	4.27	0.77	3.21	16.19	0.50	3.02	0.60	1.65	0.26	1.68	0.26
1.8	2	5.23	25.58	40.63	4.70	17.67	3.32	0.63	2.73	14.33	0.42	2.54	0.54	1.53	0.24	1.61	0.22
2	2.2	4.62	19.87	35.37	4.09	15.38	2.90	0.62	2.34	13.53	0.37	2.41	0.53	1.53	0.26	1.52	0.23
2.2	Sink	4.41	14.38	25.58	3.02	10.67	2.33	0.41	1.67	11.29	0.30	1.90	0.41	1.08	0.17	1.10	0.17
Total		3.95	14.31	23.50	2.74	11.02	2.44	0.52	2.19	10.96	0.33	1.93	0.41	1.10	0.17	1.03	0.15

Appendix D. REE analysis of the Wishbone Hill coal sample with size and density fractions (data reported on "Whole Coal" basis).

Wishbone Hill Coal																	
U.S. Mesh Size		Sc	La	Ce	Pr	Nd	Sm	Eu	Gd	Y	Tb	Dy	Ho	Er	Tm	Yb	Lu
		ppm	ppm	ppm	ppm	ppm	ppm	ppm	ppm	ppm	ppm	ppm	ppm	ppm	ppm	ppm	ppm
	+1/4 inch	13.51	19.12	39.12	4.79	18.44	4.37	0.93	4.10	23.07	0.69	3.88	0.86	2.58	0.37	2.55	0.35
-1/4 inch	+30M	14.44	16.11	36.09	4.27	18.39	4.31	0.87	3.96	20.58	0.65	3.81	0.81	2.34	0.38	2.18	0.30
-30M	+100M	13.57	18.29	39.94	4.62	19.59	4.52	0.98	4.23	21.71	0.62	3.78	0.82	2.16	0.36	2.27	0.34
-100M		13.55	19.55	42.79	5.13	21.04	4.94	1.15	4.89	25.36	0.77	4.56	1.01	2.78	0.43	2.59	0.39
TOTAL		14.26	16.64	36.81	4.37	18.54	4.34	0.89	4.01	20.99	0.65	3.82	0.82	2.35	0.38	2.23	0.31
Wishbone Hill -1/4 inch+30Mesh																	
Washability		Sc	La	Ce	Pr	Nd	Sm	Eu	Gd	Y	Tb	Dy	Ho	Er	Tm	Yb	Lu
SINK	FLOAT	ppm	ppm	ppm	ppm	ppm	ppm	ppm	ppm	ppm	ppm	ppm	ppm	ppm	ppm	ppm	ppm
FLOAT	1.3	7.09	4.75	10.64	1.30	5.70	1.42	0.34	1.74	13.03	0.30	2.05	0.48	1.37	0.24	1.50	0.23
1.3	1.5	11.92	15.31	31.93	3.80	15.80	3.68	0.75	3.64	19.40	0.57	3.38	0.74	2.11	0.35	2.17	0.33
1.5	1.6	13.30	19.02	41.37	4.92	20.75	4.43	0.89	4.25	21.37	0.63	3.94	0.84	2.35	0.36	2.27	0.36
1.6	1.7	13.34	21.02	46.31	5.55	22.46	4.84	1.08	4.86	22.83	0.71	4.32	0.91	2.41	0.39	2.33	0.35
1.7	1.8	15.40	23.09	49.53	5.98	24.38	5.57	1.04	5.09	23.54	0.76	4.39	0.93	2.50	0.40	2.49	0.35
1.8	2	17.11	25.59	55.06	6.67	27.30	6.55	1.24	5.52	27.06	0.94	5.27	1.09	2.73	0.43	2.71	0.37
2	2.2	19.51	25.36	54.30	6.32	26.42	6.34	1.31	5.80	28.53	0.90	5.27	1.10	2.87	0.48	2.71	0.41
2.2	Sink	17.68	24.08	51.69	6.26	25.43	5.87	1.27	5.56	27.28	0.91	5.09	1.05	2.85	0.45	2.55	0.40
Total		13.12	16.39	35.32	4.25	17.54	4.09	0.87	3.97	21.12	0.64	3.80	0.81	2.21	0.36	2.15	0.33
Wishbone Hill -30Mesh+100Mesh																	
Washability		Sc	La	Ce	Pr	Nd	Sm	Eu	Gd	Y	Tb	Dy	Ho	Er	Tm	Yb	Lu
SINK	FLOAT	ppm	ppm	ppm	ppm	ppm	ppm	ppm	ppm	ppm	ppm	ppm	ppm	ppm	ppm	ppm	ppm
FLOAT	1.3	7.17	4.21	8.49	1.03	4.68	1.20	0.30	1.44	11.21	0.26	1.77	0.42	1.21	0.21	1.31	0.20
1.3	1.5	10.60	15.50	33.06	3.98	16.73	3.76	0.85	3.79	18.68	0.57	3.38	0.75	1.99	0.33	1.89	0.31
1.5	1.6	12.15	21.26	44.07	5.28	21.08	5.02	1.01	4.60	21.92	0.65	4.12	0.86	2.45	0.38	2.36	0.36
1.6	1.7	9.16	23.75	49.65	5.87	24.50	5.49	1.09	4.99	22.89	0.69	4.52	0.87	2.45	0.39	2.36	0.34
1.7	1.8	16.66	25.94	55.29	6.59	27.13	6.13	1.25	5.46	25.31	0.80	4.93	0.95	2.87	0.40	2.29	0.35
1.8	2	10.60	26.27	54.21	6.62	26.12	6.11	1.28	5.72	25.06	0.84	4.72	1.00	2.48	0.42	2.53	0.39
2	2.2	11.84	22.03	46.82	5.46	23.29	5.01	1.03	4.67	22.82	0.69	4.32	0.88	2.56	0.39	2.44	0.36
2.2	Sink	19.86	23.49	49.66	5.80	24.61	5.04	1.26	5.04	24.53	0.79	4.48	0.98	2.54	0.40	2.70	0.38
Total		15.48	18.12	38.22	4.48	19.07	4.02	0.98	4.03	20.72	0.63	3.73	0.81	2.18	0.35	2.28	0.33

Appendix E. REE analysis of the Healy and the Wishbone Hill composite coal samples with size and density fractions (data reported on "Whole Coal" basis).

Healy 1/4 inch to 0																	
Washability		Sc	La	Ce	Pr	Nd	Sm	Eu	Gd	Y	Tb	Dy	Ho	Er	Tm	Yb	Lu
SINK	FLOAT	ppm	ppm	ppm	ppm	ppm	ppm	ppm	ppm	ppm	ppm	ppm	ppm	ppm	ppm	ppm	ppm
FLOAT	1.3	3.45	8.67	17.56	2.04	8.65	2.08	0.45	1.98	9.84	0.29	1.63	0.33	0.94	0.13	0.83	0.12
1.3	1.5	4.55	16.49	33.10	3.94	15.84	3.62	0.76	3.35	16.31	0.53	2.94	0.59	1.59	0.25	1.53	0.24
1.5	1.6	5.33	16.86	30.36	3.47	14.21	3.08	0.73	2.85	13.90	0.42	2.45	0.50	1.40	0.21	1.28	0.20
1.6	1.7	4.83	18.50	33.03	3.82	15.16	3.24	0.77	3.02	14.29	0.45	2.55	0.55	1.46	0.23	1.46	0.20
1.7	1.8	6.44	25.38	44.15	4.98	19.21	4.00	0.80	3.17	16.40	0.49	2.96	0.61	1.72	0.27	1.77	0.25
1.8	2	9.48	28.39	48.98	5.82	21.57	4.26	0.83	3.42	17.05	0.48	3.10	0.68	1.89	0.28	1.86	0.30
2	2.2	12.04	30.84	55.56	6.57	23.56	4.43	0.91	3.55	19.12	0.59	3.45	0.77	2.08	0.34	2.24	0.36
2.2	Sink	7.76	32.34	73.66	9.24	36.24	8.48	1.08	7.40	35.79	1.27	7.23	1.38	3.55	0.53	2.81	0.35
Total		4.95	15.68	30.44	3.60	14.36	3.22	0.67	2.93	14.40	0.45	2.56	0.52	1.43	0.22	1.34	0.20
Wishbone Hill 1/4 inch to 0																	
Washability		Sc	La	Ce	Pr	Nd	Sm	Eu	Gd	Y	Tb	Dy	Ho	Er	Tm	Yb	Lu
SINK	FLOAT	ppm	ppm	ppm	ppm	ppm	ppm	ppm	ppm	ppm	ppm	ppm	ppm	ppm	ppm	ppm	ppm
FLOAT	1.3	7.09	4.72	10.47	1.28	5.61	1.41	0.34	1.71	12.93	0.30	2.03	0.48	1.37	0.24	1.50	0.23
1.3	1.5	11.88	15.36	32.00	3.82	15.81	3.68	0.76	3.64	19.42	0.57	3.37	0.74	2.11	0.35	2.18	0.33
1.5	1.6	13.29	19.08	41.43	4.93	20.75	4.44	0.89	4.25	21.40	0.63	3.94	0.84	2.36	0.36	2.28	0.36
1.6	1.7	13.26	21.11	46.41	5.56	22.49	4.85	1.08	4.86	22.86	0.71	4.32	0.91	2.41	0.39	2.33	0.35
1.7	1.8	15.51	23.39	50.10	6.04	24.63	5.62	1.06	5.13	23.73	0.77	4.44	0.93	2.54	0.40	2.48	0.35
1.8	2	17.05	25.71	55.16	6.69	27.27	6.55	1.24	5.52	27.11	0.94	5.26	1.09	2.74	0.43	2.73	0.37
2	2.2	18.82	25.19	53.75	6.26	26.13	6.23	1.29	5.69	28.11	0.88	5.18	1.08	2.86	0.47	2.71	0.41
2.2	Sink	17.98	24.43	51.85	6.27	25.30	5.75	1.28	5.47	27.18	0.89	4.98	1.05	2.87	0.45	2.66	0.40
Total		13.37	16.84	36.03	4.33	17.80	4.12	0.89	4.00	21.32	0.65	3.81	0.82	2.25	0.36	2.21	0.33

Appendix F. Wet High Intensity Magnetic Separation (WHIMS) of the Healy and the Wishbone Hill coal samples (<100 Mesh fractions).

	Moisture	% Dry Weight	Ash	Volatile Matter	Fixed Carbon	Total Sulphur
	air dried %		air dried %	air dried %	air dried %	air dried %
Healy Magnetics	NSS	0.67	48.59	NSS	NSS	NSS
Healy Non-Mags	9.42	99.33	32.78	44.75	13.05	0.52
Wishbone Hill Magnetics	1.53	12.02	74.78	23.69	0	<0.01
Wishbone Hill Non-Mags	3.71	87.98	58.38	20.77	17.14	0.18

Appendix G. REE distributions after Wet High Intensity Magnetic Separation (WHIMS) of the Healy and the Wishbone Hill samples (<100 Mesh fractions) on whole coal basis.

	Sc	La	Ce	Pr	Nd	Sm	Eu	Gd	Y	Tb	Dy	Ho	Er	Tm	Yb	Lu
	ppm	ppm	ppm	ppm	ppm	ppm	ppm	ppm	ppm	ppm	ppm	ppm	ppm	ppm	ppm	ppm
Healy Magnetics	NSS	NSS	NSS	NSS	NSS	NSS	NSS	NSS	NSS	NSS	NSS	NSS	NSS	NSS	NSS	NSS
Healy Non-Mags	6.68	20.95	42.52	4.94	20.09	4.20	0.98	4.03	18.83	0.58	3.38	0.69	2.09	0.29	1.80	0.30
Wishbone Hill Magnetics	29.56	19.18	43.95	5.44	23.65	6.98	1.83	8.31	50.90	1.34	8.55	1.87	5.34	0.78	4.79	0.70
Wishbone Hill Non-Mags	14.81	20.36	43.69	5.37	21.54	5.02	1.08	4.39	23.02	0.68	4.33	0.88	2.41	0.39	2.52	0.37

Appendix H. Flotation of Healy and the Wishbone Hill Samples (<100 Mesh fractions) on whole coal basis.

	Yield %	Moisture	% Dry Weight	Ash	Volatile Matter	Fixed Carbon	Total Sulfur
		air dried %		air dried %	air dried %	air dried %	air dried %
Healy Coal Floats	26.21	7.55	26.73	21.94	35.63	34.88	0.56
Healy Coal Tailings	73.79	9.97	73.27	34.13	33.37	22.53	0.57
Wishbone Hill Coal Floats	30.74	3.41	30.60	26.5	29.93	40.16	0.39
Wishbone Hill Coal Tailings	69.26	2.73	69.40	74.24	17.50	5.53	0.03

Appendix I. REE Distribution after flotation of Healy and the Wishbone Hill Samples (<100 Mesh fractions) on whole coal basis.

	Sc	La	Ce	Pr	Nd	Sm	Eu	Gd	Y	Tb	Dy	Ho	Er	Tm	Yb	Lu
	ppm	ppm	ppm	ppm	ppm	ppm	ppm	ppm	ppm	ppm	ppm	ppm	ppm	ppm	ppm	ppm
Healy Coal Floats	6.63	16.95	34.15	3.98	15.93	3.43	0.78	3.26	16.56	0.51	2.99	0.60	1.60	0.22	1.50	0.22
Healy Coal Tailings	8.70	22.38	44.68	5.26	20.92	4.35	1.00	4.23	21.87	0.65	3.87	0.83	2.34	0.31	2.10	0.34
Wishbone Hill Coal Floats	9.00	11.19	23.76	2.91	12.01	2.83	0.65	3.09	18.76	0.48	2.98	0.70	1.97	0.31	1.95	0.31
Wishbone Hill Coal Tailings	18.82	26.66	56.70	7.01	28.31	6.68	1.29	6.22	33.80	0.96	6.06	1.33	3.52	0.47	3.22	0.46

Appendix J. Proximate and sulfur analysis of UAF power plant products.

	Weight %	Moisture	Dry Weight %	Ash	Volatile Matter	Fixed Carbon	Total Sulfur
		air dried %		air dried %	air dried %	air dried %	air dried %
UAF BOTTOM ASH	100	0.09	99.91	99.63	0.28	0.00	<0.01
UAF FLY ASH	100	1.95	98.05	84.17	7.84	6.04	1.71
UAF CINDERS	100	3.54	96.46	67.17	7.23	22.06	0.24

Appendix K. REE distribution of UAF power plant products on ash basis.

	Sc	La	Ce	Pr	Nd	Sm	Eu	Gd	Y	Tb	Dy	Ho	Er	Tm	Yb	Lu
	ppm	ppm	ppm	ppm	ppm	ppm	ppm	ppm	ppm	ppm	ppm	ppm	ppm	ppm	ppm	ppm
UAF BOTTOM ASH	23.89	31.86	66.11	7.41	30.37	6.36	1.58	6.28	32.56	0.98	5.91	1.25	3.56	0.53	3.34	0.49
UAF FLY ASH	20.74	26.35	56.6	6.4	26.96	5.94	1.44	5.83	29.72	0.96	5.45	1.13	3	0.47	2.87	0.48
UAF CINDERS	17.63	20.38	42.03	4.82	19.6	4.33	1.09	4.15	21.37	0.64	4.03	0.83	2.31	0.35	2.13	0.37

Appendix L. Proximate Analysis of the 17 Box-Behnken Flotation products for Wishbone Hill.

	% Weight	Moisture air dried %	% Dry Weight	Ash air dried %	Volatile Matter air dried %	Fixed Carbon air dried %
Wishbone Hill Floats-1	80.5	2.50	80.5	32.4	37.54	27.54
Wishbone Hill Tailings-1	19.5	2.50	19.5	75.3	16.10	6.10
Wishbone Hill Floats-2	84.6	2.40	84.6	34.1	37.04	26.44
Wishbone Hill Tailings-2	15.4	2.40	15.4	77.6	15.30	4.70
Wishbone Hill Floats-3	81.0	3.00	81.0	32.7	37.06	27.26
Wishbone Hill Tailings-3	19.0	3.00	19.0	75.4	15.70	5.90
Wishbone Hill Floats-4	83.6	2.50	83.6	33.7	37.11	26.71
Wishbone Hill Tailings-4	16.4	2.50	16.4	77.1	15.40	5.00
Wishbone Hill Floats-5	21.6	2.90	21.6	24.8	35.28	36.98
Wishbone Hill Tailings-5	78.4	2.90	78.4	45.2	25.10	26.80
Wishbone Hill Floats-6	73.0	3.00	73.0	27.8	39.35	29.85
Wishbone Hill Tailings-6	27.0	3.00	27.0	75.9	15.30	5.80
Wishbone Hill Floats-7	75.3	2.90	75.3	29.0	38.76	29.36
Wishbone Hill Tailings-7	24.7	2.90	24.7	76.9	14.80	5.40
Wishbone Hill Floats-8	76.7	2.90	76.7	29.6	38.96	28.56
Wishbone Hill Tailings-8	23.3	2.90	23.3	77.7	14.90	4.50
Wishbone Hill Floats-9	76.8	2.90	76.8	29.4	38.87	28.87
Wishbone Hill Tailings-9	23.2	2.90	23.2	78.7	14.20	4.20
Wishbone Hill Floats-10	77.6	2.60	77.6	30.4	38.21	28.81
Wishbone Hill Tailings-10	22.4	2.60	22.4	77.0	14.90	5.50
Wishbone Hill Floats-11	76.0	2.70	76.0	29.1	39.06	29.16
Wishbone Hill Tailings-11	24.0	2.70	24.0	78.0	14.60	4.70
Wishbone Hill Floats-12	76.4	2.60	76.4	29.5	38.49	29.39
Wishbone Hill Tailings-12	23.6	2.60	23.6	77.3	14.60	5.50
Wishbone Hill Floats-13	54.4	3.10	54.4	20.2	41.30	35.40
Wishbone Hill Tailings-13	45.6	3.10	45.6	65.4	18.70	12.80
Wishbone Hill Floats-14	76.9	2.70	76.9	30.0	38.54	28.74
Wishbone Hill Tailings-14	23.1	2.70	23.1	76.7	15.20	5.40
Wishbone Hill Floats-15	18.9	3.30	18.9	40.4	26.96	29.36
Wishbone Hill Tailings-15	81.1	3.30	81.1	40.9	26.70	29.10
Wishbone Hill Floats-16	19.9	2.80	19.9	29.9	32.58	34.68
Wishbone Hill Tailings-16	80.1	2.80	80.1	43.5	25.80	27.90
Wishbone Hill Floats-17	72.1	2.70	72.1	27.1	39.62	30.62
Wishbone Hill Tailings-17	27.9	2.70	27.9	76.3	15.00	6.00
Wishbone Hill Composite	100	4.20	100	40.8	26.20	28.80

Appendix M. Proximate Analysis 17 Box-Behnken Flotation products for Healy.

	% Weight	Moisture air dried %	% Dry Weight	Ash air dried %	Volatile Matter air dried %	Fixed Carbon air dried %
Healy Floats-1	46.3	7.60	46.33	23.13	32.74	24.64
Healy Tailings-1	53.7	7.60	53.67	20.28	34.90	26.80
Healy Floats-2	48.7	6.10	48.66	23.13	33.64	25.24
Healy Tailings-2	51.3	6.10	51.34	20.15	35.90	27.50
Healy Floats-3	51.1	6.10	51.11	23.18	33.55	25.25
Healy Tailings-3	48.9	6.10	48.89	19.95	36.00	27.70
Healy Floats-4	62.3	6.40	62.26	21.96	34.48	25.88
Healy Tailings-4	37.7	6.40	37.74	21.01	35.20	26.60
Healy Floats-5	12.4	4.00	12.36	29.57	30.42	20.82
Healy Tailings-5	87.6	4.00	87.64	20.48	37.30	27.70
Healy Floats-6	66.8	7.40	66.80	21.01	34.95	25.85
Healy Tailings-6	33.2	7.40	33.20	22.79	33.60	24.50
Healy Floats-7	65.5	7.90	65.46	21.57	33.88	25.58
Healy Tailings-7	34.5	7.90	34.54	21.67	33.80	25.50
Healy Floats-8	56.3	6.20	56.30	22.52	33.90	25.80
Healy Tailings-8	43.7	6.20	43.70	20.41	35.50	27.40
Healy Floats-9	61.7	7.50	61.74	22.54	33.44	24.94
Healy Tailings-9	38.3	7.50	38.26	20.08	35.30	26.80
Healy Floats-10	73.5	8.80	73.55	21.22	33.89	25.19
Healy Tailings-10	26.5	8.80	26.45	22.66	32.80	24.10
Healy Floats-11	64.6	7.90	64.57	22.11	33.52	25.12
Healy Tailings-11	35.4	7.90	35.43	20.68	34.60	26.20
Healy Floats-12	77.6	10.30	77.57	21.58	32.86	24.16
Healy Tailings-12	22.4	10.30	22.43	21.67	32.80	24.10
Healy Floats-13	23.0	7.70	23.02	28.89	28.43	20.13
Healy Tailings-13	77.0	7.70	76.98	19.42	35.60	27.30
Healy Floats-14	60.3	7.30	60.32	25.29	30.65	23.75
Healy Tailings-14	39.7	7.30	39.68	15.99	37.70	30.80
Healy Floats-15	14.4	8.70	14.37	46.79	14.13	6.33
Healy Tailings-15	85.6	8.70	85.63	17.37	36.40	28.60
Healy Floats-16	16.6	7.60	16.63	28.55	28.99	20.19
Healy Tailings-16	83.4	7.60	83.37	20.21	35.30	26.50
Healy Floats-17	58.9	10.10	58.95	24.22	30.67	22.57
Healy Tailings-17	41.1	10.10	41.05	17.83	35.50	27.40
Healy Composite	100	17.55	100.00	21.6	33.70	25.30

Appendix N. REE distribution in 17 Box-Behnken Flotation products for Wishbone Hill.

	Sc	La	Ce	Pr	Nd	Sm	Eu	Gd	Y	Tb	Dy	Ho	Er	Tm	Yb	Lu
	ppm	ppm	ppm	ppm	ppm	ppm	ppm	ppm	ppm	ppm	ppm	ppm	ppm	ppm	ppm	ppm
Wishbone Hill Floats-1	24.3	49.1	99.5	12.3	23.1	10.9	2.3	11.1	65.1	1.6	10.1	2.2	6.7	1.0	6.1	1.0
Wishbone Hill Tailings-1	18.0	33.9	74.0	8.8	12.1	7.7	1.7	7.7	41.5	1.1	6.9	1.3	4.1	0.6	3.6	0.6
Wishbone Hill Floats-2	24.1	48.4	99.5	12.1	22.4	10.6	2.2	10.9	64.2	1.6	9.9	2.1	6.5	0.9	5.9	1.0
Wishbone Hill Tailings-2	17.0	32.0	68.0	8.5	11.1	7.5	1.7	7.4	38.3	1.0	6.4	1.3	3.8	0.6	3.5	0.5
Wishbone Hill Floats-3	23.6	48.2	99.4	12.1	22.9	10.7	2.3	11.1	65.9	1.6	10.0	2.2	6.6	1.0	6.0	1.0
Wishbone Hill Tailings-3	19.0	35.1	73.4	9.1	12.1	7.9	1.7	7.6	39.4	1.0	6.8	1.3	4.1	0.6	3.7	0.5
Wishbone Hill Floats-4	22.4	47.9	97.2	12.0	22.4	10.6	2.2	10.7	62.4	1.5	9.8	2.1	6.4	0.9	5.8	0.9
Wishbone Hill Tailings-4	21.0	34.0	75.0	8.9	11.7	7.8	1.8	8.1	43.7	1.1	6.9	1.5	4.3	0.6	3.8	0.6
Wishbone Hill Floats-5	17.3	63.3	121.2	10.0	31.5	8.6	0.0	6.3	72.3	0.0	2.9	0.0	0.8	0.0	0.2	0.0
Wishbone Hill Tailings-5	31.0	39.9	84.9	10.5	16.5	9.2	2.1	9.7	53.5	1.3	9.1	1.9	5.8	0.9	5.2	0.8
Wishbone Hill Floats-6	22.0	52.1	105.4	13.2	26.2	11.7	2.5	12.0	74.0	1.8	11.1	2.4	7.5	1.1	6.9	1.1
Wishbone Hill Tailings-6	22.0	35.2	75.4	9.0	12.1	7.8	1.7	7.8	39.4	1.0	6.7	1.3	4.0	0.6	3.6	0.6
Wishbone Hill Floats-7	24.6	50.7	101.0	13.0	25.3	11.4	2.4	11.6	68.9	1.7	10.8	2.3	7.1	1.0	6.6	1.1
Wishbone Hill Tailings-7	19.0	35.4	78.0	8.9	12.0	7.7	1.7	7.9	42.4	1.0	6.7	1.4	4.2	0.6	3.6	0.6
Wishbone Hill Floats-8	23.6	50.5	102.8	12.8	25.2	11.1	2.3	11.6	70.3	1.7	10.6	2.3	7.0	1.0	6.5	1.1
Wishbone Hill Tailings-8	20.0	35.0	74.7	8.8	11.5	7.9	1.7	7.8	39.4	1.1	6.8	1.3	4.1	0.6	3.6	0.6
Wishbone Hill Floats-9	25.2	50.6	102.7	12.6	25.2	11.3	2.4	11.6	70.7	1.7	10.7	2.3	7.1	1.1	6.6	1.1
Wishbone Hill Tailings-9	18.0	34.9	75.0	9.2	11.6	7.7	1.7	7.8	39.2	1.0	6.7	1.4	4.1	0.6	3.5	0.6
Wishbone Hill Floats-10	25.6	51.3	104.6	12.8	24.6	11.3	2.3	11.5	70.8	1.7	10.7	2.3	7.1	1.1	6.5	1.1
Wishbone Hill Tailings-10	17.0	33.0	70.7	8.6	11.6	7.6	1.7	7.6	37.2	1.0	6.4	1.3	3.9	0.6	3.5	0.6
Wishbone Hill Floats-11	26.2	51.4	103.6	12.8	25.4	11.3	2.4	12.0	71.2	1.7	10.7	2.4	7.1	1.1	6.5	1.1
Wishbone Hill Tailings-11	17.0	34.4	74.6	9.0	11.7	7.9	1.6	7.4	39.3	1.0	6.8	1.3	4.1	0.6	3.7	0.6
Wishbone Hill Floats-12	22.0	51.7	104.4	12.7	25.1	11.1	2.4	11.6	71.5	1.7	10.8	2.3	7.1	1.1	6.4	1.1
Wishbone Hill Tailings-12	22.0	33.6	72.9	9.0	11.7	8.0	1.7	7.7	38.2	1.1	6.6	1.4	4.1	0.6	3.7	0.6
Wishbone Hill Floats-13	32.8	63.1	120.9	15.0	37.8	13.4	2.8	14.5	94.0	2.2	13.2	3.0	8.7	1.3	8.2	1.4
Wishbone Hill Tailings-13	18.0	36.4	79.0	9.6	12.2	8.3	1.8	8.2	42.8	1.1	7.3	1.5	4.6	0.7	4.1	0.6
Wishbone Hill Floats-14	21.2	50.7	101.6	12.6	24.9	11.2	2.4	11.6	69.0	1.7	10.5	2.3	7.0	1.0	6.4	1.0
Wishbone Hill Tailings-14	23.0	34.4	75.6	9.0	11.5	7.8	1.7	7.7	40.4	1.0	6.8	1.4	4.1	0.6	3.6	0.6
Wishbone Hill Floats-15	19.8	44.9	82.5	9.8	19.6	7.2	0.0	7.8	47.5	0.0	4.6	0.0	2.7	0.0	2.4	0.0
Wishbone Hill Tailings-15	29.0	42.8	91.6	10.9	18.5	9.8	2.1	9.9	58.2	1.4	9.4	1.9	5.9	0.9	5.4	0.9
Wishbone Hill Floats-16	27.8	56.5	100.2	12.2	26.7	9.9	1.9	8.1	65.4	1.7	6.6	1.5	4.8	0.7	3.3	0.9
Wishbone Hill Tailings-16	21.0	41.4	88.6	10.9	17.8	9.7	2.1	10.2	55.1	1.4	9.3	2.0	5.9	0.9	5.5	0.8
Wishbone Hill Floats-17	27.5	52.9	106.6	13.5	27.2	11.7	2.5	12.3	75.5	1.7	11.5	2.5	7.7	1.1	6.9	1.1
Wishbone Hill Tailings-17	17.0	35.1	75.4	8.8	11.7	7.9	1.7	7.7	39.3	1.1	6.6	1.3	3.9	0.6	3.6	0.6
Wishbone Hill **Composite**	22.0	43.6	90.3	11.1	19.1	9.7	2.1	9.9	56.6	1.4	8.9	1.9	5.7	0.8	5.2	0.8

Appendix O. REE distribution in 17 Box-Behnken Flotation products for Healy.

	Sc	La	Ce	Pr	Nd	Sm	Eu	Gd	Y	Tb	Dy	Ho	Er	Tm	Yb	Lu
	ppm	ppm	ppm	ppm	ppm	ppm	ppm	ppm	ppm	ppm	ppm	ppm	ppm	ppm	ppm	ppm
Healy Floats-1	28.1	56.9	113.0	13.1	18.7	10.6	2.2	9.7	53.0	1.4	8.9	1.8	5.5	0.7	5.0	0.7
Healy Tailings-1	16.0	55.9	115.0	13.6	17.9	10.2	2.5	10.6	55.2	1.4	9.5	1.9	5.6	0.9	5.0	0.8
Healy Floats-2	21.1	55.4	111.2	13.2	19.0	10.3	2.3	9.5	50.8	1.4	9.0	1.7	5.4	0.7	5.0	0.7
Healy Tailings-2	23.0	57.5	117.0	13.6	17.5	10.6	2.4	10.9	57.7	1.4	9.4	2.0	5.7	0.8	5.0	0.8
Healy Floats-3	21.2	56.6	114.8	13.7	19.0	10.6	2.3	9.7	53.7	1.4	9.2	1.8	5.7	0.8	5.1	0.8
Healy Tailings-3	23.0	56.1	113.0	12.9	17.4	10.2	2.4	10.8	54.6	1.4	9.3	1.9	5.3	0.8	4.9	0.8
Healy Floats-4	19.1	56.4	114.6	13.5	18.5	10.4	2.3	9.9	54.5	1.4	9.4	1.8	5.6	0.8	5.0	0.8
Healy Tailings-4	27.0	56.4	113.0	13.1	17.9	10.5	2.4	10.5	53.4	1.4	8.9	1.8	5.5	0.8	5.1	0.7
Healy Floats-5	17.1	52.0	109.1	12.6	19.8	6.5	2.1	7.2	49.7	1.2	8.5	1.2	4.6	0.5	4.2	0.5
Healy Tailings-5	23.0	57.3	115.0	13.5	18.0	11.2	2.4	10.8	55.0	1.5	9.4	2.0	5.8	0.8	5.2	0.8
Healy Floats-6	24.2	57.3	116.7	13.8	18.3	10.8	2.5	10.3	56.1	1.5	9.7	1.9	5.7	0.8	5.2	0.8
Healy Tailings-6	18.0	54.8	109.0	12.5	18.3	9.6	2.2	9.8	50.3	1.3	8.4	1.7	5.2	0.8	4.6	0.7
Healy Floats-7	23.1	56.8	115.6	13.9	18.3	10.6	2.4	10.1	53.7	1.4	9.3	1.8	5.7	0.8	5.0	0.8
Healy Tailings-7	20.0	55.7	111.0	12.3	18.3	10.0	2.4	10.3	54.9	1.4	9.0	1.9	5.4	0.8	4.9	0.8
Healy Floats-8	22.7	56.8	115.4	13.8	19.1	10.4	2.3	9.8	55.2	1.4	9.4	1.8	5.6	0.8	5.1	0.8
Healy Tailings-8	21.0	55.8	112.0	12.8	17.1	10.4	2.4	10.7	52.5	1.4	8.9	1.8	5.5	0.8	4.8	0.7
Healy Floats-9	22.0	56.9	113.4	13.3	18.7	10.2	2.4	10.0	54.3	1.4	9.3	1.8	5.6	0.8	5.0	0.7
Healy Tailings-9	22.0	55.5	115.0	13.5	17.5	10.8	2.4	10.5	53.7	1.4	9.2	1.8	5.4	0.8	5.1	0.8
Healy Floats-10	23.2	58.1	118.4	13.9	18.5	10.8	2.5	10.5	56.4	1.5	9.6	1.9	5.8	0.8	5.2	0.8
Healy Tailings-10	19.0	51.9	102.5	11.9	17.7	9.3	2.1	9.2	48.2	1.3	8.1	1.6	4.9	0.7	4.4	0.7
Healy Floats-11	23.0	56.7	115.3	13.7	18.7	10.5	2.4	10.2	55.1	1.4	9.6	1.9	5.6	0.8	5.1	0.8
Healy Tailings-11	20.0	55.8	111.5	12.8	17.5	10.2	2.4	10.1	52.1	1.4	8.5	1.8	5.4	0.8	4.8	0.8
Healy Floats-12	22.0	57.2	114.9	13.5	18.4	10.6	2.4	10.2	54.9	1.4	9.4	1.8	5.7	0.8	5.1	0.8
Healy Tailings-12	22.0	53.6	111.0	12.8	18.0	9.7	2.3	9.9	51.3	1.3	8.4	1.7	5.2	0.8	4.6	0.8
Healy Floats-13	28.7	52.8	106.1	12.8	20.1	8.9	1.9	8.8	47.1	1.4	8.9	1.6	4.6	0.6	4.7	0.7
Healy Tailings-13	19.0	58.0	117.5	13.6	17.5	11.1	2.6	10.8	57.2	1.4	9.4	1.9	6.0	0.9	5.1	0.8
Healy Floats-14	17.8	54.5	109.2	12.9	18.8	9.7	2.2	9.2	49.2	1.3	8.5	1.7	5.1	0.7	4.8	0.7
Healy Tailings-14	32.0	61.0	125.5	14.5	17.1	12.2	2.7	12.4	66.0	1.6	10.9	2.2	6.6	1.0	5.6	0.9
Healy Floats-15	4.3	46.2	91.9	10.9	20.7	7.1	1.7	6.1	37.3	1.0	7.2	1.2	4.4	0.5	4.0	0.6
Healy Tailings-15	30.0	61.0	124.0	14.5	17.2	11.9	2.7	12.0	61.7	1.6	10.2	2.1	6.1	0.9	5.5	0.8
Healy Floats-16	22.0	56.4	103.4	11.4	20.1	7.0	2.1	7.3	48.1	1.2	7.9	1.5	5.3	0.5	4.1	0.7
Healy Tailings-16	22.0	56.4	117.0	13.9	17.8	11.4	2.5	11.0	55.8	1.5	9.6	1.9	5.6	0.9	5.2	0.8
Healy Floats-17	19.4	53.5	107.6	12.6	18.1	9.6	2.1	8.9	49.4	1.3	8.6	1.7	5.2	0.7	4.7	0.7
Healy Tailings-17	27.0	62.0	126.5	14.8	18.6	12.0	2.9	12.5	63.3	1.6	10.4	2.1	6.3	0.9	5.6	0.9
Healy Composite	22.0	56.4	114.0	13.4	18.3	10.4	2.4	10.2	54.1	1.4	9.2	1.8	5.6	0.8	5.0	0.8

Appendix P. Cost analysis of the project over a period of 7 years.

Year	1	2	3	4	5	6	7	TOTAL
PRODUCTION								
Operating days/year	350	350	350	350	350	350	350	2,450
Waste (t/day)	0	0	0	0	0	0	0	
Ore (t/day)	7000	7000	7000	7000	7000	7000	7000	
Ore milled (000 t)	2,450	2,450	2,450	2,450	2,450	2,450	2,450	17,150
Ore grade (g/t)	130	130	130	130	130	130	130	
Mill recovery (%)	73%	73%	73%	73%	73%	73%	73%	
REE recovered (000 g)	231,231	231,231	231,231	231,231	231,231	231,231	231,231	1,618,617
Remaining recoverable REE (000 g)	1,387,386	1,156,155	924,924	693,693	462,462	231,231	0	
REVENUE								
REE price ($/g)	1.00	1.00	1.00	1.00	1.00	1.00	1.00	
Gross income ($ 000)	231,231	231,231	231,231	231,231	231,231	231,231	231,231	1,618,617
OPERATING COSTS								
Mill Operating Cost ($/t)	17.5	17.5	17.5	17.5	17.5	17.5	17.5	
Total Milling Cost ($ 000)	42,875	42,875	42,875	42,875	42,875	42,875	42,875	300,125
Total Operating Cost ($ 000)	42,875	42,875	42,875	42,875	42,875	42,875	42,875	300,125
DEPRECIATION								
Var. Dep. Year 1 (DB-SL) ($ 000)	2,231	1,702	1,298	990	796	773	750	8,541
Var. Dep. Year 2 (DB-SL) ($ 000)	0	473	345	251	183	169	164	1,583
Cumulative Depreciation ($ 000)	2,231	2,175	1,643	1,241	979	941	-311	8,900
DEPLETION								
Percentage Depl. Allowance ($ 000)	6,590	6,590	6,590	6,590	6,590	6,590	6,416	45,956
50% Taxable Income Limit ($ 000)	0	0	0	0	40	59	103	202

Appendix P. Cost analysis of the project over a period of 7 years (continued).

Depletion Taken ($ 000)	6,590	6,590	6,590	6,590	40	59	103	26,562
Cumulative Depletion ($ 000)	6,590	13,180	19,770	26,360	26,400	26,459	26,562	145,323
TAX								
Gross Revenue ($ 000)	231,231	231,231	231,231	231,231	231,231	231,231	230,006	1,617,392
Less: Refinery Charges ($ 000)	184,985	184,985	184,985	184,985	184,985	184,985	184,985	1,294,894
Net Smelter Return ($ 000)	46,246	46,246	46,246	46,246	46,246	46,246	45,021	322,498
Less: Royalty Payment ($ 000)	2,312	2,312	2,312	2,312	2,312	2,312	2,251	16,125
Net Revenue ($ 000)	43,934	43,934	43,934	43,934	43,934	43,934	42,770	306,373
Add: Salvage Value ($ 000)	0	0	0	0	0	0	1,225	1,225
Less: Operating Costs ($ 000)	42,875	42,875	42,875	42,875	42,875	42,875	42,875	300,125
Less: Depreciation ($ 000)	2,231	2,175	1,643	1,241	979	941	-311	8,900
Less: Depletion ($ 000)	6,590	6,590	6,590	6,590	40	59	103	26,562
Taxable Income ($ 000)	-7,762	-7,706	-7,174	-6,773	40	59	1,328	-27,989
Less: Tax ($ 000)	-3,571	-3,545	-3,300	-3,115	18	27	611	-12,875
CAPITAL INVESTMENT								
Mine/Mill Capital ($ 000)	10,413	1,838	0	0	0	0	0	12,250
Working Capital ($ 000)	13,000	0	0	0	0	0	-13,000	0
Total Capex Cash Flow ($ 000)	23,413	1,838	0	0	0	0	-13,000	12,250

Appendix P. Cost analysis of the project over a period of 7 years (continued).

CASH FLOW								
Net Income After Tax ($ 000)	-4,192	-4,161	-3,874	-3,657	22	32	717	-15,114
Add: Depreciation ($ 000)	2,231	2,175	1,643	1,241	979	941	-311	8,900
Add: Depletion ($ 000)	6,590	6,590	6,590	6,590	40	59	103	26,562
Less: Capital Cost ($ 000)	10,413	1,838	0	0	0	0	0	12,250
Less: Working Capital ($ 000)	13,000	0	0	0	0	0	-13,000	0
Net Cash Flow ($ 000)	-18,783	2,766	4,359	4,174	1,040	1,032	13,509	8,098
Cumulative Cash Flow ($ 000)	-18,783	-16,017	-11,658	-7,483	-6,443	-5,411	8,098	
NPV @ 10% ($ 000)	-552.4							
IRR	9%							
Payback Period	CCF-Negative	CCF-Negative	CCF-Negative	CCF-Negative	CCF-Negative	CCF-Negative	6.40	